

Exploiting a mmWave Large Antenna Array from a High-Altitude Platform (HAP) for Rural Vehicular Communications

Kayode Popoola

Doctor of Philosophy

University of York
Electronic Engineering

February 2022

Abstract

Intelligent Transport Systems (ITS) are envisioned to revolutionize the quality of experience for drivers and passengers by facilitating a broad array of vehicular services and applications. Several network architectures have been proposed in the literature which exploit cellular infrastructure and Roadside Units (RSUs). However, these approaches suffer from various challenges, particularly on rural roads. First, because of the rural topology, coverage and connectivity issues arise due to the need to deploy a sufficient number of RSUs. Second is that current technologies, i.e., Dedicated Short-Range Communications (DSRC), can only support a maximum data rate of 27 Mbps. This is grossly inadequate considering the growing requirements of next-generation vehicular applications.

In this thesis, we address some of these challenges by proposing the exploitation of a High-Altitude Platform (HAP), operating in the mmWave band, and equipped with a large antenna array. Firstly, a framework for characterizing the HAP-assisted vehicular network with a representative traffic demand is presented. Our approach is efficient, scalable, incorporates real-world maps and publicly available demographic data. To improve the network management, we propose a clustering scheme for grouping vehicles into clusters and show the effectiveness of our algorithm in achieving stable clusters. Secondly, by exploiting the HAP model, we investigate the coverage and capacity performance of the clustered group of vehicular users. To the best of our knowledge, this is the first such attempt that characterizes the performance of a HAP-assisted vehicular network for a rural scenario. Finally, we propose an optimal relay selection scheme for extending the performance of vehicles with poor radio conditions. In lieu of an exhaustive search, the relay selection is formulated as an optimization problem and solved using the Kuhn-Munkres algorithm. Simulation results show our scheme can provide an 82.4% improvement in throughput when compared to without relaying.

Table of Contents

List of Figures	v
List of Tables	vii
Acknowledgements	viii
Declaration	ix
List of Symbols	x
List of Abbreviations	xi
1 Introduction	1
1.1 Research Background	1
1.2 Scenario Background and Description	4
1.3 Research Hypothesis and Objectives	6
1.4 Thesis Scope	7
1.5 Research Contributions and Thesis Outline	7
1.6 Publication List	9
2 Literature Review	10
2.1 Introduction	10
2.2 mmWave Air-to-Ground (A2G) Channel	10
2.2.1 Key Technical Advantages and Challenges	11
2.3 The Antenna Array	18
2.3.1 Array Beamforming	19
2.3.2 Beam Optimization	20
2.3.3 Windowing Weights	21
2.4 Related Work on High Altitude Platforms (HAPs)	21
2.5 Vehicular Network Overview	23
2.5.1 Vehicular Mobility Models	23
2.5.2 Traffic Mobility Simulators	25
2.6 Vehicular Network Services and Applications	27
2.7 Vehicular Network Clustering	28

2.8	Conclusion	29
3	The Vehicular Traffic Demand and Clustering Model	31
3.1	Introduction	31
3.2	Contribution and Organisation	32
3.3	Traffic Demand Generation	33
3.3.1	Study Area	34
3.3.2	SUMO Traffic Generation Tool	35
3.4	Vehicular Clustering Model	39
3.4.1	Centroidal Voronoi Tessellation (CVT) <i>k-means++</i> Clustering Approach	41
3.4.2	The Silhouette Coefficient (SC)	43
3.4.3	Ant Colony Clustering	47
	Multi-Objective optimisation	48
	Original Ant Colony Clustering System (ACCS)	49
	ACS Problem Formulation	51
3.5	Simulation Results	54
3.5.1	Performance Metrics	55
3.6	Conclusion	57
4	Coverage and Capacity Analysis of a HAP System with Large Antenna Arrays	59
4.1	Introduction	59
4.2	Contribution and Organisation	60
4.3	System Model	61
4.3.1	The HAP Antenna Array	61
4.3.2	HAP Wireless Channel Propagation	64
4.3.3	HAP Beamforming Gain	67
4.4	Performance Analysis Characterisation	69
4.4.1	SNR and SINR Coverage Analysis	70
4.4.2	Capacity Analysis	71
4.5	Simulation Results and Discussion	71
4.5.1	Contour Footprint Performance	72
4.5.2	SINR Boxplot Distribution	74
4.5.3	SINR Coverage Performance	75
4.5.4	CDF Distribution	81
4.5.5	UE Throughput Performance	81
4.6	Coverage Probability and Throughput Performance under Ideal Interference Mitigation	83
4.7	A Dynamic Fractional Frequency Reuse (D-FFR) Scheme	86
4.8	UE Trajectory Performance	89
4.9	Throughput Trajectory Scenario	94

4.10	Conclusion	96
5	Optimal Relay Selection for a HAP-assisted Vehicular Network	98
5.1	Introduction	98
5.1.1	Cooperative Relay Transmission Protocol	98
5.2	Related Work	100
5.2.1	Contributions and Organization	102
5.3	System Model	103
5.3.1	Outage Probability of the HAP Link	104
5.3.2	Channel Propagation Model	105
5.4	Problem Formulation	106
5.4.1	Interference Characterisation	107
5.5	Relay Selection Scheme	108
	Kuhn Munkres Algorithm	109
5.6	Performance Metrics	112
5.6.1	Outage Probability and Transmission Success Probability	112
5.7	Simulation Results	113
5.8	Conclusion	118
6	Conclusion and Future Work	121
6.1	Chapter Summary and Conclusion	121
6.2	Research Hypothesis Revisited and Summary of Original Contributions	123
6.3	Future Work	123
6.3.1	A Heterogeneous Traffic Model with Network Virtualization	124
6.3.2	Intelligent beamforming	124
6.3.3	Energy Management of the HAP Antenna Payload	125
6.3.4	Local Search method and Learning for clustering weights	125
6.3.5	Worst-case Interference control with Link adaptation	126
6.3.6	Consideration of Uplink	127
6.3.7	Resource Division and Transmit Power Control	127
6.3.8	Constellation of Inter-connected HAPs	127
	Appendix A Study Area	128
	Appendix B Simulation Snapshot	129
	Appendix C Proof of Theorem 1	130
	Bibliography	131

List of Figures

1.1	Global predicted IoT growth as reported in [1] with connected vehicles having the highest at 30% CAGR by 2023, reproduced from [1]	2
1.2	A simple illustration of the proposed system scenario.	5
2.1	Path-loss as function of distance between transmitter and receiver	14
2.2	Three State Semi-Markov Process [directly reproduced from [66]	17
2.3	(a) Antenna Array with beamforming (b) Analog beamforming (c) Digital beamforming (d) Hybrid beamforming	20
2.4	Normalized gains due to different windowing functions with sub-platform point at $54.315^{\circ}N, -0.9^{\circ}E$	22
3.1	High-level abstraction of SUMO traffic demand model	36
3.2	Simulation output of vehicle UE distribution over time	38
3.3	The average and standard deviation of critical parameters	39
3.4	Centroidal Voronoi Tessellation (CVT) of the Area of Interest (AoI).	44
3.5	CDF of Silhouette Coefficient (SC).	45
3.6	Box plot of Silhouette Coefficient (SC).	46
3.7	Average duration of cluster head vehicle	56
3.8	Average duration of cluster member vehicle	56
3.9	Average duration of cluster head vehicle Vs Maximum Speed	57
4.1	Phased Array Antenna System	62
4.2	Phased Array Antenna System with Beam Footprint	62
4.3	The average and standard deviation of critical parameters	63
4.4	Total free space path loss at 28 GHz from the model in [188]	66
4.5	The average and standard deviation of critical parameters	69
4.6	SINR contour with 6 clusters with a 40×40 antenna element array	72
4.7	SINR contour with 100 clusters with a 40×40 antenna element array	73
4.8	Boxplot of SINR - 6 clusters with a 20×20 Antenna element array	74
4.9	Boxplot of SINR - 100 clusters with a 40×40 Antenna element array	75
4.10	SINR coverage probability for different χ_{SINR}	76
4.11	SINR coverage probability as a function of the average vehicle UE per cluster	77
4.12	SINR coverage probability for a different number of clusters	78

4.13	SINR coverage probability for different number of UEs	79
4.14	SINR Coverage probability for different number of clusters	80
4.15	CDF of SINR for 50 clusters	81
4.16	Average Throughput per cluster vs Number of antenna elements	82
4.17	Average User throughput vs number of UEs per cluster	83
4.18	CDF of Capacity for different antenna elements	84
4.19	SNR coverage probability for different SNR thresholds	85
4.20	Average Throughput per cluster vs Number of antenna elements	86
4.21	Geometry of Dynamic Fractional Frequency Reuse (D-FFR)	87
4.22	CDF of SINR with and without D-FFR	88
4.23	CDF of UE capacity with and without D-FFR	89
4.24	Coverage Map of vehicle trajectory	90
4.25	The average and standard deviation of critical parameters	91
4.26	30-cluster SNR/SINR trajectory	93
4.27	40-cluster SNR/SINR trajectory	93
4.28	50-cluster SNR/SINR trajectory	94
4.29	30-cluster SNR/SINR Throughput	95
4.30	40-cluster SNR/SINR Throughput	95
4.31	50-cluster SNR/SINR Throughput	96
5.1	A V2V relay assisted communication	100
5.2	Network Architecture of relaying scheme	103
5.3	CDF of 5 th percentile UE Capacity	104
5.4	Interference scenario for relay selection	108
5.5	Bipartite Matching Graph for relay assignment and adjacency matrix	111
5.6	Transmission success probability vs Average Link Contact Durations	116
5.7	Transmission success probability vs V2V Link distance	116
5.8	Transmission success probability vs Average Vehicle Speed	117
5.9	Outage Probability vs SNR	118
5.10	Outage Probability Vs Interference Threshold of UE	119
5.11	CDF plot of UE Throughput	119
6.1	Interference to Noise ratio (INR) for different number of clusters	126
A.1	Study Area comprising rural road way of North Yorkshire- Kirkbymoorside and Helmsley	128
B.1	A SUMO simulation snapshot at t=20 s	129
B.2	A SUMO simulation snapshot at t = 30s	129

List of Tables

3.1	Traffic Demand Data	36
3.2	ACO Simulation Parameters	54
4.1	System Parameters for HAP Model	68
5.1	V2V Simulation Parameters	114

Acknowledgements

First, my deepest gratitude goes to the Almighty for giving me the grace to successfully complete this remarkable Ph.D journey. A big thank you to my supervisors, Prof. David Grace and Mr. Tim Clarke, for their invaluable guidance over the course of my study. This work would not have been feasible without their kind support, encouragement and insightful supervision. I would also like to thank my thesis advisor, Prof. Paul Mitchell for his helpful suggestions and guidance.

To my beloved wife, Ghaniyyah Olaide Popoola, my profound and heartfelt gratitude to you for your moral and emotional support from the first day I began this journey. I could not have done this without you. To my girls, Fareedah and Zahrah, I can only say thank you for providing those moments that kept me going.

To my Mum and Dad, words alone cannot express my gratitude. I say a big thank you to you guys for always being there for me and supporting me through thick and thin. You laid the foundation for me and never stopped believing in me. For this, I am forever grateful to you guys and I owe you a big debt of gratitude. To Taibat, Seun, Abdulwasiu, Abdulaziz and Balqis, words alone cannot express how deeply grateful I am for your support and encouragement.

To my colleagues in the Communications Research group - Steve Arum, Muheeb Ahmed, Qiao Wang and Junfei Qui, I say thank you for providing a memorable and enjoyable experience. It was never dull with you guys!

Finally, I thank the Petroleum Technology Development Fund (PTDF), Nigeria for providing the funding for my studies. For this, I am forever grateful.

Declaration

I, Kayode Popoola, declare that this thesis titled, "Exploiting a mmWave Large Antenna Array from a High-Altitude Platform (HAP) for Rural Vehicular Communications" is a presentation of original work and I am the sole author. This work has not previously been presented for an award at this, or any other, University. All sources are acknowledged with appropriate references.

List of Symbols

x	Matrix
\mathbf{X}	Vector
$\log_{10}(x)$	Logarithm of x to base 10
$\min(\cdot)$	Minimum of a function
$\max(\cdot)$	Maximum of a function
\cup	Union Operation
\cap	Intersection Operation
\sum	Summation Operator
$ \cdot $	Cardinality Operator
\in	Element Operator
\subseteq	Subset Operator

List of Abbreviations

3-GPP	3 rd Generation Partnership Project
5G-NR	5G New - Radio
A2G	Air to Ground
ACO	Ant Colony Optimization
CAGR	Cumulative Annual Growth Rate
CH	Cluster Head
CM	Cluster Member
C-V2X	Cellular - Vehicle to Everything
CVN	Cooperative Vehicular Network
CVT	Centroidal Voronoi Tessellation
D2D	Device to Device
DSRC	Dedicated Short Range Communications
FSO	Free Space Optics
GPS	Global Positioning System
GUI	Graphical User Interface
HAP	High Altitude Platform
ITS	Intelligent Transport System
ITU	International Telecommunication Union
IoT	Internet of Things
IoV	Internet of Vehicles
LAP	Low Altitude Platform
LoS	Line of Sight
MCS	Modulation and Coding Scheme

MIMO	Massive Input MassiveOutput
NLoS	Non Line of Sight
NR-V2X	New - Radio Vehicle to Everything
OBU	On Board Unit
OSM	Open Street Map
POI	Point of Interest
QoS	Quality of Service
RF	Radio Frequency
RSU	Road Side Unit
SC	Silhouette Coefficient
SDN	Software Defined Network
SINR	Signal to Interference and Noise Ratio
SLL	Side Lobe Level
SNR	Signal to Noise Ratio
SPP	Sub Platform Point
SUMO	Simulation of Urban Mobility
TAZ	Traffic Assignment Zone
UAV	Unmanned Aerial Vehicle
UE	User Equipment
UPA	Uniform Planar Array
V2I	Vehicle to Infrastructure
V2V	Vehicle to Vehicle
V2X	Vehicle to Everything
VANET	Vehicular Ad-hoc Network

Chapter 1

Introduction

1.1 Research Background

It is widely expected that the vehicular network landscape will change substantially over the next few years as vehicles are expected to have growing levels of autonomous functions and capabilities. This, in combination with 5G wireless connectivity is expected to be an important enabler for the next generation of vehicular networks. Therefore, an explosion in the number of connected devices and unprecedented opportunities for the provision and facilitation of a host of innovative applications and services such as the Internet-of-Things (IoT) are envisaged. The IoT ecosystem is a prevalent system of interconnecting people, devices, processes, and data to each other and the internet that has revolutionized the global connectivity landscape with an expected increase in global population penetration and a predicted cumulative annual growth rate (CAGR) of 66% by 2023 [1]. A fusion of the internet and IoT technology has led to the emergence of the Internet of Vehicles (IoV) and, with that, the concept of the connected and autonomous vehicle and its associated applications; otherwise called an Intelligent Transport System (ITS).

The ITS paradigm reflects the efficient and safe way in which transportation infrastructure, vehicles, people, and passengers are able to apply information and communication technologies (ICT) to provide services to end-users through the utilization of advanced storage, processing and computing capabilities which will ultimately aid vehicle decision making processes. This will, (a) ensure a safe driving environment by requiring vehicles to exchange accurate and timely information with other neighbouring vehicles via on-board units (OBUs) and Global Positioning Systems (GPS), thereby facilitating cooperative perception applications such as collision warning and blind-spot detection, (b) provide an efficient traffic management system in which vehicles can communicate with the road infrastructure while providing real-time status information on the current road network conditions and, (c) enhance the user quality experience by delivering multimedia and infotainment content to both driver and passengers.

As shown in Fig. 1.1, a Cisco Annual Internet Report [1] forecast that connected vehicles will be the fastest-growing category for connected devices with an expected CAGR of 30% by 2023.

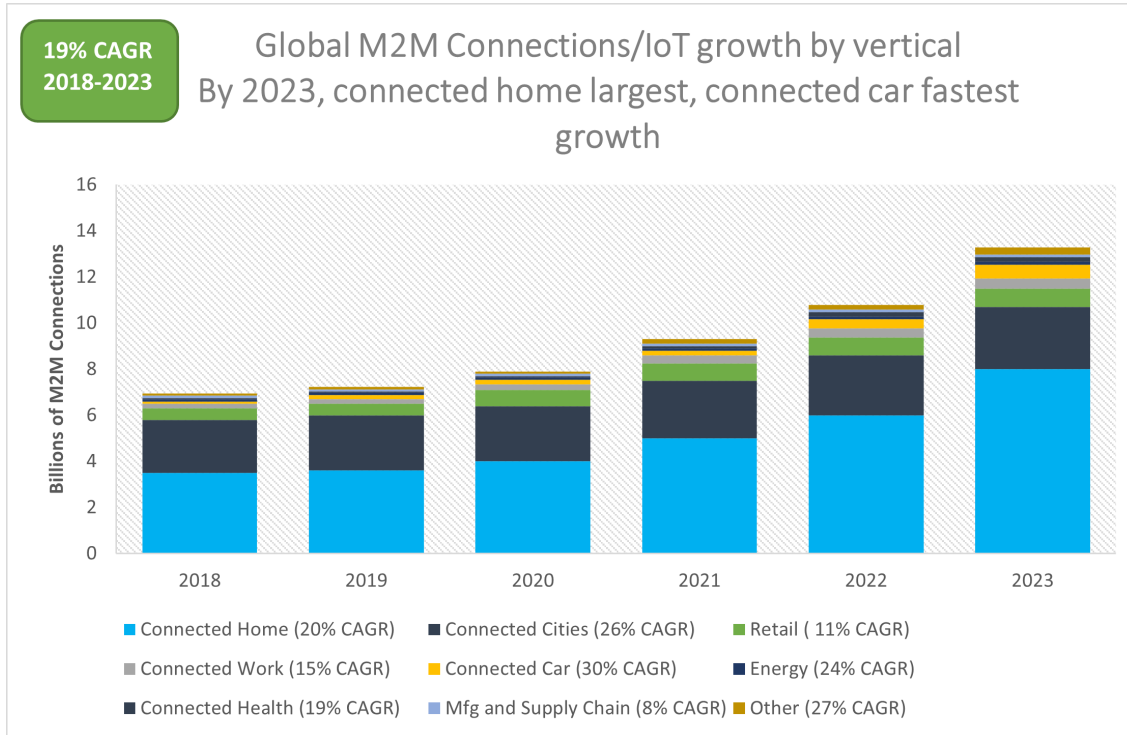


FIGURE 1.1: Global predicted IoT growth as reported in [1] with connected vehicles having the highest at 30% CAGR by 2023, reproduced from [1]

Unsurprisingly, vehicle manufacturers, governmental institutions, and researchers have worked collaboratively to develop and drive this emerging field with various ITS projects initiated. For instance, in February 2020, a government-backed Nissan Leaf autonomous vehicle successfully completed a 230-mile self-navigated journey in the United Kingdom [2] and the Multi-Car Collision Avoidance (MuCCA) project [3] aims to use artificial intelligence (AI) and vehicle-to-vehicle (V2V) communications to aid autonomous vehicles to cooperatively make decisions and avoid potential incidents.

Various regulatory frameworks, standards, and policies aimed at fast-tracking the development of autonomous vehicle technology have also been announced. Specifically, the U.S. Department of Transportation (US DOT), in 2009, allocated 75 MHz of licensed spectrum in the 5.850-5.925 GHz spectrum band (otherwise referred to as 'Safety Band' spectrum) for the dedicated short-range communication (DSRC) designed to support a variety of V2V safety applications [4], and in February 2020, a broad agency announcement (BAA) was released for the procurement of vehicle-to-everything (V2X) communication devices to support testing at the "Safety Band" spectrum and determine whether DSRC and/or 5G-New Radio (5G-NR) technologies can meet the requirements for V2V and vehicle-to-infrastructure (V2I) systems [5]. Considering the growing requirements of

the vehicular networking applications and the need to optimize the utilization of the 5.9 GHz spectrum resources, the Federal Communications Commission (FCC), in November 2020, subsequently split the 75 MHz of the formerly-DSRC spectrum between unlicensed and ITS use and allocated the upper 30 MHz for ITS that use the Cellular-V2X (C-V2X) communication technology [6].

C-V2X was published by the 3rd Generation Partnership (3GPP) Release 14/15 as an evolution of the Long-Term Evolution (LTE) standard and within Release 16 with support for New Radio V2X (NR-V2X) to complement more advanced C-V2X use cases. This offered an alternative to IEEE 802.11p with support for direct communication between vehicles, independent of the cellular network infrastructure using the so-called Proximity-based Communication interface - *PC5 interface/LTE side-link* - otherwise, referred to as Mode 4. If the vehicle is dependent on the existing cellular infrastructure to send and receive information about neighbouring vehicles and traffic conditions, it uses the LTE User-to-user interface - *Uu interface* - otherwise, referred to as Mode 3 [7]. However, some disadvantages include the additional network overhead introduced with sharing the same resource with other mobile users and data transmission problems in overcrowded conditions [8].

Tremendous efforts have been made to realise connectivity for V2V and V2I communication for both safety and non-safety applications with most of the research efforts predominantly focused on DSRC and C-V2X in urban and suburban roads [9]. However, DSRC performance has been shown to degrade in dense traffic scenarios [10] with support for a maximum coverage range of 1 km and theoretical data rates of 6 - 27 Mbps [11]. This limits its adoption for the high bandwidth requirements of vehicular network services and applications. Similarly, the utilization of C-V2X in Mode 3 and Mode 4 and/or NR-V2X have also been proposed to provide connectivity, with actual field trials on highways investigated for the former as reported in [12]. However, both modes have inherent challenges. The business justification for operation in Mode 3 for both the Original Equipment Manufacturers (OEMs) and cellular operators remains its biggest challenge [13]. Vehicles will be required to constantly send and receive scheduling messages that are processed in a short-latency central server that could span multiple operators. The question arises as to who pays for the communication infrastructure, bandwidth and servers. C-V2X in Mode 3 will require the support of the cellular infrastructure or the placement of a sufficient number of road side units (RSU's) and/or distributed units (DUs) to process the physical layer and RF front-end [14]. When rural roads are considered, this becomes increasingly challenging for deployment, where, hitherto, the communication infrastructure is sparse and/or virtually non-existent, with connectivity gaps ranging from regions of partial not-spots (where there is partial coverage) to complete not-spots (areas with no coverage).

Furthermore, the optimal placements of RSUs in rural roadways, as well as the economic consideration of deploying a sufficient number to provide adequate connectivity becomes increasingly difficult. This is largely due to the inverse relationship between the density of users per RSU and the cost of the infrastructure, and therefore, making a compelling business case for such deployment becomes difficult. To add to these challenges, the rapid proliferation of IoV applications (i.e., multi-media infotainment content delivery such as Ultra high definition (UHD), traffic information e.t.c) has led to an explosion in mobile internet traffic with the sub-6 GHz frequency bands incapable of supporting these bandwidth-intensive applications. To tackle this spectrum crunch and provide the high bandwidth and data rates, a promising approach that has gained increasing traction over the last decade is communication over the mmWave bands, with carrier frequencies ranging from 30 - 300 GHz. With the availability of larger licensed and unlicensed bandwidth at the mmWave frequency band, support for a wide variety of wireless broadband services is envisioned.

To address the aforementioned challenges, and complement or provide wireless vehicular communication in an under-served or un-served rural road, an alternative approach, proposed in this thesis, is the utilization of a High-Altitude Platform (HAP) equipped with a large antenna array and operating at the mmWave frequency band. With a direct LoS link, HAPs offer an exciting and promising alternative to provide both coverage and capacity to rural vehicular user equipment (UEs). HAPs are aerial platforms deployed in a quasi-stationary position in the stratosphere at an altitude of between 17 – 22 km above the Earth's surface to provide line-of-sight (LoS) wireless communication links to ground UEs within a large coverage area. HAPs combines the best characteristics of terrestrial and satellite communication systems while avoiding their drawbacks [15]. They are particularly suitable for rural and sparsely populated scenarios due to their relatively fast and low-cost deployment capabilities and their ability to cover considerably large areas compared to terrestrial deployments. Research on the utilization of HAPs as a means of wireless communication is not new.. Previous studies have demonstrated HAP deployment for last-mile internet connectivity [16], in hot-spot and disaster relief scenarios [17], and to provide capacity and extended coverage [18].

1.2 Scenario Background and Description

Motivated by several AP projects [19], [20], coupled with recent advancements in sensor and hardware technologies for the connected vehicle, there exists a clear scope for the integration of APs, specifically, a HAP in a vehicular network architecture. This is because, in comparison to a satellite or a LAP, a HAP offer an agile and flexible solution for facilitating the provision of vehicular network applications. While previous work in this domain have primarily focused on the LAPs, i.e, UAVs [21] and satellite communication

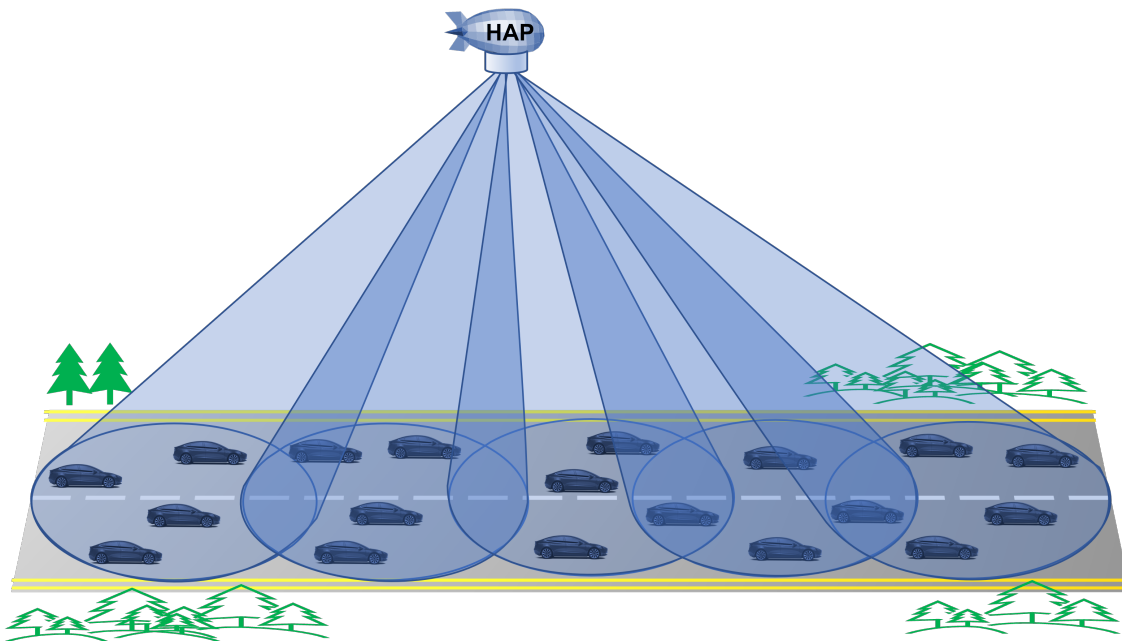


FIGURE 1.2: A simple illustration of the proposed system scenario.

architectures [15], we motivate the exploitation of a HAP to provide wireless communication in a rural AoI due to the following: HAPs have a favourable radio propagation condition and a reduced latency as opposed to satellites with the ability to serve a wide coverage area with a predominant LoS connectivity. Therefore, HAPs can be exploited to complement the coverage and capacity challenges of current vehicular network architectures while simultaneously providing new and innovative applications to vehicles UEs. Fig. 1.2 depicts a simple scenario illustration of the proposed network architecture. In the considered architecture, the HAP is exploited to provide content to the ground UEs via a direct HAP-to-ground UE communication. We assume that the HAP, equipped with large antenna arrays, is deployed at the centre of the coverage area with a line-of-sight (LoS) communication link to the ground UEs. To aid content dissemination and resource allocation [22], the vehicle UEs will be grouped into clusters with each cluster served by a HAP beam. For every cluster, a cluster center vehicle to which the HAP beam is directed is determined based on the mobility metric of the UEs. For this purpose, the clustering scheme considered will aim to minimize the mobility difference of the UEs in the cluster by considering the clustering as an optimization problem. If a UE cannot be served directly by the HAP beam via a direct transmission, it can establish communication links with UEs that are served directly by the HAP via a V2V relaying, thereby extending the network coverage.

It is therefore our opinion that, with HAPs providing a viable alternative for wireless connectivity from the sky, coupled with the possibility of operating at the mmWave frequencies and utilizing antenna arrays with a large number of antenna elements, a logical

approach is to combine these in a mmWave HAP-assisted wireless communication network. The work described in this thesis, therefore, investigates the exploitation of a HAP to provide and extend wireless communication for ITS services and applications on a rural un-served/under-served road, thereby assisting to enhance our understanding and, contributing to the growing body of literature in this domain.

1.3 Research Hypothesis and Objectives

The central hypothesis that has driven the research work presented in this thesis is that:

"A HAP, operating in the mmWave frequency band and deployed with a large number of antenna elements per HAP antenna array can provide adequate wireless communication for vehicular UEs specifically in rural scenarios where the terrestrial network infrastructures are inadequate or unavailable.

A HAP offers advantages such as rapid deployment, low-cost alternatives, and a high probability of LoS links over a large coverage area. Furthermore, HAPs can provide global knowledge of the channel gain of UEs in the coverage area and can centrally perform resource allocation with a full knowledge of the interference power from all UEs. In comparison to previous research work that has investigated Low Altitude Platform (LAP)-assisted vehicular communication networks [23], [24], in this thesis, we attempt to leverage the advantages of a HAP and present an alternative perspective for providing capacity and connectivity to vehicle UEs in a rural area of interest (AoI) through an investigation of the performance characterization of the network. Moreover, with future 5G enabled vehicle UEs expected to provide a diverse range of new services and applications that differ from the existing paradigm, it is critical to investigate alternative enabling architectures that can improve system performance and the overall user quality-of-service (QoS). In this context, our objectives are as follows:

1. Use publicly available geographical population distribution data to derive vehicular traffic demand for a given geographical AoI which achieves an acceptable level of realism.
2. Implement a clustering strategy for effective network management and information dissemination using the HAP by considering cluster formation as both an unsupervised learning and an optimization problem for the traffic scenario.
3. Conduct a performance analysis for the SINR coverage probability and the achievable UE capacity for a varying number of clusters and antenna elements per HAP antenna array.
4. Investigate an optimal relay selection scheme for extending the network performance in terms of the probability of successful transmission, outage probability and

throughput of vehicular UEs that have poor link quality or that cannot be served by the HAP.

1.4 Thesis Scope

To investigate the performance of the HAP for rural vehicular communications, we examine the impact of different numbers of clusters and different number of antenna elements for the HAP antenna array and how these affect the coverage and achievable UE throughput. We also determine the appropriate number of clusters and corresponding number of UEs that maximize the coverage probability in terms of the total number of UEs that can be served by the HAP. More importantly, we address the following important questions:

- What are the coverage and/or capacity trade-offs with the different numbers of antenna elements?
- What is the appropriate number of clusters that will ensure an acceptable coverage for vehicle UEs?
- From a UE-centric perspective, what is the achievable throughput for vehicle UEs for a different number of clusters?
- what performance gains are obtainable with different frequency reuse factors?
- How can vehicle relays be optimally selected to extend the coverage and throughput performance for UEs not served by the HAP or with poor radio conditions?

1.5 Research Contributions and Thesis Outline

This research makes several noteworthy contributions to the growing body of research in the aerial-platform assisted vehicular network domain. Specifically, we outline our contributions below:

- we motivate a new perspective on exploiting a HAP equipped with a large antenna array to provide vehicular communication in an unserved rural area. The HAP network architecture can serve as a viable option to support the ubiquitous coverage and high-capacity requirements of future vehicular network applications and services. To the best of our knowledge, this is the first such attempt to characterize the performance of a HAP-assisted vehicular network for a rural scenario.
- An investigation of the performance of the proposed system in terms of the coverage probability and achievable UE throughput for a varying number of clusters and antenna elements per HAP antenna array. The proposed model provided an insight into the system performance and the characterization of the coverage-capacity

trade-off behaviour of the system. For the considered traffic scenario, the model indicated the upper and lower bounds for the number of clusters and UEs required to achieve maximum coverage and capacity for a different number of antenna elements. The proposed model's optimal best-case performance levels in terms of the coverage probability and achievable UE capacity have also been shown.

- an optimal relay selection scheme to provide connectivity to UEs not served by the HAP. In lieu of an exhaustive search, we formulated the relay selection as an optimization problem and solved it using the Kuhn-Munkres (KM) algorithm. The performance of the proposed algorithm against benchmark relay selection schemes in the literature was investigated. The simulation results show that our proposed algorithm provides better performance when compared to a scenario without relaying, i.e., a direct transmission from the HAP. Similarly, the proposed approach was compared to benchmark relaying approaches in the literature, indicating the superiority of our proposed scheme.
- the implementation of a clustering scheme to aid the HAP beamforming and group UEs into clusters using UE mobility information. In particular, two clustering algorithms were investigated: a k-means++ clustering and an ant-colony based clustering approach. Unlike comparable clustering approaches, our approach incorporated the UE mobility and nodal degree connectivity. The simulation results show that our proposed clustering approach performs better than the k-means++ clustering and benchmark clustering approaches in terms of achieving stable clusters. This contribution has been presented in [25]
- the generation of representative and realistic traffic demand for the rural study area. Unlike similar research in this domain requiring a high level of detail and complexity, our approach incorporates real-world topographical maps, publicly available demographic data with the traffic demand generated in each traffic assignment zone (TAZ) similar to an origin-destination (O-D) matrix.

The organization of the thesis is as follows: Chapter 2 presents a review of related literature that forms a background of the work subsequently presented. Firstly, an overview of mmWave communication for an aerial-assisted wireless communication network is presented. Here, we discuss relevant work in this domain, examine key technical advantages, practical applications and highlight potential challenges. Secondly, we review key antenna techniques used for aerial platform communications and discuss HAP networks as a promising and alternative for rural wireless vehicular communication. Finally, we provide insights into traffic mobility models and examine vehicular clustering architecture for network management.

In Chapter 3, we present the network scenario, the traffic mobility model, and clustering models that have been used to characterize the network. Detailed insights into

the network simulator used, as well as the traffic demand generation are also presented. Additionally, we consider clustering approaches that are based on; (a) a k-means++ clustering algorithm and (b) an optimization problem using Ant Colony Clustering (ACO). A performance comparison of this algorithm alongside a benchmark algorithm in the literature is presented.

Chapter 4 introduces the framework for the HAP to vehicle UE wireless communication links. This framework is characterized by a mmWave path loss-dependent model. We present the beamforming model and characterize the important performance metrics of Signal-to-Noise ratio (SNR), Signal-to-Interference plus Noise ratio (SINR), coverage probability, and achievable user capacity. We then present a user-centric analysis for arbitrary ground vehicles to study the impact of different antenna element configurations on achievable user capacity.

In Chapter 5, we extend the model in order to expand the coverage and capacity to vehicle UEs not served by the HAP and with poor channel conditions below a specified link quality threshold. In the proposed approach, we investigate an optimal selection of relay UEs, thereby extending the connectivity and enhancing the capacity of this set of UEs. A performance comparison of our proposed algorithm with comparable algorithms in the literature is investigated in this chapter. Results obtained show that our proposed approach minimizes the outage probability and improves the throughput performance.

Finally, the conclusions of the work conducted in this thesis and the potential research directions for future work are presented in Chapter 6.

1.6 Publication List

Conference Papers

- K. Popoola, D. Grace and T. Clarke, "Capacity and Coverage Analysis of High Altitude Platform (HAP) Antenna Arrays for Rural Vehicular Broadband Services," 2020 IEEE 91st Vehicular Technology Conference (VTC2020-Spring), 2020, pp. 1-5, doi: 10.1109/VTC2020-Spring48590.2020.9129557.
- K. Popoola, D. Grace, T. Clarke and M. Ahmed, "An Iterative k-means++ and Ant Colony Clustering Scheme for Vehicular Networks," 2022 IEEE Nigeria 4th International Conference on Disruptive Technologies for Sustainable Development (NIGERCON), 2022, pp. 1-5, doi: 10.1109/NIGERCON54645.2022.9803091.

Chapter 2

Literature Review

2.1 Introduction

The success of a connected and autonomous vehicle - ultimately aimed at a fully autonomous vehicle as defined in [26], and the associated delivery of innovative services and applications supporting both the driver and passenger, depends significantly on the wireless communication between the vehicles. Therefore, a study into the characteristics of the wireless propagation channel becomes paramount. The first section of this chapter presents salient characteristics and pertinent background work on mmWave air-to-ground (A2G) channel propagation based on existing state-of-the-art research solutions. Secondly, we present key technical advantages as well as the challenges. Thirdly, an insight into the antenna design characterization for a mmWave wireless communication is presented, and we subsequently examine the various research activities for wireless connectivity in the HAP domain. Fourthly, a brief overview of related work on vehicular mobility models is presented, and lastly, we present related work on clustering techniques for network management in vehicular networks.

The organization of this chapter is as follows: Related work on the mmWave Air-to-Ground (A2G) channel is presented in Section 2.2. In Section 2.3, a brief introduction on the antenna arrays and beamforming for the air-to-ground network is presented. Section 2.4 presents related work on HAPs, and in Section 2.5, background studies on vehicular mobility models are presented. Section 2.7 presents a review of clustering schemes in the literature and finally, in Section 2.8, concluding remarks are presented.

2.2 mmWave Air-to-Ground (A2G) Channel

Typically, the A2G network is either a LAP (i.e., a UAV) , a HAP (i.e., a stratospheric airship or balloon) or a satellite A2G network, depending on the altitude

to the earth's surface of the communication channel between the aerial network and the ground UE, usually termed as the A2G channel. The mmWave frequencies have also attracted significant research attention due to the large availability of bandwidth and there have been extensive studies to characterize the mmWave channel in different scenarios over the last few years. Seminal studies in [27] and [28] provide an extensive characterization of the channel. Particularly, the authors of [27] present a comprehensive overview of the channel modelling efforts by various groups and standards with propagation parameters such as LoS probability, large-scale path loss, e.t.c., considered for the mmWave channel propagation.

Advancing the work in [27], the study in [28] presents path-loss propagation measurements at 73 GHz for rural Virginia using field data to predict rural macro-cell (RMa) path-loss as a function of the base station antenna height. A comparison of their result with rural RMa path-loss model by the 3rd Generation Partnership Project (3GPP) TR38.900 Release 14 [29] is provided. Their results demonstrate that mmWave communication can achieve remarkable link distances, exceeding the 5 km coverage distance for a rural non-LoS (NLoS) model in [29]. Although their work did not involve an aerial platform as part of the communication system, their results are fundamental in advancing the understanding of rural propagation at mmWave.

For the A2G channel, much of the previous research has investigated channel models for UAV-assisted wireless networks, [30], [31], for satellites channels [32], [33] and for the HAP channel [34], [35]. However, in contrast to a HAP A2G channel, the operating frequencies, and altitude for a UAV A2G networks are significantly lower compared to that of a HAP channel, which is characterized by long link distances, usually greater than 17 km, and therefore, a higher likelihood of LoS propagation. Furthermore, mmWave HAPs A2G propagation channels are susceptible to atmospheric attenuation due to signal absorption by oxygen and water molecules, which is typically not a factor in UAV A2G channels. Therefore, channel models for the latter are not representative of the former without appropriate modifications. To the best of our knowledge, no specific channel measurements or analysis has been conducted on channel models for a mmWave HAP channel in a vehicular context, as majority of the measurement efforts have been in the LAP [36], [37] and land-mobile satellite domains [38].

2.2.1 Key Technical Advantages and Challenges

The integration of a mmWave HAP assisted wireless network can undoubtedly provide advantages to ground vehicle UEs. This include higher data rates due to higher bandwidths, increased antenna gains due to the ability to pack more antenna elements in a small form factor, reduced interference due to highly directional

mmWave beams etc. We now discuss some of these advantages, plus a consideration of related challenges.

Large Bandwidth Availability: One of the key advantages of mmWave communication is the large amount of both licensed and unlicensed bands of spectrum in the 30 GHz to 300 GHz range (including slightly lower frequencies) and channel bandwidths of up to 400 MHz as defined in the *3GPP Release 15* [39]. The use of mmWave in a vehicular context is not new. It has applications at 24 and 77 GHz for automotive radar and cruise control respectively [40]. With DSRC and C-V2X unable to provide the Gbps throughput and bandwidth requirements of vehicular network services and applications, the mmWave band offers an abundance of bandwidth to meet these requirements. This has been theoretically verified by the Shannon-Hartley theorem which shows a linear increase in capacity with bandwidth [41].

Available frequency bands with potential application for use in mmWave communication include the 24 GHz band (24.25-27.5 GHz), 28 GHz band (27.5-29.5 GHz), 38 GHz band (37-40 GHz), 45 GHz (42.3-47.3 GHz or 47.2-48.4 GHz), and E band (71-76 GHz, 81-86 GHz, and 92-95 GHz) [42]. In addition to the dedicated International Mobile Telecommunications (IMT) bands in the 2 GHz and 6 GHz bands, the designated spectrum for HAPs is in the frequency bands 47.2/48.2 GHz for global usage and the 21.4/22 GHz and 24.25/27.5 GHz for fixed services in Region 2 (including the Americas) [43]. To further underscore the growing need to expand the available spectrum for HAPs, ITU-R at the WRC-19 [43] identified additional mmWave spectrum bands for HAP use with the 31-31.3 GHz, 38-39.5 GHz allocated for worldwide use.

Small form factor antenna: Operation in the higher frequency spectrum means signals will have extremely short wavelengths. In comparison to operation in the sub-6 GHz, the mmWave wavelength spans the range from 10 mm at 30 GHz to 1 mm at 300 GHz with 28 GHz and 60 GHz having wavelengths 10.7 mm and 5 mm, respectively [44].

For example, for a square antenna array with 400 antenna elements operating at the sub-6 (2 GHz) or mmWave frequency (28 GHz) band with a half-wavelength inter-element spacing, the linear dimension is $20 \times \frac{\lambda}{2} = 1.5 \text{ m}$ and $20 \times \frac{\lambda}{2} = 0.11 \text{ m}$ with an area of 2.25 m^2 and 0.012 m^2 respectively. Clearly, the physical sizes of the antenna elements decrease proportionally to a higher mmWave frequency and therefore, it is possible to have small form-factor antenna arrays with increased flexibility for antenna placement.

With a reduced array dimension, additional space for other on-board communication systems such as the back-haul unit and mechanical/monitoring devices can

be incorporated on the platform. Smaller antenna dimensions also enable more elements per HAP antenna array and, with adaptive beamforming, higher antenna gains can be achieved with LoS propagation which can compensate for the higher propagation losses.

mmWave Challenges: Despite the potential benefits of mmWave, this section will be incomplete without careful consideration of some of the associated challenges associated with mmWave bands in order to achieve a holistic understanding of the signal propagation in this spectrum band. For signal propagation in free space the free space, path loss is expressed as [27]:

$$\begin{aligned} PL_{[dB]} &= 10 \log_{10} \left(\left(\frac{4\pi df}{c} \right)^2 \right), \\ &= 92.4 + 20 \log f_{[GHz]} + 20 \log d_{[km]}. \end{aligned} \quad (2.1)$$

where d is the separation distance between the transmitting and receiving antennas in km , f is the operating frequency in GHz and the first term in (2.1) is a constant due to d and f increasing by factors of 10^3 and 10^9 respectively. According to Equation (2.1), the path loss is proportional to the square of the separation distance and operating frequency. Therefore, as the frequency approaches the mmWave band, with a reduced wavelength through the relationship, $\lambda = \frac{c}{f}$, the path loss increases. This effect is shown in Fig. 2.1 where the path-loss is expressed as a function of frequency for different transmit-receive distances. A higher path loss is therefore experienced with an increasing distance between the transmitter and receiver and also increases with frequency. This demonstrates that the increasing path-loss observed at higher mmWave frequencies is non-trivial.

Additionally, the mmWave propagation channel can also be significantly affected by atmospheric attenuation caused by the interaction of the radio frequency signals with molecules in the physical environment. For the mmWave HAP system, rain attenuation is considered to be the most significant propagation impairment causing an absorption and scattering of the signal, especially for low altitude and tropical regions. In [45], a detailed procedure for the calculation of the loss due to water vapour can be found with other works in [46], [47] presenting rain attenuation prediction for an accurate evaluation of link budget requirements. It is important to note that the additional attenuation caused by operation at higher mmWave frequencies depends on the characteristics of the physical environment and the height of the platform above the ground level [48]. Other challenges associated with the mmWave spectrum include the increased effect of blockages, with results in [49] showing that outage probability increases as blockage factor increases.

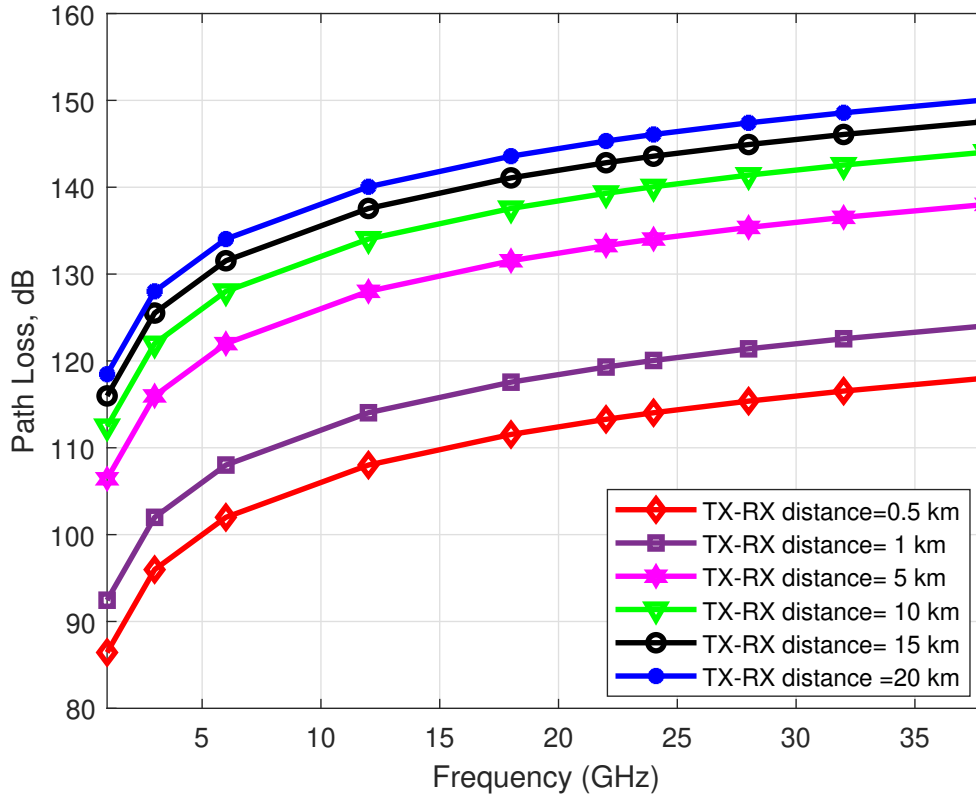


FIGURE 2.1: Path-loss as function of distance between transmitter and receiver

To address these challenges, several solutions have been proposed in the literature. Specifically, techniques such as beamforming using a large number of antenna elements per antenna array with large array gain [50], massive multiple-input multiple-output (MIMO) technologies [51], re-configurable intelligent surfaces (RIS) such as re-configurable reflect arrays (RRAs) in the form of an intelligent-omni surface (IOS) to enhance coverage and spectral efficiency [52], [53] and Hyper Surfaces [54] to provide connectivity via programmatic reflection. This is applicable to all frequency spectrum and wireless architecture. In this thesis, we will exploit the inherent advantages a HAP offers, complemented by beamforming using antenna arrays with a large number of antenna elements. This can compensate and mitigate the effects of higher path loss and increased atmospheric attenuation as they can provide high-gain narrow directional beams to the intended UE.

Next, we briefly review related research for the mmWave Air-to-Ground (A2G) channel propagation to provide a more complete summary of these channel propagation models. The A2G mmWave channel model can be broadly categorized into:

(a) Empirical channel models:

These models are based on environment-specific measurement campaigns which do not require specific knowledge of the propagation environment and are represented by path-loss equations and probability density functions (PDFs) elicited from measurement data [55]. Some standardized measurement models such as the *Third Generation Partnership Project (3GPP), TR 38.901* [39] and *International Telecommunication Union-Radio (ITU-R) M.2135-1* [56] have various channel models based on environment-specific measurement results for traditional cellular networks. However, actual measurements for an A2G channel in the mmWave band are limited due to the tremendous challenges primarily because of platform size, strict payload requirements and power limitations [57]. As such, measurements studies have focused on the sub-6 GHz band, C-band (4-8 GHz), and IEEE 802.11n bands [58] with ray tracing simulations and large-scale statistics such as path-loss and shadowing effects considered for various environments.

In [59], the authors proposed an empirical altitude-dependent path-loss model for A2G mmWave network considering LoS, reflection and, diffraction conditions with their result showing that the proposed model can be effectively extended for low and high altitude platforms. Similarly, in [60], a height-dependent A2G LoS model for mmWave communication suitable for both a LAP and HAP was presented for built-up areas. Building height distribution, width and space were geometric factors considered in the model and with known transmitter and receiver coordinates, they considered the probability of a LoS path based on all buildings along the propagation path being below the height of the transmitter-receiver connection line. The LoS probability is defined as:

$$P_{LoS} = \prod_{i=0}^{N_b} P_i = \prod_{i=0}^{N_b} P(h_i < h_{LoS}), \quad (2.2)$$

where h_i represents the building height, h_{LoS} is the LoS height and N_b is the number of buildings. The authors in [61] present an empirical measurement model using directive steerable antennas to evaluate the mmWave A2G radio link at 28 GHz and 38 GHz in a dense urban environment. Measurements were obtained for the power angle profiles for the directional antennas in both azimuth and elevation with their results showing agreement with previous studies in [62]. This study provided insights into the effects of reflection and scattering for signal propagation from a street canyon environment to the air and vice-versa.

(b) Analytical channel models:

Analytical models are focused on the impulse response between the transmit and receive arrays with each response allocated to a MIMO channel matrix. Various works have been presented in the literature that have focused on statistical channel

models for an A2G channel such as in [63] and [64]. In [63], the authors present an analytical channel model for an integrated ground-HAP Free Space Optics (FSO) link. They studied the effect of antenna directivity and gain under different channel conditions required to achieve a minimum outage probability. Their results show that the link performance is dependent on the receiver field of view and received beamwidth. The work presented in [64] derived a physical-statistical channel model used in the prediction of statistical time series and power delay profiles for a multi-antenna, multi-satellite A2G scenario. A 3-D HAP MIMO channel model was also presented in [65] where a space-time correlation function under different fading environments was derived. To improve on a single-state channel model, the authors in [66] and [34] proposed a multi-model approach using a three-state semi-Markov channel model of a HAP station in the Ka-band. Specifically, [66] consider a three-state dynamic Markov model based on a LoS state, shadowed state, and blocked state with the three-state Markov model represented by a state probability vector S defined as:

$$S = (w_A \quad w_B \quad w_C) \quad (2.3)$$

where w_A , w_B and w_C are the three channel states of the Markov model. The state transition probability matrix P and the state probability vector S is expressed as:

$$S(I - P) = 0 \quad (2.4)$$

where I is an identity matrix, and P is given by:

$$P = \begin{pmatrix} p_{AA} & p_{AB} & p_{AC} \\ p_{BA} & p_{BB} & p_{BC} \\ p_{CA} & p_{CB} & p_{CC} \end{pmatrix} \quad (2.5)$$

p_{ij} denotes the probability of change from one state to another and $\sum_{j=1}^n p_{ij} = 1$. Therefore, the probability density function of the three state semi-Markov model is defined as:

$$f(r) = w_A f_{LOS}(r) + w_B f_{Shadowed}(r) + w_C f_{Blocked}(r) \quad (2.6)$$

where $f_{LOS}(r)$, $f_{Shadowed}(r)$ and $f_{Blocked}(r)$ are the probability density function of LoS state, shadowed state, and blocked states respectively. Their results show that tropospheric weather and complex ground conditions have a significant effect on

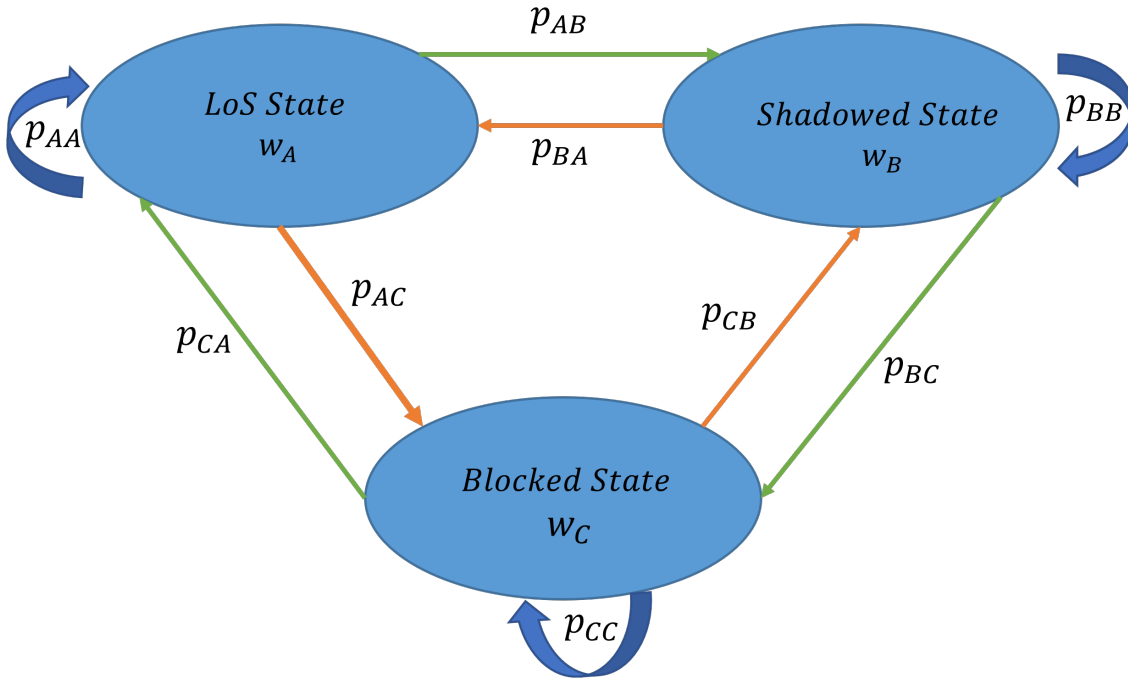


FIGURE 2.2: Three State Semi-Markov Process [directly reproduced from [66]]

transmitted signals with a 5-10 dB and 10-15 dB fading observed in open and suburban scenarios, respectively.

However, as these channel models have been developed for a LAP in either an urban or suburban environment, their results cannot be generalized for a HAP platform due to differences in, for example, the platform height and propagation environment. Nonetheless, these channel models can be extended to a HAP if these differences are taken into consideration.

For various physical operating environments, frequency ranges and propagation path types (LoS and NLoS), corresponding path-loss propagation models are as defined in [67]. With the HAP A2G communication link assumed to be predominantly LoS, the signal attenuation can be represented by large-scale path-loss fading, a log-normal distributed shadow fading and scenario-specific standard deviation [67]. Similarly, [18], [68] also report that using a large-scale channel propagation model (path loss, shadowing loss) for a HAP channel can provide reasonable results. Therefore, in this thesis, we adopt the free space path loss (FSPL) for the HAP A2G channel and account for signal attenuation owing to atmospheric rain effects as presented in Section 4.3.2.

2.3 The Antenna Array

For the full benefits of a HAP mmWave system to be realized, the size of the HAP antenna is a critical consideration due to the increased propagation loss and the effect on coverage, beam footprint, signal-to-noise ratio (SNR), and, ultimately, overall network performance. Traditionally, and owing to their versatility and ease of practical implementation, phased array antennas have been used to provide point-to-point (PtP) or point to multi-point (PmP) spot beams over the coverage area for a HAP system. Specifically, in a test demonstration by the authors of [69], antenna arrays were designed to support RF links for mechanically steered user terminals in the Ka-band using a 256-element antenna array. With the additional propagation losses experienced at mmWave frequencies, the HAP antenna array is, therefore, of great significance in the realization of a mmWave HAP network. For the work presented in this thesis, we have utilized a phased array antenna as the HAP antenna payload. In this vein, we present related research in this domain in terms of the HAP antenna array, array beamforming and beam optimization.

The size of the antenna arrays at sub-6 GHz is of the order of a few square metres while for mmWave systems, significantly smaller sized antennas can be realized due to the shorter wavelengths. This enables more antenna elements to be packed into a small form factor. In [70], the authors considered the performance of the uniform rectangular planar array (URPA), uniform hexagonal planar array (UHPA), and uniform circular planar array (UCPA) in the mmWave frequency band in terms of maximum array gain, beamwidth, and achievable spectral efficiency. For stratospheric platforms, the authors in [71] investigate a high gain, steerable antenna array for service footprint maximization of a HAP communication system. Their method entailed the demonstration of the beamforming and beam steering performance at approximately $\pm 60^\circ$ at the Ka-band (26 - 40 GHz). They also characterized the radiation pattern of the 256- antenna element array and computed the far-field performance with a ± 2.5 dB in gain variations observed for a 256-antenna element with a total mass of 90 g. The performance results show that the antenna array can be exploited for broadband LoS HAP communications to serve multiple users over a wide coverage area.

In [72], the authors present an analysis of a HAP operating in the 5G NR frequency bands (24.25-29.5 GHz) with a 64-antenna element array for both a triangular and rectangular geometry. Performance metrics of array gain, side lobe level (SLL), and mutual coupling were highlighted. Also, they show that a triangular or rectangular array geometry provide a better signal-to-interference ratio (SIR) and, thus, better performance in terms of spectral efficiency (SE) compared to the square antenna

array geometry. Specifically, they demonstrate that for a 64-element antenna array serving 20 users deployed in different cells, the triangular array lattice exhibit the most efficient performance with between 8.5% and 12% improvement in spectral efficiency observed when compared to a square lattice planer array. A further analysis of the performance of the triangular and rectangular planer arrays shows no substantial improvement in SE between both array geometry. An extensive review of the state-of-the-art in antenna array design and technologies for mmWave communications can be found in [73], and the references therein.

2.3.1 Array Beamforming

Antenna array beamforming utilizes multiple antennas to concentrate the signal power transmission to a specified area via signal processing techniques thereby improving the system performance. With different antenna array architectures, beamforming ensures the main beam and null directions can be dynamically shaped according to the UE location, thereby reducing interference and delivering an improved overall QoS.

Beamforming can be categorized as: (a) fully digital beamforming (DBF) (b) fully analog beamforming (ABF) and, (c) hybrid beamforming (HBF) architecture. In the DBF architecture, each antenna has a dedicated radio frequency (RF) chain with the phases and amplitude controlled by the baseband processing. However, they are expensive, exhibit high power consumption, and incur significant signalling overheads. In contrast to DBF, ABF utilizes a single, common RF chain that is connected to all the antenna elements with the beam controlled by adjusting the phase shifters along the RF path [74]. This is more energy efficient but comes at the expense of fewer degrees of freedom. HBF combines aspects of both DBF and ABF to achieve a trade-off with RF chains connected to a large number of antenna elements via analog phase shifters as shown in Fig. 2.3.

Several beamforming techniques have been proposed for HAPs to minimize interference [75], extend coverage and enhance capacity [51], [76]. In [51], a multiple beam antenna technology is proposed which satisfies coverage link quality and improves wireless system capacity. Their technique involved utilizing multiple antennas which improves the cell link SNR by increasing the inner circle beam width and reducing the outer beam. Other existing works have been presented on spatial and polarization diversity to improve channel capacity [77] and resource allocation [78]. A beamforming scheme for an integrated HAP and satellite system was also proposed in [79].

However, due to the highly mobile and fast-moving environment of vehicular networks, a fast and accurate monitoring of the directional signal i.e. beam-tracking

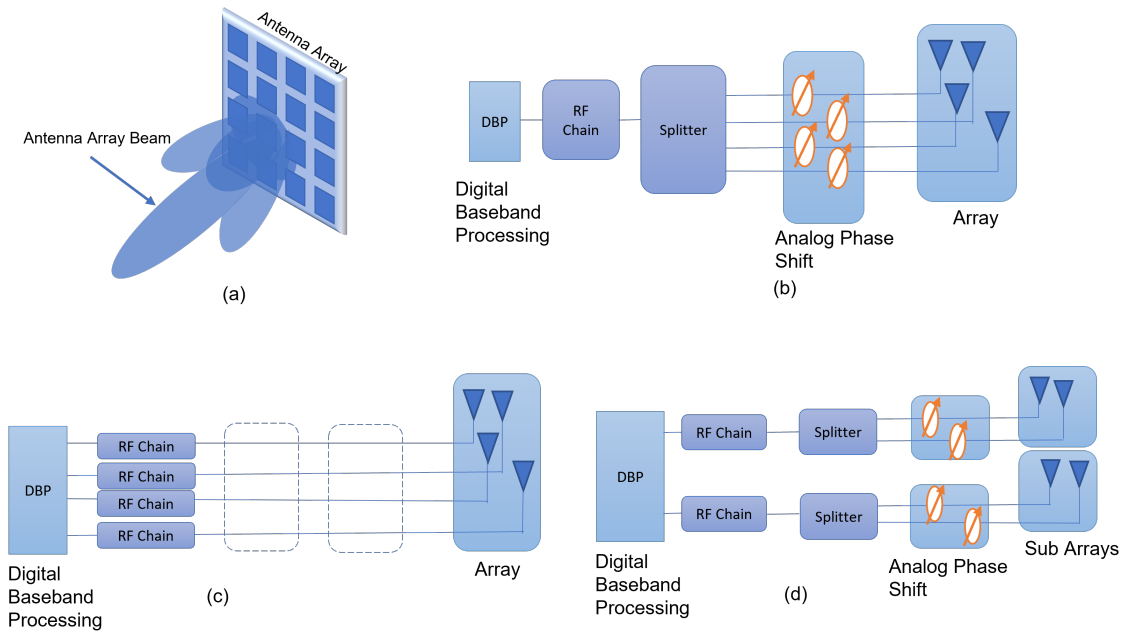


FIGURE 2.3: (a) Antenna Array with beamforming (b) Analog beamforming (c) Digital beamforming (d) Hybrid beamforming

is required to maintain a reliable communication link. To address these challenges, the authors in [80] presented a stochastic approximation and recursive estimation algorithm for beam-tracking using analog beamforming for mmWave communications. By formulating the beam tracking error as a constrained control and estimation problem, they were able to optimize both the beam direction estimator and the analog beamforming vectors. They established, via extensive simulations, that the recursive beam tracking algorithm achieves a higher tracking speed, higher tracking accuracy, and a higher data rate compared to reference algorithms such as the IEEE 802.11ad beam sweeping and tracking [81] and the Extended Kalman Filter (EKF) algorithms [82]

In contrast, the authors in [83] proposed a beam tracking algorithm based on the position, velocity, and channel coefficient in a mmWave V2I network. Using a robust adaptive, multi-feedback (RAF) algorithm, their results showed a significant improvement in the tracking performance with a 14% and 75.5% reduction in channel estimation and feedback overhead respectively. However, some of these algorithms have high processing complexity and will be challenging for a HAP system due to its power limitations. It is, therefore, important that the HAP beamforming scheme has low processing complexity.

2.3.2 Beam Optimization

To reduce interference from neighbouring beams over a coverage area, the concept of beam optimization will have a bearing on the overall SINR and consequently, the

QoS. Seminal research studies in this domain include the work in [84] and [85] to suppress the side-lobe levels of the antenna radiation pattern with low power levels in the direction of interferers. Also, [86] details a window-function beam optimization design for a uniform linear array. With an array response for N elements, the array factor, as a function of the elevation angle of the mmWave beam response, is written as:

$$AF(\theta) = w(\theta)p(\theta) = \sum_{n=0}^{N-1} w_n e^{j\frac{2\pi}{\lambda} nd \sin \theta} \quad (2.7)$$

where $w(\theta)$ is the the beam weighting vector, $p(\theta)$ is the array response, λ is the wavelength, N is the number of antenna array elements, w_n is the beam weight of the n^{th} antenna array element and d is the inter-element separation distance.

2.3.3 Windowing Weights

The selection of appropriate antenna element weights is important for the optimization of the beam pattern as it determines the side lobe level (SLL) and beamwidth. By applying appropriate windowing weights, an optimization of the beam pattern via a reduction of the SLL and beamwidth can be achieved. In Fig. 2.4, we compare the normalized antenna gains for different windowing functions: Rectangular (no windowing), Hann, Dolph-Chebyshev, Blackman-Harris, and a Kaiser windowing with shape parameter $\beta = 5$. The Dolph-Chebyshev has a specified SLL of -40 dB which can be adjusted based on the design requirements. The Hann window has a relatively narrower beamwidth compared to the Blackman-Harris and also a good attenuation of the first few SLL. The SLL of the Kaiser window is determined by the parameter β . As β increases for the Kaiser window, the main lobe beamwidth increases with a corresponding increase in SLL attenuation. Rectangular windowing is a poor choice due to its minimal SLL attenuation. In this work, we have used the Hann windowing function due to its sufficiently favourable tradeoff between the main lobe beamwidth and the attenuation of the SLL [74].

2.4 Related Work on High Altitude Platforms (HAPs)

Previous research work on the utilization of HAPs for wireless communication applications include the Japanese Stratospheric Platform (SPF) project [87], the Helinet and CAPANINA projects [88], [89] with various successful trials conducted. Despite being discontinued, Google's Project Loon [90] kick-started interests in the HAP domain. In recent times, SoftBanks HAPSMobile [19] has successfully

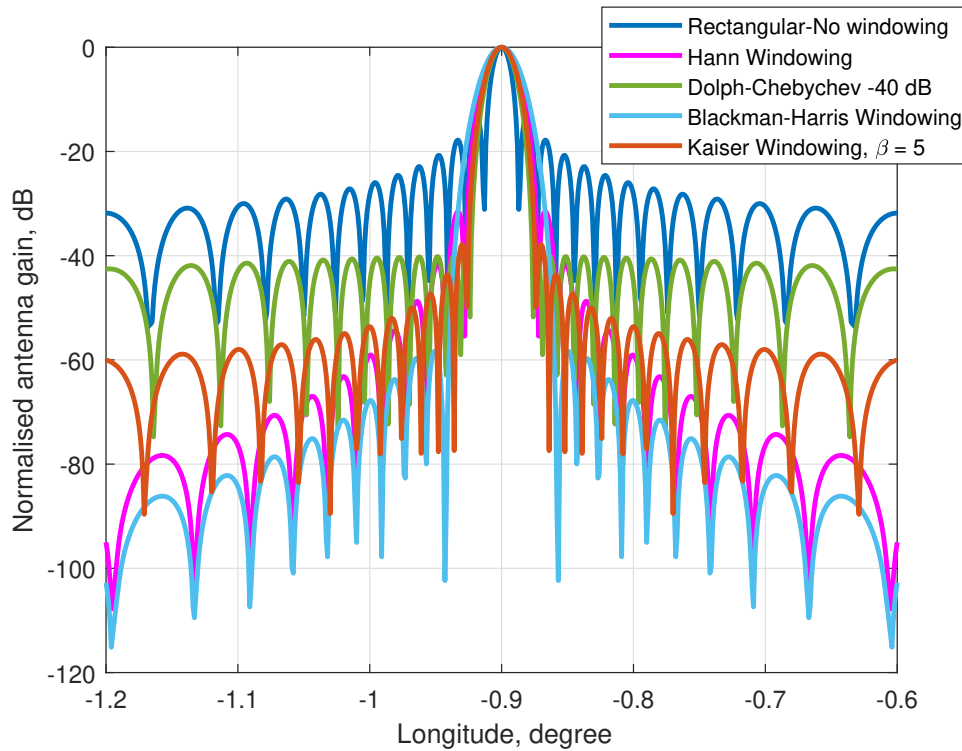


FIGURE 2.4: Normalized gains due to different windowing functions with sub-platform point at $54.315^{\circ}N, -0.9^{\circ}E$

conducted test flight trials and internet connectivity test for its solar powered unmanned aircraft system “Sunlider”, and the Cambridge-based Stratospheric Platforms (SPL), backed by Deutsche Telekom, has proposed a zero emission hydrogen-powered HAP (Stratomast) that can provide coverage for remote and rural regions of Scotland spanning across a $140km^2$ area with significantly higher data rates compared to those obtainable with satellites [20]. Other promising HAP projects around the world include the ECOSAT project [91], SCEYE project [92] and the Thales Alenia Stratobus project [93].

The research on HAPs is not limited to the commercial domain. Various research studies have also been presented with notable early work in [94] where they investigated the provision of high data rate links to trains using ‘smart’ antenna arrays on the HAP. Similarly, and motivated by the shortcomings in [95], where the effect of coverage and system capacity on a multi-beam antenna located on an AP utilizing planar arrays was presented, the authors in [96], report the effect of co-channel interference on elliptical HAP beams at cell edges with marginal link budgets using different cluster sizes and sidelobe levels. In [55], an overview of HAP based broadband communications and the use of Free-Space-Optics (FSO) to provide high capacity backhaul links was investigated, while in [97], using directive antenna arrays, the authors studied the effect of HAP antenna beamwidth, antenna

spacing radius, and beamforming on the system capacity for single and multiple HAP deployments utilizing different antenna models. Their results showed that a narrower beamwidth provides a better downlink SNR over 75% of the coverage area. Typically, a narrower antenna beamwidth will provide a higher transmit gain and steeper antenna roll-off. However, this is at the expense of a reduced SNR for users at the cell edge, not covered by the HAP beam.

More recently, in [98], the authors proposed a scheme using an efficient Markov chain channel model to support IoT services and applications while in [99], an integrated air-ground heterogeneous network architecture for HAPs and LAPs to expand coverage for un-served areas and enhance capacity was presented. Here, the authors proposed a software-defined network (SDN) as a central controller to manage the different tiers of the system and discussed several enabling technologies required to sustain the air-ground network. Finally, a case study of the proposed architecture evaluating the system performance in terms of outage probability and user throughput was investigated. In [18], the authors provided a literature survey from a coverage and capacity extension perspective for HAPs in remote un-served and under-served rural areas.

Taking into account current technological advancements in the wireless technology domain, the authors in [100] proposed a HAP deployment as a next-generation super macro base-station (SMBS) to address the high capacity requirements in urban and densely populated areas. Other works have investigated radio resource and interference management [101], channel modelling [34], energy management [102] and HAP-based FSO communication systems [103]. An in-depth review of the opportunities, latest advancements, future networking applications and use-cases for a HAP system can be found in [68] and the references therein.

2.5 Vehicular Network Overview

In this section, we briefly examine the framework required to properly describe vehicular movements and depict realistic vehicular traffic scenarios. Then, a brief description of the traffic simulator used in this thesis is presented and an overview of the various research work in this domain is presented.

2.5.1 Vehicular Mobility Models

The simulation of vehicular networks in a real test-bed environment is often challenging due to the complexity, cost and safety concerns associated with the implementation of such test-bed environments. As a result, researchers have resorted

to computer-based simulations with a broad array of traffic mobility models categorized based on the level of detail, operation and/or representation of the process. Traffic modelling approaches that consider the level of detail and operation are grouped into [104]:

- *microscopic models*, which consider the time-space behaviour of vehicles (i.e., position, trajectory, distance, time) under the influence of other vehicles in their proximity.
- *macroscopic models*, which describe vehicle behaviours by considering aggregated vehicle dynamics (i.e, density, flow intensity) and;
- *mesoscopic models*, which analyse vehicle elements in small groups of vehicle dynamics.

Various authors [105], [106] have proposed that, for accurate vehicular network analysis, the mobility model employed must be able to depict realistic microscopic and macroscopic dynamic vehicular movement patterns. Simplistic models such as the Random Way Point (RWP), Random Walk Model (RWM) and, the Gauss Markov Models (GMM) are unable to give a correct representation for the realistic vehicular movement. As such, for any vehicular simulation model to depict realistic vehicular movement, it must incorporate one or more of the following [104]:

- **An accurate and realistic topological map:** map topology should have multiple lanes and intersections as well as varying speed limits for each lane
- **Obstacles:** obstacles to vehicle motion such as neighbouring cars and pedestrians as well as wireless communication impediments should be incorporated in a realistic mobility simulator.
- **Attraction and repulsion points:** vehicles do not move randomly. A vehicle should have a start point and an endpoint corresponding to journey origin-destination.
- **Vehicle characteristics:** various vehicle categories found on a realistic road network are to be accounted for with their corresponding speed limits, acceleration, and deceleration.
- **Path Motion:** vehicles do not just move randomly when travelling from an origin to destination. Their movement pattern is dictated by factors such as the personal habit of the driver, traffic congestion, the shortest distance to destination, time of day, and speed limits. The path motion is therefore, described as a set of nodes and edges traversed by the vehicle from the beginning of the journey to the end.

From the foregoing, the classification of vehicular mobility models is now further refined by categories such as those discussed in [104] which includes models based on vehicular traces [107], [108], models based on vehicular network surveys [109], synthetic or mathematical-based models [110] and, traffic simulator models [111], [112].

Synthetic models are otherwise referred to as mathematical-based models i.e., random way point (RWP) model. A significant limitation of the synthetic models is the difficulty in modelling detailed human behaviour [104]. For trace-based models, mobility patterns are extracted from publicly available real-world vehicular movement such as bus or taxi traces obtained via GPS or Wi-Fi. The quality of such traces is often impacted by spatial and temporal gaps due to long periods not observed which could affect the reliability of the results. For survey-based models, extensive statistical data from vehicle driving patterns are obtained and integrated into a generic model. The random or deterministic behaviour of the model is then observed. However, obtaining large-scale surveys and trace data for vehicular network simulation is usually non-trivial with only a handful of publicly available and location-dependent trace datasets and surveys available [113], [114]. Due to these challenges, the traffic demand used in this thesis is generated using a traffic mobility simulator whose advantages are discussed next.

2.5.2 Traffic Mobility Simulators

Traffic mobility simulators are based on refined synthetic models which have been validated using real vehicular traces or surveys and can model highly detailed microscopic interactions between vehicles. Examples of traffic mobility simulators include SUMO [115], VISSIM [116] and, MOVE [117]. A detailed discussion of the current state-of-the-art of the various traffic simulators available to the vehicular network community is not presented in this thesis. However, we refer interested readers to [104] and [109] for a comprehensive survey and analysis of such simulators. We now briefly introduce the traffic simulator used in this thesis: Simulation of Urban Mobility (SUMO).

Simulation of Urban Mobility (SUMO)

SUMO is an open-source, time-discrete, microscopic vehicular mobility simulator, developed by the Institute of Transportation Systems at the German Aerospace Centre (DLR) [115]. SUMO is implemented in C++ and has portable libraries offering microscopic simulation, online interaction, and the simulation of multi-modal traffic designed to handle large and complex road networks. It is highly portable across Windows and Linux platforms and is inter-operable with a number of external applications. It is also integrated with a graphical user interface (GUI) that can

be used to visualize the behaviour of vehicle mobility and allows for the representation of both synthetic and realistic road networks. SUMO has been widely adopted by the V2X community due to it being open-source with the ability to provide realistic vehicular traces and can interact with network simulators for both physical and MAC layer evaluations

Using SUMO, two inputs are required for a vehicular network simulation:

- **the network topology:** where either synthetic maps are generated by the user or vector maps of the AoI are downloaded from open repositories such as Open Street Map (OSM) [118] and;
- **the traffic demand pattern:** which is generated as a collection of edges, nodes and vehicle definitions. OSM is a collaborative, crowd-sourced mapping of the world's geographic database, with data contributed from a variety of sources including human surveys, GPS, and aerial photography.

With over two million registered users, an active user community, and the geographic data set available in an easily readable Extensible Markup Language (XML) output data format and, more recently, the Protocol Buffer Binary Format (PBF), it has become a much-preferred geographic database system in the research community, as opposed to proprietary data sources like Google Mapmaker, TomTom, and Waze. The SUMO edges represent roads, streets, and pedestrian pathways with capabilities for multiple lanes including position and speed limits while nodes represent junctions. Each vehicle in SUMO can be modelled explicitly and is defined by an identifier (i.e., vehicle name) with the vehicle departure time, position and velocity obtained at every time instant.

In recent years, various research work using SUMO, has been conducted to create traffic mobility scenarios for various purposes and applications. The TAPAS Cologne project [119] was a project that utilized SUMO to generate traffic mobility for a period of 24 hours in the city of Cologne. The generated traffic mobility covered a region of approximately 400 km^2 . Using an origin-destination (O/D) matrix obtained by exploiting travel patterns of local residents, the authors were able to generate a data set of the traffic demand comprising over 1.2 million individual vehicle trips. However, this scenario was highly complex and required a high computation time due to the large network size.

In the Bologna Ringway project [114], the utilization of SUMO for the representation of realistic vehicular traffic was presented. Using data from navigation services for validation, the authors investigated the road traffic mobility for approximately 22, 000 vehicles covering an area of 25 km^2 . More recently, in [112], the authors utilized SUMO for the generation of a multi-modal scenario with traffic mobility

based on user activity chains. This was used to support various travel modes of walking, public transportation, and user-defined vehicles that represented daily generic routines.

In this thesis, we utilize SUMO for the generation of an activity-based traffic demand for the rural geographical AoI. Realistic mobility traces representative of the mobility patterns of UEs in the AoI is obtained and integrated with MATLAB for evaluating the trace data. This is described in Section 3.3.

2.6 Vehicular Network Services and Applications

Future 5G vehicular network services and applications are expected to provide a host of new services, applications, and use-cases ranging from multimedia infotainment (4K videos, virtual and augmented reality (VR/AR) gaming, etc.) to connected and automated vehicles, smart traffic and parking management, remote vehicle diagnosis, and windshield advertising, among others. Various authors have investigated terrestrial communications (via RSUs) [120], [121] and aerial communications via LAPs [30] with a direct communication link over the sub-6 GHz frequency spectrum. However, operation over this band typically has low data rate requirements and is prone to interference with the existing cellular infrastructure [122]. Moreover, most of the research in this domain have been conducted in the urban domain with, to the best of our knowledge, little or no research work conducted on rural roads. For instance, in [100] the authors conduct an investigation on the integration of HAPs as a super macro base station in urban metropolitan areas for next generation 5G use-cases and applications. Similarly, in [123], the authors investigate the provision of 5G services via a HAP in an urban area with specific focus on the interference characterization and analysis of an integrated HAP and terrestrial system. Along the same lines, [68] also draw on an extensive range of previous research into HAP-assisted communication in urban roads. While much of the available literature has been focused on the urban connectivity for 5G use-case and applications in urban and densely populated areas, rural road have been largely neglected even though a report in [124] suggest rural residents travel approximately 22% more than their urban residents. With the connected and autonomous vehicles being at the forefront of the 5G connectivity, we take a different approach in this thesis and investigate a performance analysis for the provision of 5G paradigms on rural roads via a HAP. Furthermore, we also motivate the provision of these services on the mmWave band which are closely aligned to the 5G seamless and reliable delivery of enhanced mobile broadband (eMBB), ultra-reliable, low-latency communications (URLLC) and Massive machine type communication (mMTC) for

reliable and seamless connectivity and delivery of 5G vehicular application and use-cases.

2.7 Vehicular Network Clustering

For the facilitation of various use-cases and applications, vehicles are expected to be able to communicate with other vehicles via V2V and the infrastructure via V2I communications. However, due to the unique vehicular network characterized by a highly dynamic network topology, a variable network density and a heterogeneity of vehicular network applications, wireless communication to vehicles within a geographical area in a flat network architecture can cause network scalability challenges and frequent link disconnections during data transmissions. This can lead to unreliable and frequent link disconnections for V2X message delivery and this impact the high throughput requirement of vehicular network applications and services as a significant amount of the bandwidth will be wasted [125] due to the increased communication overhead incurred. An effective way to tackle this challenge and support a reliable and stable network connection can be achieved via vehicular network clustering. Clustering is a category of unsupervised learning which groups nodes in a network into several distinct entities based on certain pre-defined criteria. Clustering helps to simplify network functions such as information routing and bandwidth allocation to the members of the network.

In a vehicular network, each cluster has a Cluster Head (CH), Cluster Members (CMs) and Cluster Gateways (CGs), [126]. The cluster head serves as the coordinator within the cluster by managing intra and inter-cluster communications and data forwarding. A CG can communicate with its own cluster and CHs of other clusters while CMs are ordinary nodes within a cluster that are not a CH. It is important that the clustering algorithm improves the stability of the network structure while simplifying routing. A number of clustering algorithms have been proposed in the literature [127], [128] for establishing stable clusters in vehicular networks with parameters such as vehicle position, speed, direction, and link quality used as metrics for evaluating the performance of the clustering algorithm. In [129], the authors considered a highway scenario where the first vehicle is selected as a CH with all other vehicles within a predetermined distance to the CH grouped as cluster members. Affinity propagation [130] is a clustering algorithm that select CHs based on a UEs suitability (responsibility) or desire (availability). The authors in [131] proposed a position-based clustering algorithm based on the geographic position of the UEs. They used a cross-layer algorithm that depends on a geographical data collection mechanism based on road segmentation. However, the performance is highly reliant on the availability of infrastructure.

Other clustering algorithms consider weighting coefficients w for clustering solutions by standardizing clustering metrics and multiplying each standardized value by their assigned weight. Weight coefficients are assigned based on which clustering metric has a higher importance for stable cluster formation such that $\sum_{k=1}^N w_k = 1$, where N is the total number of vehicles. Vehicles are selected as CHs if they have the least average distance to CMs, the closest speed to the average cluster speed, or the highest number of neighbouring UEs. This was demonstrated in [132] where road identifiers and node direction were used to achieve stable clusters.

Intelligence bio-inspired clustering techniques have also been proposed in [133] and [134]. A multi-agent-based intelligent clustering approach was proposed in [135] where single or multi-agents, acting as autonomous systems that could sense their environment (system or network) and acted based on knowledge gained from the environment in order to achieve their goals. They utilized a blackboard architecture for inter-agent communication with the network consisting of cluster manager agents (static agents) and cluster information collection/dissemination agents (mobile agents). This architecture was based on a distributed artificial intelligence model with the agents iteratively updating the knowledge base (which consists of information about the agent and other neighbouring nodes) until an optimal solution is achieved. In this work, the cluster manager agents were deployed along the road junctions and CHs selected based on node mobility and density. The agents were able to dynamically learn the traffic patterns from the direction of traffic flow and node mobility and perform clustering based on the information. A reward or penalty was associated with each agent action and the value of the learning parameter incremented or decremented based on the corresponding agent action until an optimal solution was attained. For our clustering approach presented in Section 3.4, we propose a k-means++ and ant-colony clustering approach for the network. The k-means++ algorithm was chosen for its relative simplicity, scalability to large networks, and fast convergence. However, it has some drawbacks, such as a limited ability to adapt to dynamic traffic conditions and a sensitivity to outlier UEs. As a result, and in order to improve the clustering solution even further, we investigate an intelligent-based clustering approach using ant colony clustering (ACC). Our ACC approach optimizes the UE mobility metric and UE node degree and determines an appropriate number of clusters for the network thereby improving cluster stability.

2.8 Conclusion

In this chapter, we have presented background information relevant to the work conducted in this thesis. Current state-of-the-art research studies in the various

domains have been highlighted. In summary, important concepts of the mmWave A2G propagation channel, as well as the key technical challenges, were presented to provide a better understanding of the propagation conditions. The choice of propagation model employed is influenced primarily by the assumption that the HAP is predominantly LoS. We thereafter introduced the antenna arrays and highlighted the advantages associated with utilizing a large number of antenna elements per HAP antenna array. Related work on the antenna array beamforming, beam optimization and various windowing weights required for the optimization of the HAP beam have also been introduced. In particular, we presented related work on array windowing weights to achieve beam optimization and highlighted the benefits of the Hann windowing function, one of which is a good trade-off advantage in terms of SLL attenuation and mainlobe beamwidth. We subsequently presented key related work in the HAP domain. In this vein, we provide an overview on the state-of-the-art from various commercial and academic initiatives that are advancing the exploitation of HAPs for 5G applications and use cases. Furthermore, we also present a summary of related work on traffic mobility models and clustering models for the vehicular network. For the traffic mobility, we consider traffic demand generation via microscopic trace files which has the advantage of depicting the behaviour of individual vehicles and their interaction with the road network achieved via SUMO. The choice of SUMO for the traffic demand generation is motivated by its ability to model detailed and realistic microscopic vehicular movements, scalability and interoperability with external applications such as MATLAB. From the background literature conducted in this chapter, and to the best of our knowledge, none of the existing works have considered exploiting a HAP system operating at mmWave wave frequency, complemented by antenna arrays with a large number of antenna elements to provide service to rural vehicular UEs.

Chapter 3

The Vehicular Traffic Demand and Clustering Model

3.1 Introduction

As highlighted in Section 1.1, the explosive growth in the demand for IoV applications has prompted the need for exploring innovative architectures and enabling technologies to cater for these growing requirements. This is because the current existing architectures and technologies have inherent challenges particularly when remote unserved or under-served rural roads are considered. In this context, we consider a HAP system where vehicle UEs will be served via a HAP equipped with a large antenna array providing content to multiple grouped UEs simultaneously via HAP spot-beams with full frequency reuse. Within this framework, an important consideration is related to the accurate representation of the movement pattern of vehicles, otherwise called the mobility model, and how vehicle UEs are grouped, otherwise referred to as clustering for an efficient network management. In this vein, we therefore present a traffic mobility demand and clustering model for the network.

Due to the prohibitive cost and implementation complexity of real-world deployments, most vehicular network mobility models rely on computer simulations for performance evaluation. Legacy mobility models such as the Random Way-point Mobility, Gauss-Markov model, and variants [109] are unable to adequately capture the characteristics of vehicular movements whose mobility patterns have a spatial and temporal dependence on the road topology, the UE velocity and behavioural human driving patterns. The limitations of these models have attracted the interest of the research community to develop mobility models that can adequately capture and mimic realistic vehicle mobility. In this regard, various studies with varying degrees of complexity have been presented in the literature [136], [112].

Motivated by these works and understanding the need for a realistic vehicular mobility model tailored to our scenario, we present in this chapter, a framework that reflects realistic vehicular movement for a rural area of interest. In this case, realism refers to the model's ability to reproduce rural traffic phenomena as closely as possible to what is obtainable in the real world. Thereafter, and in a bid to plan for the coverage of the beam footprint, we formulate the grouping of vehicle UEs as a clustering problem with a partition of all the vehicle UEs in the network such that UEs in a cluster are served under a beam. The beam centre will correspond to a position where the HAP antenna gain is maximum.

Therefore, in this chapter, we will present the approaches for:

1. generating realistic vehicular traffic mobility demand using a microscopic traffic mobility simulation suite - Simulation of Urban Mobility (SUMO) software.
2. investigating a clustering solution using a k-means++ and an ant colony clustering (ACC) approach.

Vehicular mobility traces of the traffic demand for the area of interest is obtained from (1), and using the trace data, vehicle UEs are grouped into clusters in (2). Thereafter, we investigate the performance of the clustering solution using cluster stability (in terms of a Silhouette Coefficient for the k-means++ algorithm and the average duration of the cluster head vehicle and cluster member vehicles for the ACC approach, respectively) as a measure of performance.

We have chosen SUMO [137] and MATLAB [138] as our simulation tools. SUMO represents a viable choice of traffic simulator because it is:

- open source with an active and engaged user community.
- a widely adopted and validated traffic simulator software for microscopic vehicular traffic mobility modelling in the vehicular research community.

The Krauss' car-following model [139] defines the movement of vehicles in SUMO, enabling the generation of mobility traces that can be loaded into a standard network simulator such as NS-2 [140], OMNeT++ [141] or MATLAB. MATLAB is adopted for trace analysis due to its flexibility and ease of use and a huge library of tested pre-defined functions, which makes data visualisation, as well as matrix and vector manipulations easier.

3.2 Contribution and Organisation

This chapter considers the generation of a realistic traffic demand and a clustering solution for the HAP-assisted vehicular network. In this vein and for the generation of mobility traces, we utilise an activity-based traffic demand using SUMO. For the

clustering problem and as a first attempt, we investigate a k-means++ clustering approach using UE position information and velocity differences to group vehicle UEs into simultaneously served clusters. Thereafter, we extend the clustering solution by investigating a swarm-based clustering approach using ant-agents with an ant colony clustering approach. The significant contributions in this chapter are summarised below:

- using SUMO’s traffic demand generation tool, we generate a representative and realistic traffic demand for a rural district of North Yorkshire, UK - Kirkbymoorside and Helmsley. This incorporates real-world topographical maps and publicly available demographic data to generate vehicular trace data. This is important so that unrealistic traffic flows do not bias the simulation results for the wireless propagation model which may impact the performance of the overall system.
- we investigate a clustering scheme for vehicle UEs based on a Centroidal Voronoi Tessellation (CVT) k-means++ clustering, which leverages the UE position information and mobility difference to determine the beam centre and the cluster head UEs. We examine the performance of the proposed clustering scheme in terms of a Silhouette Coefficient (SC) metric. Thereafter, we extend the clustering analysis and investigate a clustering scheme based on a multi-objective ant colony clustering approach. We compare the performance of the proposed clustering schemes in terms of cluster stability to existing clustering approaches in the literature. Results obtained demonstrate the effectiveness of the ACC scheme in maintaining a stable cluster.

The organisation of this chapter is as follows: A description of the vehicular traffic demand generation using the SUMO simulation suite is presented in Section 3.3. In Section 3.4, we present the proposed vehicular clustering model. Finally, simulation results and concluding remarks are presented in Section 3.5 and Section 3.6 respectively.

3.3 Traffic Demand Generation

Over the past few years, the vehicular network research community has investigated the generation of mobility models for vehicular networks using synthetic models [110], trace-based models [108], traffic survey-based models [142] and traffic simulator based models [111]. Specifically, in evaluating services for ITS using SUMO, several works based on realistic vehicular mobility have been proposed. For instance, in [143], a realistic multi-modal traffic for the Principality of Monaco termed the Monaco SUMO Traffic (MoST) was presented. In that scenario, the authors integrated vulnerable users (cyclists and pedestrians) into the evaluation

of advanced parking management with consideration for realistic communication models. In [136], the authors presented Luxembourg SUMO Traffic (LuST), a realistic vehicular traffic scenario for the city of Luxembourg over a 24 hour period using SUMO. Their model was verified for consistency and realism by comparing the rush hour traffic (i.e., 8:00 am traffic) generated in their scenario to traffic data provided by Google Maps.

In SUMO, a straightforward approach for traffic demand generation is implemented via a SUMO tool *randomTrips* with source and destination edges chosen randomly and trips generated subsequently. This approach was presented in [144] where the authors evaluated a context-aware and traffic-adaptive scheme to maximise the location privacy of vehicular networks. However, with a random traffic demand, if the destination edge is unreachable by the vehicle UE, the trip is considered incomplete and usually discarded. In this case, the network is not fully connected and therefore, lacks realism. As a result, we employ the SUMO utility tool *ACTIVITYGEN* to generate a realistic traffic demand using the population distribution of the AoI to achieve a realistic traffic scenario that is representative of real-life vehicular mobility.

However, with random trip traffic generation, incomplete UE trips are discarded if the network is not fully connected, i.e. if the destination edge is unreachable, and as a result, they lack realism. As a result, we use the SUMO utility *ACTIVITYGEN* to generate realistic traffic using the AoI population distribution to achieve a realistic traffic scenario that is representative of actual vehicular traffic.

3.3.1 Study Area

Yorkshire is the largest county in the United Kingdom, encompassing over 15,000 square kilometres and a population of over 5.4 million people spread across the North, South, East and West, with North and East Yorkshire considered to be predominantly rural [145]. According to a report in [146], 85% of the county is considered to be "rural or super sparse". Typically, such areas are associated with low population densities and scattered housing, making inhabitants highly vehicle dependent. This was reported in a 2020 Department for Transport (DfT) report [124] which states over 72% of trips by rural residents was utilised using a vehicle compared with 50% in an urban area. This is also while simultaneously travelling twice as far per year than those in urban areas. Typically, urban roads as defined by the DfT are those within a settlement of 10,000 people or more with all other roads considered "rural". With such rural dependence on vehicles coupled with the sparse network connectivity, it is imperative to understand the traffic demand in such territories. Therefore, for our simulation, a rural region of North Yorkshire is selected as the area of study.

Specifically, the chosen study area comprises rural roadways in the Ryedale district of North Yorkshire, Kirkbymoorside and Helmsley, whose landscape is rural and consists of a moderately sized population with travel demand behaviour and activity pattern similar to those observed on rural roads. Kirkbymoorside has a population of about 3,413, while Helmsley has just over 3,128 inhabitants according to a 2016 mid-year population estimate [147]. We illustrate an area abstraction in Fig. A.1 of Appendix A.

3.3.2 SUMO Traffic Generation Tool

It has been established, from travel theory, that the demand for travel is derived from the demand for activities [148]. Primarily, an activity trip is characterised by a sequence of tasks that a user needs to accomplish before the end of the day, usually orderly. It is made up of primary trips, intermediary trips and secondary trips. This fundamental mobility strategy is the central concept of the SUMO *ACTIVITYGEN* tool. The literature has presented various studies and modelling approaches using *ACTIVITYGEN* for multi-modal traffic assignments [112] and [149]. However, these studies are predominantly for urban scenarios and require a detailed description of the properties of the cities. They are also cumbersome and complex to configure, especially with increased network size.

Therefore, in our study, we propose a simple and straightforward approach to the vehicular traffic demand modelling for a rural AoI using *ACTIVITYGEN*. This approach incorporates traffic assignment zones (TAZs) with the traffic demand generated based on the activities specific to each TAZ. This is similar to the well-known origin-destination (O-D) matrix [114]. To generate the traffic demand, publicly available demographic data for the AoI (Kirkbymoorside and Helmsley) is utilized. This information, along with general statistical information as presented in Table 3.1 is written to a statistics file and used to generate the UE trips. Simulation snapshot abstractions are depicted in Figs. B.1 and B.2 of Appendix B.

We outline the detailed steps for the traffic demand generation below with a high-level abstraction illustrated in Fig. 3.1.

- **Generate study area:** Using geographic coordinates, the study area radius is specified and projected to the Open Street Map (OSM) format with a map view of the network as illustrated in Fig. A.1 of Appendix A. The study spans a coverage area of approximately 30 km radius with coordinates at Lat. ($54.1045^{\circ}N, 54.3392^{\circ}N$) and Long. ($-1.1042^{\circ}E, -0.7552^{\circ}E$).
- **Extract road network:** The road network data for North Yorkshire is extracted from OSM using Geofabrik [150] and the coordinates for the bounding box passed to OSMOSIS [151]. This is necessary to process the OSM data.

TABLE 3.1: Traffic Demand Data

Parameter	Value
Total Population	6631
No of Households	500
Unemployment Rate	0.08
Car Ownership Rate	0.60
Children Age Limit	18
Retirement Age Limit	65
No of Nodes	12584
No of Edges	27778
Total length edges	4967 km
Total lane length	5076 km

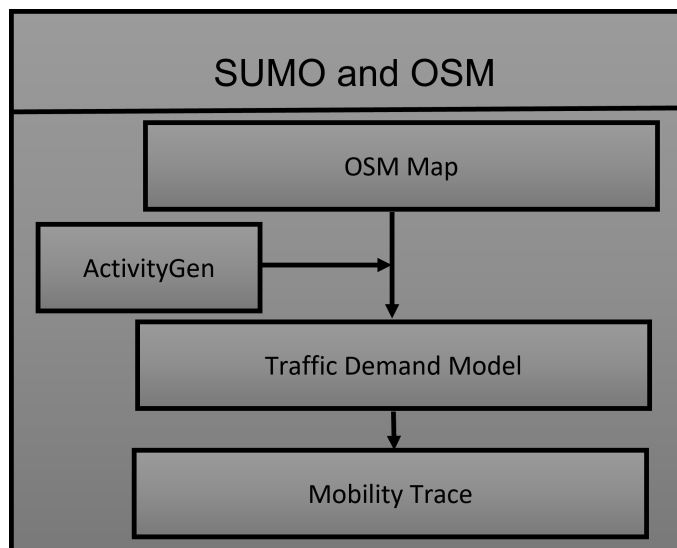


FIGURE 3.1: High-level abstraction of SUMO traffic demand model

- **Filter OSM Data:** Using OSMOSIS, the generated OSM data is processed to remove unwanted data. This is because, in addition to the OSM road data, the data also contains complex shapes, i.e., waterways, which can be very large. Therefore, filtering out such unwanted data is important to speed up processing when converted into a routable street network. The resulting output is a .OSM human-readable XML-structured file.
- **Generate SUMO Network:** Using *NETCONVERT* utility in SUMO, the data is converted into a SUMO network file with lanes specified by edges and junctions referenced by nodes. Edges and nodes are inspected and visualised for correctness using SUMO graphical user interface (SUMO-GUI).

- **Build the Statistics file:** Attributes specific to the AoI such as total inhabitants, number of households, retirement age limit, unemployment rate, e.t.c, are as specified in Table 3.1. The total population is divided by the total length of the network edge to obtain the population per meter street. Other parameters, such as free time and random traffic rates, are assumed at 0.15 and 0.20, respectively [152]. We note that *ACTIVITYGEN* cannot account for all traffic types with specific traffic types such as taxi journeys and bus trips not captured.
- **Define traffic assignment zones (TAZ) and points of interest (POI):** for the network, Gaussian distributed TAZs and POIs within each TAZ is defined. Using the *DUAROUTER* utility in *SUMO*, each UE utilises the ‘user equilibrium’ principle as originally proposed in [153] where no individual UE can reduce its travel time unilaterally by changing its travel path.
- **Generate Traffic Demand:** using input statistical data described above, the traffic demand is generated with *ACTIVITYGEN* utility which describes the sequence of vehicular activity for the population over the simulation period. The simulation was allowed to run for 3600 s (1 hour) with a warm-up period of 1400 s to ensure a steady-state distribution of UEs and achieve stability in the network. A total of 508 vehicles UEs was obtained at a steady state for 800 s as shown in Fig. 3.2. With a total lane length of approximately 5,076 km, the simulation indicates an approximate density of 10 *veh./lane/km* over the steady-state period. The trace file output contains the vehicle index id, location data and, speed over the steady-state period. The trace data is used as input to the clustering model.

Due to the movement of the vehicle UEs over time, the network exhibits a high degree of spatial and temporal variation with the maximum UE speed determined from a normally distributed speed factor in the range [0.2, 2] with mean 1 and standard deviation 0.1 [137]. The speed of each vehicle is then determined by multiplying the normally distributed speed factor by the lane speed limit. At an instantaneous time t , the position of the i^{th} UE is represented by a horizontal and vertical component $x_i(t)$ and $y_i(t)$. After time interval Δt , the horizontal and vertical distance between the i^{th} vehicle UE and $(i + 1)^{th}$ UE can be expressed as:

$$\begin{aligned}\Delta p_{x_i}(t + \Delta t) &= x_{i+1}(t + \Delta t) - x_i(t + \Delta t) \\ \Delta p_{y_i}(t + \Delta t) &= y_{i+1}(t + \Delta t) - y_i(t + \Delta t)\end{aligned}\tag{3.1}$$

from which the velocity component can be easily resolved. Since the speed is normally distributed, the velocity is also normally distributed with a cumulative distribution function (CDF) expressed as [154]:

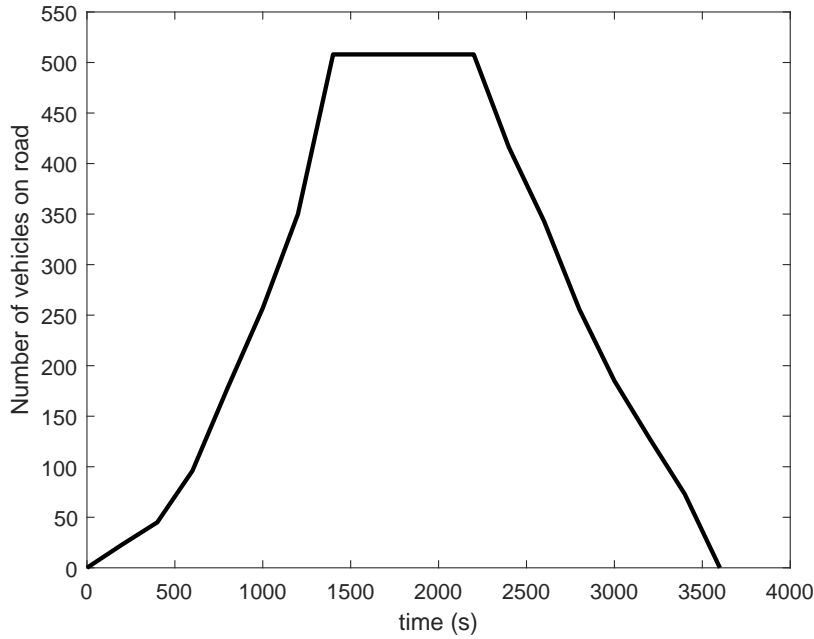


FIGURE 3.2: Simulation output of vehicle UE distribution over time

$$f(\mathbf{V} \leq \mathbf{v}) = \frac{1}{\sigma\sqrt{2\pi}} \int_0^{\mathbf{v}} e^{-\frac{(\mathbf{v}-\mu)^2}{2\sigma^2}} dv, \quad (3.2)$$

where μ and σ^2 are the mean and variance of the velocity distribution.

In Fig. 3.3a, we illustrate the CDF of the speed distribution and observe that approximately 90% of the UE speed is below a maximum speed limit of 60 mph, with only 10% of the UEs above the legal 60 mph speed limit for the rural road scenario. We also illustrate in Fig. 3.3b, a box plot of the speed distribution sampled at every 50 s interval. In the box plot, the median is represented by the central red line while the 25th and 75th percentiles are represented by the bottom and top edges of the box. The difference between these is the inter-quartile range (IQR). The dashed vertical lines represent the whisker and extend beyond both percentiles but are not considered as outliers, i.e., at 1.5IQR. The 5th and 95th percentile values are represented by a "*" and also extend above and below the whisker lines with the "+" representing the mean and the outliers marked with the "o" symbol. We observe that, for the vehicle UEs, the mean speed is below the legal speed limit for rural roads.

To check the realism of our generated traffic mobility and due to a lack of publicly available trace data of the traffic mobility pattern for the AoI, we resorted to a visual inspection to ensure that our traffic scenario mimicked what would be obtainable in real-world traffic conditions. Therefore, the generated traffic was visually examined, using SUMO-GUI for unrealistic traffic congestion and vehicle UE speeds

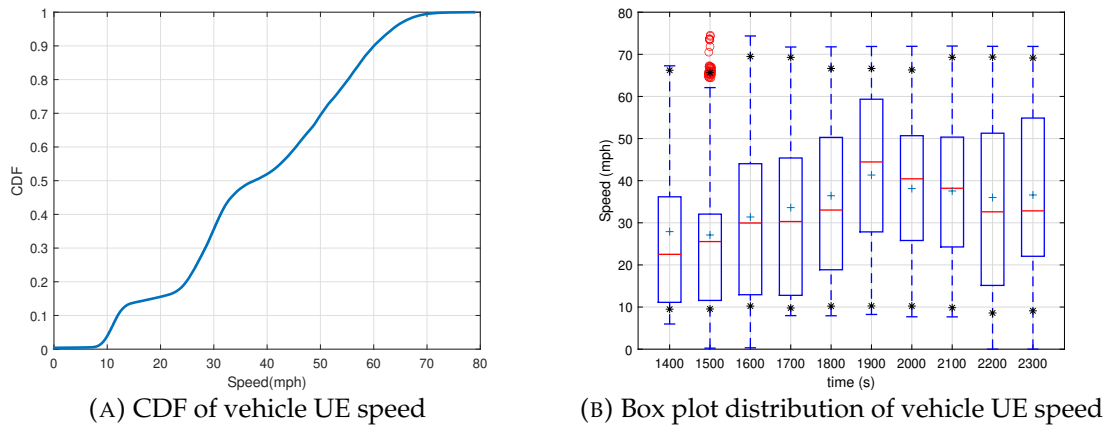


FIGURE 3.3: Speed Distribution

which can lead to traffic gridlocks and UE collisions, respectively. In our scenario, neither of these was observed. This approach is aligned with similar work by [155], [156] where visual inspection was adopted to check the realism of the generated traffic scenario.

3.4 Vehicular Clustering Model

Current wireless communication architectures exploit the concept of frequency reuse to provide coverage and enhance the capacity of ground UEs. Specifically, for a HAP system that can provide multiple spot beams over the coverage area, the concept of full-frequency reuse can be exploited to provide the high throughput requirements of vehicular network applications. By taking advantage of the available bandwidth in each beam, information can be simultaneously transmitted to UEs within a beam thereby increasing the overall UE throughput. Within this framework, an important consideration is how the UEs are grouped which we attempt to address via UE clustering. Clustering offers an efficient approach to group UEs into multiple separated, but manageable entities. This creates a network topology in which UEs are partitioned into groups based on pre-defined metrics such that UEs with similar behaviours and characteristics are grouped together. Clustering aims to improve the network stability, QoS, and data dissemination among cluster members. We note that while the overall system performance may be strongly constrained by an increased inter-beam interference caused by transmit signals from neighbouring beams radiating into corresponding beams, the implementation of effective interference mitigation measures can be employed to counter these effects. A detailed evaluation of these strategies lies beyond the scope of this thesis.

Several clustering schemes have been proposed for vehicular networks in the literature. For example, in [157], an adaptive multi-hop clustering protocol was presented which utilized a quality of path (QoP) metric. The authors utilized the trade-off between the vehicle UE mobility metric and QoS requirement to solve the routing overhead problem and the cluster head election was based on metrics of distance, speed, mobility and link quality of both one-hop and two-hop neighbours. However, this algorithm was strongly dependent on the link connectivity. Similar to [157], the authors in [158] proposed a distributed multi-hop clustering algorithm for an infrastructure-less vehicular network using a combination of UE direction, velocity and position as metrics to select stable cluster heads. The cluster head lifetime and the number of cluster head re-selection was used as the performance evaluation metric. In the results presented, they were able to show that their algorithm reduced cluster head re-selection by three times compared to the approach proposed in [159].

Optimisation approaches for vehicular network clustering have also been reported in the literature. Such clustering optimisation problems are either single-objective or multi-objective with evolutionary algorithms such as Artificial Immune System, Genetic Algorithm, Differential Evolution, and Swarm Intelligence proposed. Specifically, the authors in [160] presented a hybrid clustering algorithm based on genetic and honey bee algorithms as a solution to the clustering problem. Using a minimisation function, they proposed a multi-optimisation solution that exploited honey bees' search capability to evaluate the solution's fitness with vehicle UE degree, reliability, trust and reputation used as the clustering metric. Their results showed that the algorithm outperforms other existing schemes in the literature that implemented clustering using a zone-based architecture, among others, in terms of cluster duration, end-to-end delay and cluster re-affiliation.

In a similar vein, and inspired by the daily routine of grey wolves, the authors in [161] presented an algorithm based on grey wolf optimisation. Using the social hierarchy of the grey wolf (Alpha, Beta and Delta wolves), they modelled this mathematically and utilised the hierarchy in the exploration and exploitation operations. Their simulation results were compared to variants of the Particle Swarm Optimization (PSO) algorithm, with results showing that the scheme can significantly reduce the number of clusters and, therefore, the routing cost of the network. An exhaustive survey of vehicular network clustering algorithms, multi-hop clustering strategies, and intelligent based clustering approaches can be found in [162] and [163] and the references therein.

To adequately plan for the HAP beams, it is required that the vehicle UEs are partitioned into clusters with a cluster head UE where the HAP beams suitable to serve

each cluster can be directed. We employ vehicular traces generated from the mobility model described in Section 3.3.2 and allow a steady-state state behaviour, i.e., where the number of vehicle UEs in the coverage area remains constant over a given period as illustrated in Fig. 3.2. We assume that each UE can support a GPS device, a mmWave radio interface and a DSRC interface. Similarly, we utilise time snapshots of the network taken at regularly spaced time intervals. The time snapshot represents copies of the network at different periods with the set of network snapshots represented by $S = (S^1, S^2, \dots, S^{t+1})$ where t is the current time.

Firstly, we utilise an iterative clustering approach using a k -means++ algorithm [164] for the clustering process to group the vehicle UEs into clusters and define a Voronoi partition of the vehicular clusters from the mobility traces generated from SUMO. Subsequently, for all UEs within the clustered region, we introduce a cluster head selection index β_k to determine cluster head UEs. Furthermore, and in a bid to improve the clustering performance, we formulate the clustering as an optimisation problem and propose a solution based on a multi-objective ant colony clustering approach. This approach aims to optimize both the objective functions of vehicle mobility and node degree (i.e, number of vehicle UEs within communication range of a cluster head UE) as these parameters are considered to generate better clustering performance in a real-time environment than optimising individual parameters [165]. Our algorithm ensures that a more stable cluster head is elected therefore decreasing the frequency of cluster head re-election, which improves the stability of the clusters.

Notations: Throughout, we denote column matrices and vectors by boldfaced uppercase and lowercase letters, i.e, \mathbf{X} and \mathbf{x} respectively; x_j denotes the j^{th} column vector of the matrix \mathbf{X} . We denote the elements of the matrix \mathbf{X} by x_{ij} . Subscripts indices i and j will range from 1 to k (the number of clusters) and 1 to n (the number of vehicle UEs), respectively. \mathbb{R}^m is a set of m -dimensional real vectors.

3.4.1 Centroidal Voronoi Tessellation (CVT) k -means++ Clustering Approach

Given a set $\mathbf{U} = \{u_1, \dots, u_j, \dots, u_N\}$ of d -dimensional vehicle UE positions $u \in \mathbb{R}^d$, k -means++ clustering seeks a partition of U into K clusters, $\mathcal{C}_1, \dots, \mathcal{C}_K$ by minimizing a cost-function \mathfrak{J} , with $K \leq N$ and $\mathcal{C}_i \neq \emptyset \forall i = 1, \dots, K$; and $\mathcal{C}_1 \cup \mathcal{C}_2 \cup \mathcal{C}_K = \mathbf{U}$.

By utilizing UE position information, we define the objective function as [166]:

$$\min \mathfrak{J}(B, C) = \sum_{i=1}^K \sum_{j=1}^N w_{ij} \|u_j - c_i\|^2, \quad (3.3a)$$

$$= \sum_{i=1}^K \sum_{j=1}^N w_{ij} (u_j - c_i)^T (u_j - c_i), \quad (3.3b)$$

$$= \sum_{i=1}^K \sum_{j=1}^N \mathfrak{J}_{ij} \quad (3.3c)$$

where B is the cluster partition matrix of size $K \times N$, K is the number of clusters, N is the number of vehicle UEs and w_{ij} is given by:

$$w_{i,j} = \begin{cases} 1, & \text{if } u_j \in C_i, \\ 0, & \text{otherwise.} \end{cases}$$

Equation (3.3) is the objective function for the i^{th} UE and j^{th} cluster centroid, and $C = (c_1, \dots, c_K)$ is the matrix of cluster centers with the center of the i^{th} cluster given by:

$$c_i = \frac{1}{N_i} \sum_{j=1}^N w_{ij} u_j \quad (3.4)$$

where N_i is the number of UEs in the i^{th} cluster, $u_j \in \mathbb{R}^d$, $C \in \mathbb{R}^{K \times n}$ is a matrix of $K \times N$ cluster centers and $c_i \in \mathbb{R}^d$. w_{ij} is the cluster assignment variable for all vehicle UEs.

The algorithm requires two inputs, namely: (i) the feature vector, which describes the vehicle UEs as represented by their position vector, and (ii) the required number of clusters. Initially, a vehicle UE is randomly selected as a cluster centre and the distance vector (defined by a Euclidean distance $d_{i,j}$) of the i^{th} cluster centre to the j^{th} vehicle UE location is determined as given in Equation (3.6). All other vehicle UEs are then assigned to the nearest cluster centre UE based on the objective function by Equation (3.3) with a probability $P_{i,j}$ given by:

$$P_{i,j} = \frac{d_{i,j}^2}{\sum_{i=1}^K d_{i,j}^2}, \quad (3.5)$$

where the Euclidean distance $d_{i,j}$ between vehicle UE at a reference location $u_j \in \mathbb{R}^d$ and the center of the i^{th} cluster is expressed as:

$$d_{i,j} = \sqrt{(x_j - x_i)^2 + (y_j - y_i)^2}, \quad (3.6)$$

where x_i, y_i, x_k, y_k are the position coordinates of the UE and cluster centres respectively. The average Euclidean distance $D_{i,j}$ between vehicle UEs in the cluster is therefore given by:

$$D_{i,j} = \frac{1}{|N_i|} \sum_{i=1}^{N_i} |d_{i,j}|. \quad (3.7)$$

where N_i denotes the set of neighbouring vehicle UEs within an upper bound DSRC transmission range (i.e., 1000 m) to the reference cluster centre UE. Furthermore, given the set of clusters $\{C_1, \dots, C_K\}$, we apply a Centroidal Voronoi Tessellation (CVT) [167] where the cluster centers corresponds to the centroids of the Voronoi tessellation with each cluster grouped into a boundary of a convex set V_{u_j} (i.e regions of convex polygons) such that all vehicle UEs in a Voronoi cluster V_D are closer to the cluster center UE than to any other cluster. Mathematically, this is represented as [168]:

$$V_D(i) = \{V_{(u_i)}, u_i \in \mathbf{U}\}. \quad (3.8)$$

We show in Fig. 3.4 the CVT for the AoI where the intersection between the CVT clusters V_{u_i} and the AoI is non-empty, i.e. $V_{u_i} \cap AoI \neq \emptyset$.

Thereafter, the cluster assignment is repeatedly updated until the termination criteria are met, i.e., no changes in cluster centres and the objective function in (3.3a) cannot be minimised further. However, the cluster centre determined from above is not usually located in a vehicle position. Therefore, we utilise the nearest neighbour distance metric and designate the vehicle with the nearest distance to the cluster centre as a reference cluster centre UE. For the sake of clarity, the clustering algorithm is described in Algorithm 1.

3.4.2 The Silhouette Coefficient (SC)

The Silhouette Coefficient (SC) is a frequently applied indicator [169],[170] of clustering performance and is a widely utilized as a measure of the quality of a cluster. It gives an indication about whether UEs are clustered effectively and indicates the similarity (i.e., the average distance between the cluster head UE and all other UEs

Algorithm 1 CVT k-means++ Vehicle Clustering algorithm

- 1: Initialise the number of clusters k .
- 2: Randomly select k vehicles as the initial cluster centre vehicles.
- 3: Calculate the cost function of each vehicle UE to the initially selected centre vehicles using (3.3).
- 4: Assign each vehicle to a cluster with the least minimum distance to it.
- 5: Determine the next cluster centre with a probability proportional to $\mathfrak{J}(u_j, m_i)$.
- 6: Update cluster centroid UE.
- 7: Apply a CVT against each cluster using the cluster centre as the centre of the Voronoi polygon such that all UEs are closer to the cluster centre than any other cluster.
- 8: Iterate 3-8 until no further changes in $\mathfrak{J}(u_j, m_i)$.
- 9: Use the nearest neighbour rule and assign the closest vehicle to the cluster centre as a reference cluster head vehicle.

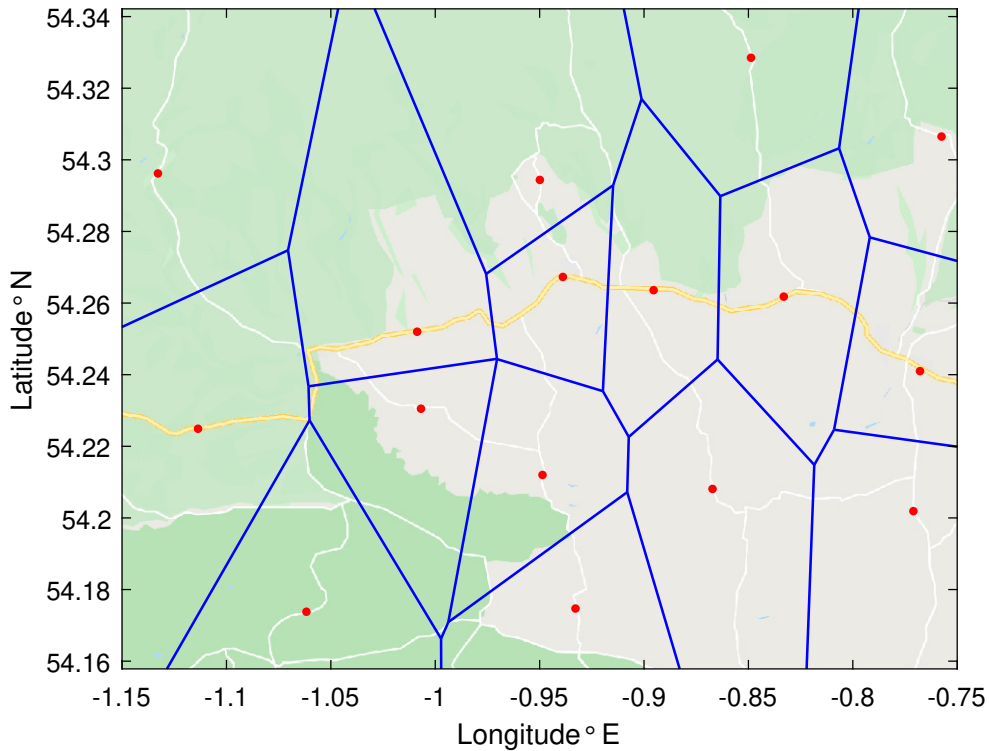


FIGURE 3.4: Centroidal Voronoi Tessellation (CVT) of the Area of Interest (AoI).

in the cluster) between members in a cluster. It also gives an indication of the cluster separation (i.e., the average distance between the cluster head UE and the UEs in the neighbouring cluster) and has values that range between -1 and 1. A SC with a value close to 1 means that the UE is closer to UEs in the cluster and far away from UEs in neighbouring clusters. This indicates a higher cluster cohesion. A SC close to -1 indicates an increasing overlap between the clusters. In other words, a

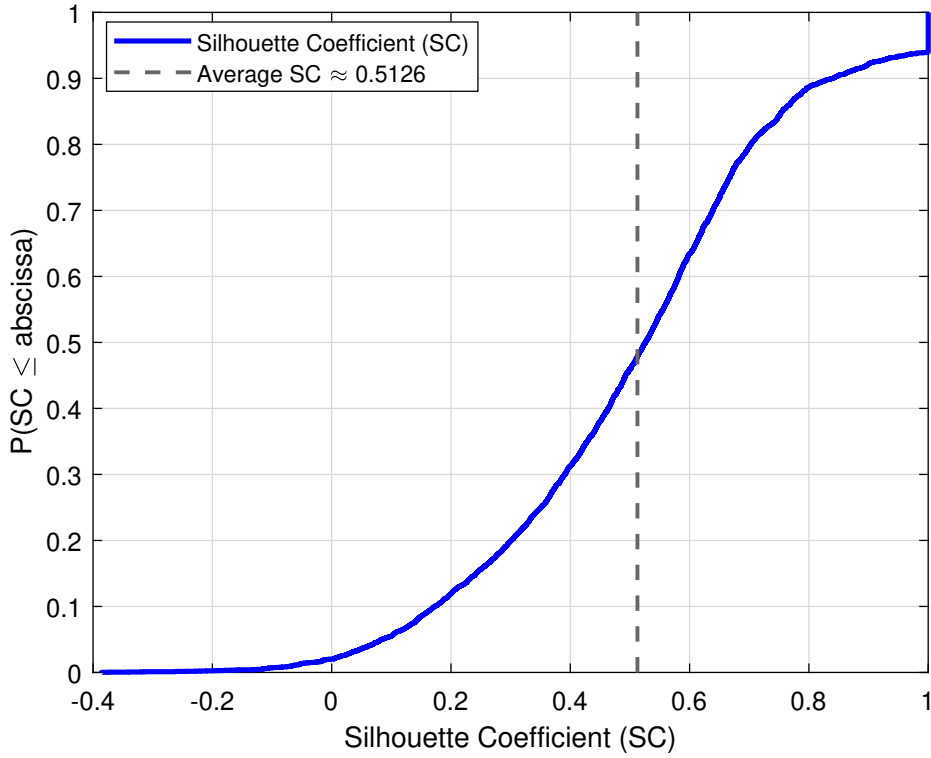


FIGURE 3.5: CDF of Silhouette Coefficient (SC).

higher SC indicates a better intra-cluster similarity and cohesion, while a lower SC is indicative of a poor match to the cluster. We utilise the SC in this work to measure the quality of cohesion among the members of the clusters. Mathematically, the SC is expressed as [171]:

$$SC = \frac{1}{n_c} \sum_{u_j \in \mathbf{U}} \frac{(b_{u_j} - a_{u_j})}{\max(a_{u_j}, b_{u_j})} \quad (3.9)$$

where n_c is the number of users in the clusters, a_{u_j} is the average intra-cluster distance and b_{u_j} is the average inter-cluster distance of the j^{th} vehicle UE location to the UEs in a different cluster. In Fig. 3.5, we illustrate a CDF of the SC for a varying number of clusters. We observe that about 0.01% of the clusters have an SC less than zero, which indicates a good performance of the clustering solution. The average SC is observed to be approximately 0.51. This indicates an acceptable level of the clustering structure and quality obtained with this algorithm. Similarly, in Fig. 3.6, we observe that as the number of clusters increases, and with a fewer number of vehicle UEs per cluster, an improvement in the SC is observed which indicates a higher cluster cohesiveness is attained with an increasing number of clusters.

Mobility Metric: Due to the high mobility associated with vehicular networks, the

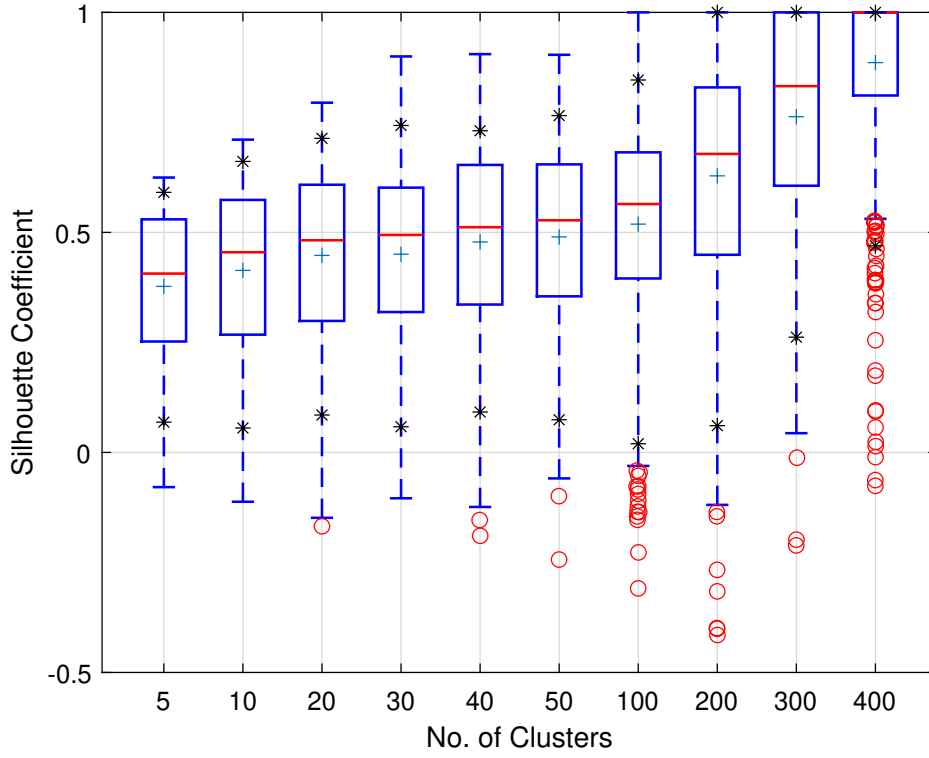


FIGURE 3.6: Box plot of Silhouette Coefficient (SC).

mobility of the vehicle UE is an important consideration for the determination of a stable cluster head vehicle. The average velocity difference between a vehicle UE at a reference location $u_j \in \mathbb{R}^d$ in the cluster and the i^{th} cluster head vehicle is given by:

$$V_{i,j} = \frac{1}{|N_i|} \sum_{i=1}^{N_i} |\mathbf{v}_j - \mathbf{v}_i|, \forall i \neq j \quad (3.10)$$

The vehicle with a lower average velocity difference in the cluster has less deviation with its neighbours and therefore can also be designated a reference cluster head vehicle. Using a cluster head selection metric β_k , we determine the overall suitability of a vehicle in the cluster to act as a cluster head. To adequately correlate the clustering metrics, we normalise $D_{i,j}$ and $V_{i,j}$ for each vehicle in the cluster. In other words, the normalised cluster head selection metric β_k is given by:

$$\beta_k = \min_{\forall k \in i,j} \left(\frac{D_{i,j}}{\max(D_{i,j})} + \frac{V_{i,j}}{\max(V_{i,j})} \right). \quad (3.11)$$

where β_k is between 0 and 2 and the UE index with the lowest value is elected as the cluster head UE. The cluster head selection procedure is described in Algorithm

2.

Algorithm 2 Cluster head Selection Algorithm**Input:** k , from Algorithm 1

```

1: repeat
2:   for each  $i \in \mathcal{C}$  do
3:     Calculate relative mobility difference of vehicles in  $\mathcal{C}$  using (3.10)
4:     Compute  $\beta_k$  from (3.11)
5:      $CH_k \leftarrow \min(\beta_k, \forall k \in i, j)$ 
6:   end for

```

Output: $CH_k \leftarrow \mathcal{C}_k$

3.4.3 Ant Colony Clustering

With a predetermined number of clusters k , the k-means++ clustering has limited flexibility in adapting to dynamic traffic and a tendency for outlier UE's, we extend the clustering solution by investigating an ant colony clustering approach for the traffic demand. In this vein, we optimizing the fitness function of each cluster while maintaining the multi-objective requirements for cluster formation, the cluster stability can be improved.

Ant colony optimisation (ACO) is a meta-heuristic population-based optimisation approach proposed by Dorigo [172]. In the original ant colony system algorithm, the authors of [172] applied it to solve a diverse set of optimisation problems such as the travelling salesman, multiple knapsack problem, graph colouring, e.t.c. Subsequently, ACO has been effectively applied to find globally optimal and feasible solutions to various static and dynamic combinatorial optimisation problems.

ACO is inspired by the foraging behaviour of biological ants in finding the shortest path between their nest and food source. By depositing a certain amount of pheromones in their local search space, each ant builds up a solution to the foraging problem, and as other ants explore the search space, a pheromone trail is established in the path with the shortest path to the food source since more ants will traverse this path, i.e. a shorter path will have a higher pheromone deposit. Therefore, as the ant's exchange information, solutions are built through a cooperative effort and pheromones are updated based on the quality of the solution and pheromone evaporation rate.

The use of ant agents to solve clustering problems is not new as variants of ACO have found applications in object clustering [173], data clustering [174], and in wireless sensor network [175]. In the VANET literature, ACO has also been utilised for routing [176] and IoV clustering [177]. Specifically, the former proposed relay-bus

selection scheme using ACO-based clustering to aid packet forwarding. They investigated a network consisting of a sparse and dense street scenario containing buses and non-buses with vehicle trace data trajectory obtained from SUMO and MOVE. ACO was then used to determine the relay-bus cluster head vehicle using maximum link reliability as a clustering metric. The network performance was investigated using metrics of packet delivery ratio, average end-to-end delay and results compared to state-of-the-art cluster-based routing schemes in the literature. Their results show that the proposed ACO clustering algorithm improves the network performance and accelerates the cluster head selection process. The authors in the latter presented an ant colony IoV clustering scheme for routing optimisation. Their proposed architecture modelled the routes as a mesh topology and allocated transmission ranges determined based on the local traffic density. Using a roulette wheel selection, they determined the initial cluster centres and using a weighted multi-objective function, ACO was used to build a clustering solution.

Similar to our work is the approach in [177] and [178], where the authors propose an ACO clustering approach for vehicular networks and IoV. However, we note that our approach is different from both approaches as our investigation is based on a subset of realistic vehicular trace mobility data obtained from the traffic demand described in Sec. 3.3 as compared to a random distribution of vehicles in the network. Moreover, our proposed scheme extends these works by maximising a multi-objective function of nodal degree and UE mobility metric. Based on the study of existing clustering algorithms and their limitations, [177], [178], our proposed architecture (1) utilises realistic trace data obtained from a realistic traffic demand rather than a synthetic road network with a random UE distribution and therefore significantly reduces the clustering overhead, and (2) facilitates an optimisation cluster head UE with the solution driven by the input trace data, the ant agent exploitation and biased exploration, pheromone deposit and evaporation and a heuristic function based on the mobility characteristics of UEs. We conduct a performance comparison of the proposed algorithm with benchmark clustering algorithms in the literature.

Multi-Objective optimisation

We begin this section by introducing fundamental preliminaries on multi-objective optimisation (MOO). MOOs are mainly concerned with minimising or maximising more than a single objective function. For an n dimensional decision variable vector (i.e., clustering metrics such as Euclidean distance, average relative velocity, interference, e.t.c) $\mathbf{x} = \{x_1, \dots, x_n\}$ in a given solution space \mathbf{X} , MOO finds a vector \mathbf{x} which minimizes or maximizes a given set of objective functions. Mathematically, this is expressed as:

$$\begin{aligned}
& \min \{f_1(\mathbf{x}), \dots, f_n(\mathbf{x})\} \\
& \max \{f_1(\mathbf{x}), \dots, f_n(\mathbf{x})\} \\
& \text{s.t. } g_i(x) = b_i(x), i = 1, 2, \dots, m
\end{aligned} \tag{3.12}$$

where the vector of decision variables is represented by $\mathbf{x} \in \mathbf{X}$, and f_j for $j=1,2,\dots,n$ represents the j^{th} objective function with the solution space \mathbf{X} restricted by constraints $g_i(x)$ and bounds $b_i(x)$ on the constraint. Therefore, if an objective function is to be minimized, a decision vector $x^* \in \mathbf{X}$ is said to be *Pareto optimal* if for all $i = 1, 2, \dots, n$ and for some $j \in \{1, 2, \dots, n\}$, $f_i(x^*) \leq f_i(x)$ and $f_j(x) \leq f_j(x)$ respectively. In other words, the decision vector is not dominated by any other solution in \mathbf{X} . In \mathbf{X} , the set of all feasible non-dominated solution is called the *Pareto optimal* set and the values of the objective function in the solution space is referred to as the *Pareto front*. Therefore for a given set of MOO problems, more than one Pareto optimal solution can be obtained.

MOO problems have been solved in the literature using fitness functions of normalised weighted sum method or Pareto ranking methods [179] amongst others. Our discussion focuses on the classical normalised weighted sum method where weights in the interval $[0, 1]$ are assigned to the normalised objective function $f'_n(x)$. This method enables us to convert the problem into a single objective function with the weights assigned based on the relative importance of each objective function to the solution. This is represented as:

$$\begin{aligned}
\min F(x) &= w_1 f'_1(x) + w_2 f'_2(x) + \dots, w_n f'_n(x) \\
&= \sum_{j=1}^n w_j f'_j(x) \\
\text{s.t. } & \sum_{i=1}^n w_i = 1, w_i \geq 0 \quad \forall i, j > 0
\end{aligned} \tag{3.13}$$

Original Ant Colony Clustering System (ACCS)

In this section, we briefly describe the details of ant colony clustering. In the next section, we first introduce the original ant colony optimisation algorithm and then address the clustering problem as an optimisation problem.

- *Graph Construction and Initialisation*: The network search space is represented by a graph $G(X, Y)$, where X is the set representing the vertices of the network, and Y is the set of edges that are the connections between vertices. Artificial ant agents start with an empty solution in the first iteration, with

the pheromone matrix initialised to a very small value. The total pheromone value is given by:

$$\sum_{i,j \in N_a} \tau_{i,j} = 1, \quad (3.14)$$

where N_a is the number of ant agents in a cluster.

- *Tour Construction*: The state transition rule is used by an ant agent to move from position r to a position s based on a probability distribution given by:

$$s = \begin{cases} \arg \max_{u \in J_{i,j}(r)} \{ \tau_j(r, u) \cdot [\eta(r, u)]^\beta \} & \text{if } q \leq q_0 \text{ (exploitation)} \\ S, & \text{otherwise} \end{cases} \quad (3.15)$$

where S is selected according to a probability distribution given by [172]:

$$P(r, s) = \begin{cases} \frac{\tau_j(r, s) [\eta(r, s)]^\beta}{\sum_{u \in J_k(r)} \tau_j(r, u) \cdot [\eta(r, u)]^\beta}, & \text{if } s \in J_{k \in i, j} \\ 0, & \text{otherwise} \end{cases} \quad (3.16)$$

with r and s representing the position vectors of ant, (r, s) denotes the edges, $\tau(r, s)$ is the pheromone level between the position vectors r and s , $\eta(r, s)$ denotes a heuristic parameter. The ant moves from one vertex to another, deposits pheromone and constructs a solution considering the pheromone trails and heuristic information over an edge. Each ant agent has a memory list which ensures a vertex is not added more than once in the ant tour. Also, $J_k(r)$ is the set of edges yet to be traversed by the k^{th} ant, and β is the pheromone control value associated with an edge. The ant exploitation and biased exploration are determined by the parameters q and q_0 , where q is a random variable in the interval $[0,1]$ and q_0 ($0 \leq q_0 \leq 1$). If $q > q_0$, then Equ. (3.16) is used to determine the probability of an edge.

- *Local and Global Pheromone Update*: For each traversal between r and s , the pheromone is updated locally on an edge by ζ :

$$\tau_j(r, s) = (1 - \zeta) \cdot \tau_j(r, s) + \zeta \cdot \tau(r, s). \quad (3.17)$$

Once the tours have been built by all ants, global pheromone is updated on all the edges with:

$$\tau_j(r, s) = (1 - \rho) \cdot \tau_j(r, s) + \rho \cdot \Delta \tau_j(r, s) \quad (3.18)$$

$$\Delta \tau_j(r, s) = \begin{cases} (L_j)^{-1} & \text{if } \tau_j(r, s) \leq \text{globalbest} \\ 0, & \text{otherwise} \end{cases} \quad (3.19)$$

where n is the number of ants, $\tau_j(r, s)$ is the pheromone level for ants in the j^{th} group given as $\tau_j(r, s) = \tau_0 = (nl)^{-1}$, l is the length of the nearest neighbour tour, n is the number of vehicles, $0 < \rho < 1$ is a pheromone decay parameter. L_j therefore consists of several ants with cost function determined by the pheromone and heuristic values of the edges.

ACS Problem Formulation

Having discussed the ACS, we subsequently describe the proposed ant colony clustering (ACC) to solve the clustering problem. This is formulated as an optimisation problem. Given N vehicle UEs, our approach aims to find a clustering solution such that the objective function as represented by (3.3) is minimised. Similar to section 3.4.1, the cluster assignment variable is subject to:

$$w_{i,j} = \begin{cases} 1, & \text{if a vehicle UE } i \text{ is assigned to a cluster } j \\ 0, & \text{otherwise} \end{cases} \quad (3.20)$$

The solution space is modelled as a graph of cluster matrix where columns denote the cluster, and the rows represent the vehicle UEs. Let \mathbf{PM}^k denote the pheromone matrix and \mathbf{ML}^k represent the ant memory list of the ant tour. Ant agents move from one vehicle UE to another in the search space and construct solutions by depositing pheromones. At each step, the ant adds a UE to its partial solution by considering the pheromone and heuristic information. The following is a step-by-step description of the algorithm:

- *step 1*: Initialize the number of ant agents K and pheromone matrix τ_0 for the UEs in the network. The pheromone τ_0 is given by:

$$\tau_0 = \frac{1}{N} \quad (3.21)$$

where N is the total number of UEs.

- *step 2*: Each ant agent randomly selects a vehicle UE not present in its memory list from the search space and adds it to its cluster matrix. Each UE is added to the cluster matrix taking into consideration the pheromone intensity and heuristic values. This is achieved via the exploitation and exploration strategies of the ant agents. Exploitation allows the ant to move to a vehicle UE with a maximum product of pheromone intensity and heuristic value as given by Equation (3.15). This means that the ant exploits its learned knowledge with a probability q_0 . The exploration strategy allows the ant to choose a vehicle UE to add to its cluster matrix with a probability according to Equation (3.16). The heuristic value of a vehicle UE i in a cluster j for an ant k is given by $\eta_{i,j}^k = \frac{1}{d_{i,j}^k}$.
- *step 3*: For each ant, update the ant memory list \mathbf{ML}^k and the pheromone matrix \mathbf{PM}^k .
- *step 4*: Determine if the memory list of each ant agent is full. If yes, go to *step 5*; otherwise, go to *step 2*.
- *step 5*: Calculate the objective function of each ant agent as given by (3.22). Subsequently, the ant solutions are ranked in ascending order of F and the best solution is the iteration-best solution.
- *step 6*: Update the local pheromone using (3.17) and reduce it by a decay factor ζ to reduce the desirability of the edge by other ants thereby allowing the exploration of edges not yet traversed.
- *step 7*: Update the pheromone matrix \mathbf{PM}^k using (3.18) and (3.19), i.e., with $\rho = 0.05$ and $\Delta\tau_{i,j} = \frac{1}{d_{i,j}^k}$.
- *step 8*: Check stopping condition. If the number of iteration has reached the maximum number of iterations, stop algorithm and output the best solution of clusters. Otherwise, go to *step 2*. The algorithm is as described in Algorithm 3.

The fitness function evaluated by each ant belonging to each cluster for the selection of cluster head UEs are the nodal degree difference and UE mobility which are defined as:

$$\max(F) = w_1\phi_1 + w_2(-\phi_2) \quad (3.22)$$

where w_1, w_2 are weighing factors assigned to ϕ_1 and ϕ_2 respectively. Both factors can be adaptively adjusted depending on the relative importance of each of the fitness functions considered. Here, we assign equal wights to each of our objectives, i.e., $w_1 = w_2 = 0.5$. The fitness parameters ϕ_1 and ϕ_2 are defined as:

Algorithm 3 Ant Clustering Algorithm**Input:** ant swarm size S , number of UEs N **Output:** $ClustH$

```

1: Initialize  $S$ , pheromone matrix  $PM^k$ ,  $ML^k$ 
2: Initialize ant agents randomly on the network
3: Calculate Euclidean distances  $d_{i,j}^k$  between UEs.
4: Initialize  $\tau_0$  as given by (3.21) on each edge.
5: while IterationCount  $\neq$  TotalIteration do
6:   for each AntAgent  $\leftarrow$  1 to  $S$  do
7:     Clustfitness(i)=fitnessfun(AntClusters)
8:     if Antfitness  $\leq$  Clustfitness then
9:       BestAnt  $\leftarrow$  AntAgent
10:      AntAgent AntAgent + 1
11:    end if
12:  end for
13: end while
14: for each AntAgent  $\leftarrow$  1 to  $S$  do
15:   Update pheromone using Eq. 3.17 and 3.18
16:   if BestAnt = LastIteration then
17:     IterationCount ++
18:   else
19:     IterationCount  $\leftarrow$  0
20:   end if
21: end for
22: for each NoClusters  $\leftarrow$  1 to  $C$  do
23:    $ClustH = GlobalBestAntTours$ 
24: end for
25: Return:  $ClustH \leftarrow S_{best}$ 

```

$$\phi_1 = 1 - \frac{v_{i,j}}{v_{max}} \quad (3.23)$$

$$\phi_2 = |d_v - \delta| \quad (3.24)$$

where ϕ_1 is the UE mobility function. The higher the value of ϕ_1 , the less the UE mobility, and therefore, a higher probability of selection as a cluster head. ϕ_2 denotes the nodal degree which is used as a measure of the UE connectivity and cluster size. We have utilized this metric to achieve appropriate cluster sizes. In other words, the clusters can neither be too small or too large to avoid an under-utilization or an over-utilization of the network resources. The d_v term denotes the number of UEs within a transmission range, i.e.,

$$d_v = \begin{cases} 1, & 0 < d_{i,j} < R \\ 0, & \text{otherwise} \end{cases}$$

and δ is the maximum number of cluster members that can be assigned to the UE. $v_{i,j} = |v_i - v_j|$, and v_{max} denotes the velocity difference and maximum UE velocity. n_v is the number of vehicles in the cluster and R is the communication radius.

3.5 Simulation Results

In this section, simulation results are presented to evaluate the performance of the proposed clustering algorithm. The total simulation time is 3600 s, and the clustering process starts at 1400 s. The performance metric of cluster stability is evaluated over a steady-state period of 800 s when all the vehicles are within the AoI. We aim to investigate the clustering performance of the algorithm in terms of cluster stability such that a stable cluster will represent all the vehicles under a HAP beam with the boresight directed at a cluster head vehicle. To justify the applicability of the proposed approach, we compare our method to (1) a dynamic transmission range clustering scheme based on a modified ant colony for IoV, otherwise called CA-COIV [177] where they investigated a clustering scheme based on the local traffic density to maintain connectivity for IoV and, (2) a moth-flame clustering algorithm termed CAMONET presented in [180]. In this algorithm, the moths are considered as search agents, and their exploration of the search space (or distance to source of light) iteratively updated until the best solution is obtained. We implement all algorithms using the parameters in Table 3.2 and perform clustering of the network at regularly spaced clustering intervals. For each of the algorithms, the simulation is performed 10 times and the result are evaluated and averaged.

TABLE 3.2: ACO Simulation Parameters

Parameter	Value
Mobility Model	SUMO <i>ACTIVITYGEN</i>
Simulation time	800 s
Evaporation rate ρ	0.05 [172]
Decay factor ζ	0.1 [172]
Weight of objective function $w_1 = w_2$	0.5
Number of simulation runs	10
Maximum iterations	100

3.5.1 Performance Metrics

Cluster stability was adopted as a metric to evaluate the performance of the proposed clustering algorithm.

Cluster Stability: The cluster stability is measured in terms of the average cluster head duration and average cluster member duration. These are defined as:

- Average Cluster Head Duration: This is defined as the average time interval between when a vehicle UE is a cluster head and when it switches state and becomes a cluster member..
- Average Cluster Member Duration: This is defined as the average time interval during which vehicles in a cluster remain as cluster members.

In Fig. 3.7, we show the result for the average duration of the cluster head vehicles as a function of the snapshot interval. A longer duration of the cluster head means a more stable cluster. We observe that the our proposed approach exhibits a higher cluster head duration with increasing snapshot interval compared to the three other approaches. It is also observed that as we vary the clustering intervals, a maximum cluster head duration for the traffic scenario is obtained at 20 s, i.e an average cluster head duration of 360 s. We utilise this clustering interval for all subsequent simulations. We note that the k-means++ algorithm exhibits the poorest performance compared to our proposed approach. A possible explanation for this result may be due to the algorithm convergence to the nearest local optimum from the initial assignment. As a result, the clusters may not be a optimal and therefore, the stability of the cluster is poor.

In Fig. 3.8, we illustrate the clustering performance in terms of the average duration of cluster members. We observe that our proposed clustering approach has a better cluster member duration for all the clustering intervals considered. For instance, we observe a lower bound difference of approximately 9% for the proposed clustering approach compared to kmeans++. This shows that the algorithm is able to form clusters that maximise the nodal degree and minimises the mobility metric between members of the cluster compared to k-means++. The proposed algorithm performs comparably better in terms of cluster stability of the cluster members taking into account both the spatial and temporal variation of vehicles on the clustering management when also compared to the CAMONET and CACOIV schemes.

Similarly, the simulation results also show that our proposed clustering approach, as well as the CAMONET and CACOIV algorithm, exhibits similar performance in terms of the average cluster head duration. We observe that our proposed clustering approach has slightly better cluster stability, especially at lower clustering intervals. Specifically, we observe approximately a 4% and 6% difference in the duration

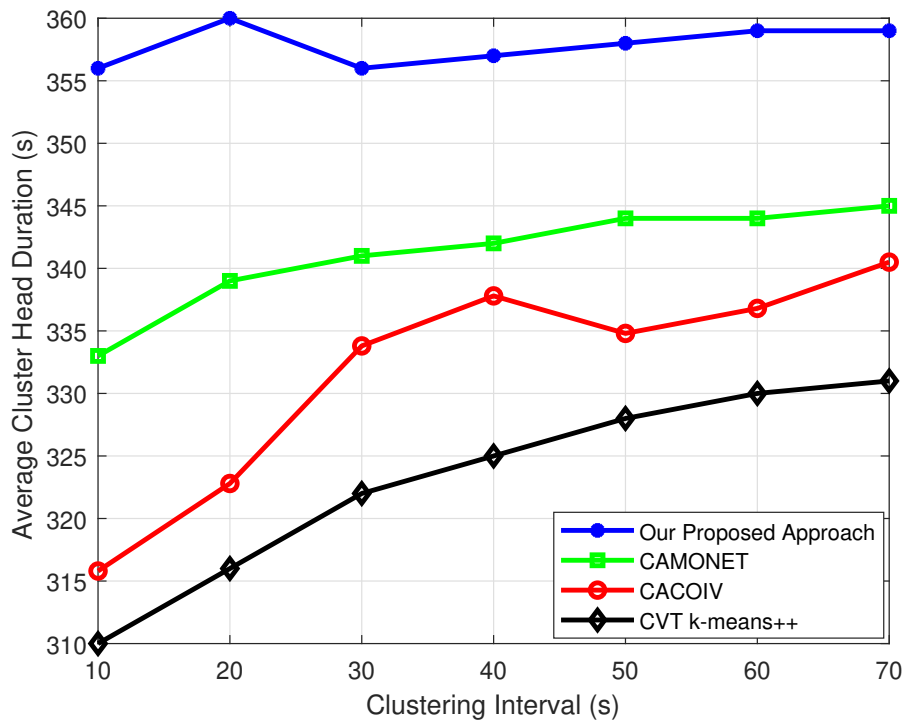


FIGURE 3.7: Average duration of cluster head vehicle

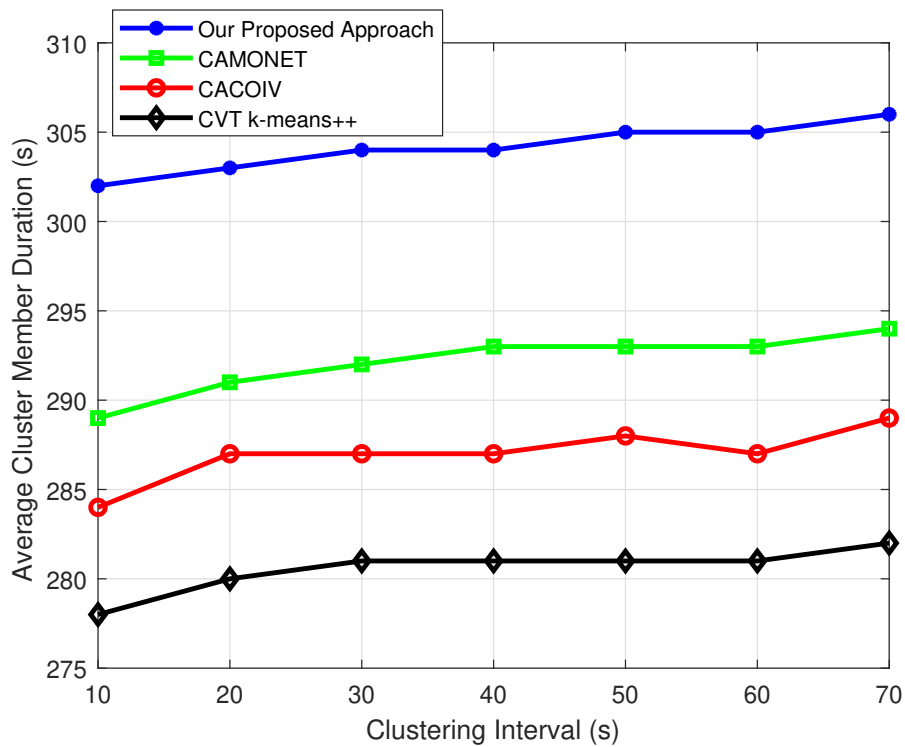


FIGURE 3.8: Average duration of cluster member vehicle

of the cluster heads for the CAMONET and CACOIV schemes at a 10 s clustering interval compared to our proposed scheme. As the clustering interval increases, the percentage difference in performance reduces with approximately 2% and 4% difference at a 70 s clustering interval observed for the two schemes respectively.

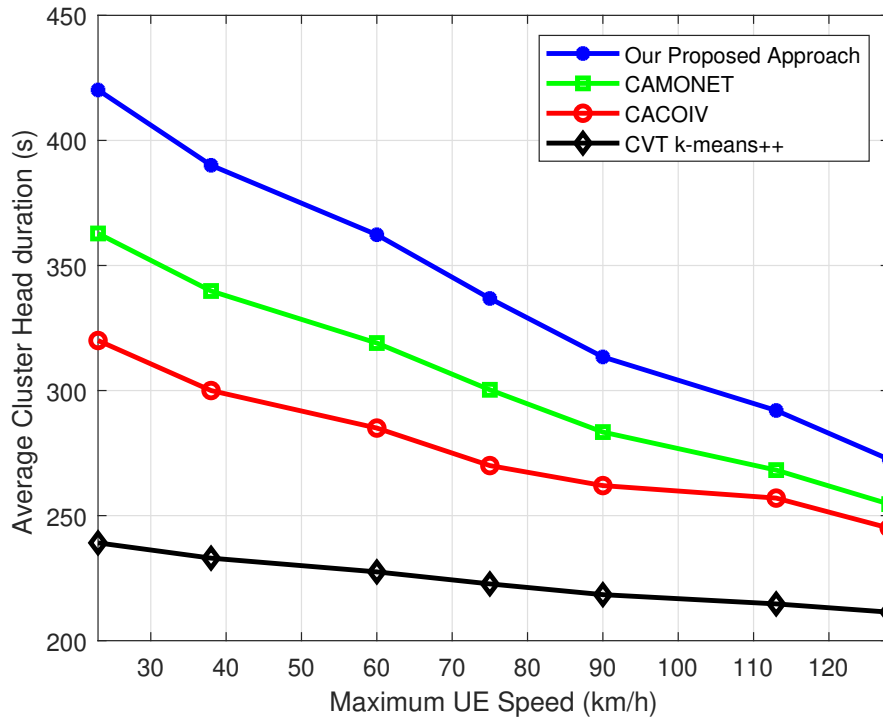


FIGURE 3.9: Average duration of cluster head vehicle Vs Maximum Speed

In Fig 3.9, we show the average cluster head duration as a function of the maximum UE speed. We observe that with an increasing UE speed, the average duration of the cluster head is decreasing for all the schemes considered. This is because with an increasing speed, the network changes rapidly and therefore a higher rate of change of cluster heads occurs. More specifically, higher UE speeds will lead to a decreased cluster stability with a corresponding decrease in the duration of the cluster heads. We observe that the proposed scheme outperforms the others as it more accurately estimates the UE mobility as well as the nodal degree.

3.6 Conclusion

In this chapter, we have investigated the generation of a traffic mobility model using SUMO with realistic traces generated from the statistical information of the AoI representing the mobility of vehicles in this area. Subsequently, we have also investigated two clustering approaches for grouping the network into clusters to achieve a stable cluster head. This is important from the point of view of the HAP

as the beam boresight of the HAP will be directed towards the cluster head vehicle. Considering this, a k-means++ clustering algorithm that utilised vehicle location and velocity information to group vehicles into clusters was presented. Results were analysed using a Silhouette coefficient with an acceptable cluster cohesiveness, which indicates a reasonable cluster quality. Furthermore, and to improve the clustering, we formulated the clustering as a multi-objective optimisation problem and investigated an ant-colony clustering approach. The algorithm performance was evaluated against the k-means and comparable benchmark clustering approaches in the literature with simulation results showing that our proposed algorithm achieves an improved cluster stability compared to the k-means and benchmark algorithms.

Chapter 4

Coverage and Capacity Analysis of a HAP System with Large Antenna Arrays

4.1 Introduction

This chapter presents a performance analysis of the HAP communication link with various numbers of antenna elements per HAP antenna array. It investigates the performance based on an SINR analysis of the coverage probability and achievable UE capacity. A performance evaluation illustrating this scenario is presented and discussed. Using different antenna elements per HAP antenna array, we also investigate the appropriate number of antenna elements required on the HAP antenna array to provide adequate coverage to vehicle UEs. Thereafter, we investigate the achievable UE throughput for both for selected vehicle UEs within the coverage area. Fundamental concepts of the HAP antenna beamforming are also presented. Finally, we investigate and discuss the trade-offs required to achieve adequate coverage and capacity for the given traffic scenario.

In investigating the coverage and capacity performance of the HAP utilising a different number of HAP antenna elements per HAP antenna array, we aim to establish that for the given traffic scenario, there exists an appropriate number of clusters and a corresponding number of antenna elements that achieves an acceptable trade-off in terms of the coverage probability and achievable UE throughput. These contributions grow in parallel with leveraging the connectivity opportunities a HAP can provide, particularly for vehicular UEs in under-served and unserved rural areas.

4.2 Contribution and Organisation

A performance evaluation on the coverage probability and achievable user capacity for a HAP utilising a different number of antenna elements per HAP antenna array is investigated in this chapter. We note that this framework is also valid for other types of aerial communication network scenarios, i.e., in the design of HAP networks as a communication framework in high user-density scenarios or during events such as football games to complement existing cellular infrastructures. Additionally, the same architecture may be designed for air-ground access in device-to-device (D2D) communications. Therefore, this chapter contributes to:

- motivating the utilisation of HAPs equipped with large antenna arrays as a viable option for rural vehicular communication in areas where the terrestrial network infrastructure is limited or non-existent. With beamforming being fundamental in mmWave communication to compensate for the higher path-loss experienced at such high frequencies, the analysis of the impact of different antenna array configurations for the HAP with a varying number of clusters helps to adequately characterise the performance of the network.
- an investigation of coverage and capacity performance of the network using an SINR link quality analysis for a different number of antenna elements and clusters is presented and discussed. Our results demonstrate the required number of clusters that maximises the coverage probability and achievable UE throughput for a different number of antenna elements. Similarly, we show the performance improvements obtainable with appropriate interference mitigation strategy when the system interference is constrained by only channel noise. We also determine the appropriate number of UEs in a cluster that maximises the system throughput. These results allows us to characterise the coverage and throughput performance of the system for the different number of antenna elements. Finally, we examine and discuss the trade-offs for simultaneously addressing the coverage and capacity requirements of the system.
- investigating the achievable throughput performance of vehicle UEs over the vehicle trajectory. To achieve this, we arbitrarily select vehicle UEs from clusters with a maximum coverage probability and present their throughput performance over the UE trajectory. Our results provide an insight into the UE-specific performance of the proposed system.

We present the HAP system model used to evaluate the system performance in Section 4.3. Here, introductory concepts of a HAP antenna array are presented in Section 4.3.1, the wireless channel model incorporating the path loss and rain attenuation model is presented in Section 4.3.2, the beamforming model is presented in Section 4.3.3, and the performance metric characterisation is presented in Section

4.4. The simulation results are presented in Section 4.5 and finally, we give concluding remarks in Section 4.10.

4.3 System Model

4.3.1 The HAP Antenna Array

We focus on the downlink transmission scenario and consider a quasi-stationary HAP operating in the mmWave frequency bands at an altitude $h \approx 20$ km and dynamically pointing its main lobe beam at the cluster centroids C_K . The set of clustered vehicle UEs is denoted by $C^{(b)} = \{C_1^{(b)}, \dots, C_K^{(b)}\}$. High gain steerable beams with high attenuation of the side-lobe levels relative to the mainlobe beam are required to meet the system requirements. The antenna array utilised on the HAP must satisfy these requirements. The high gain can compensate for the high path loss, the low side-lobe levels reduce the signal power in unwanted directions, and steerable beams can provide flexible coverage. A uniform planer array (UPA) has been adopted as the antenna payload for the HAP. The UPA has been shown to exhibit these characteristics **review** and is also reliable, versatile and easily deployable [181], and therefore, are most suited to mmWave communications.

In Fig. 4.1, we illustrate an M (x-axis) by N (y-axis) UPA with an azimuth angle ϕ_0 and an elevation angle θ_0 . The radiation pattern of the antenna array will determine how much power is radiated from the antenna towards the steering direction, and we show in Fig. 4.2 an approximate ellipse-shaped beam footprint of the UPA on the ground with a pointing direction (θ_c, ϕ_c) , a ground beamwidth of B_{θ_c} at a height h and an elevation angle θ_0 at the sub-platform point. The lines AO and BD denote the major and minor axes. With a lookup elevation angle (i. e elevation angle at the centre of the cell) given as ϵ_c and a minimum elevation angle of the cluster defined by β_c , we can express both in terms of θ_0 as [182]:

$$\epsilon_c = \frac{\pi}{2} - \theta_0. \quad (4.1)$$

$$\theta_c = \frac{\pi}{2} - \frac{B_{\theta_c}}{2} - \theta_0. \quad (4.2)$$

As highlighted in Section 2.2.1, operating the HAP at mmWave frequencies can alleviate the array size constraints compared to operation at the sub-6 GHz frequency band. For instance, given operation at a carrier frequency of 2 GHz and 28 GHz, with 400 antenna elements per HAP array, uniformly spaced at $\frac{\lambda}{2}$ separation distance, the geometric area for the UPA is $100 \lambda^2$ corresponding to a physical area of $2.25m^2$ and $0.0115m^2$ respectively. Moreover, Stratospheric Platforms Limited (SPL)

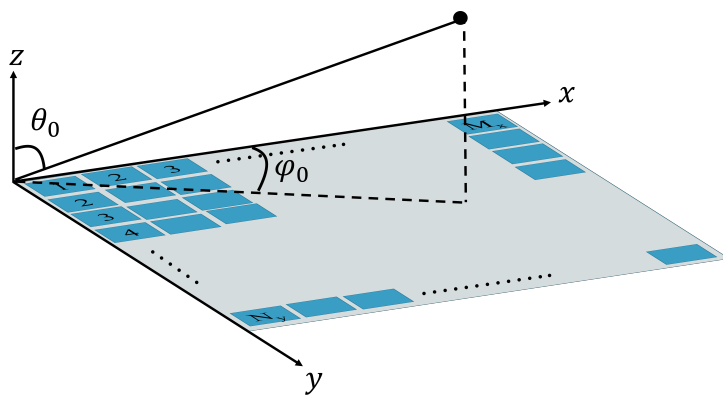


FIGURE 4.1: Phased Array Antenna System

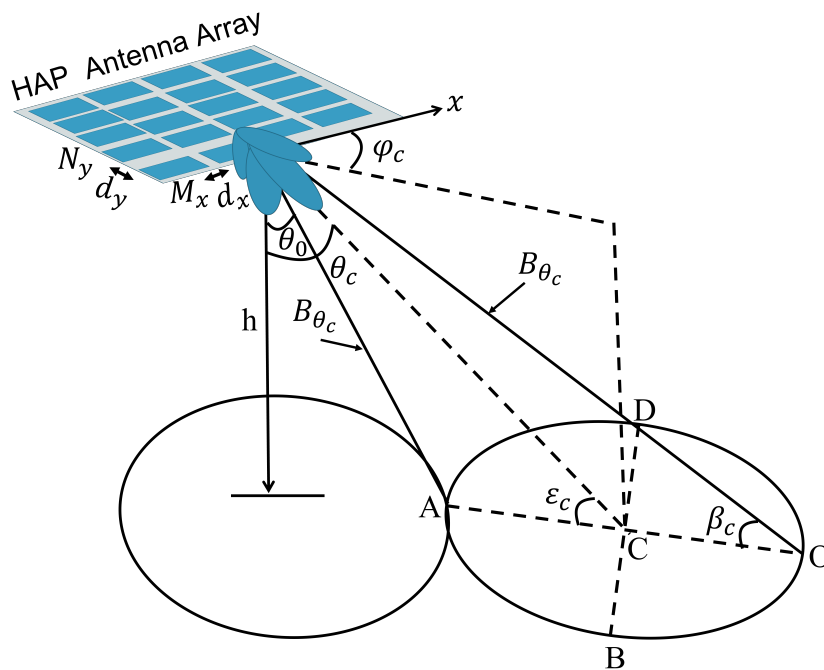


FIGURE 4.2: Phased Array Antenna System with Beam Footprint

have demonstrated a proof of concept [19] to utilise an airborne antenna on a HAP to deliver over 480 steerable beams using a phased array antenna weighing 120 kg and about 9 m^2 area. Clearly, at mmWave, the size of the antenna array with a large number of antenna elements is realisable.

This effect is explicitly illustrated in Fig. 4.3a and Fig. 4.3b. In Fig. 4.3b, we observe that with an increasing operating frequency, the size of the antenna array reduces. We observe larger antenna array sizes at the sub-6 GHz frequency band. The smaller antenna array sizes enable larger number of antenna elements per HAP antenna array which increases the antenna gain and compensates for the increased path loss as exemplified in Fig. 4.3a. In this figure, the path loss as a function of different HAP frequencies is illustrated. This shows the inverse relationship between

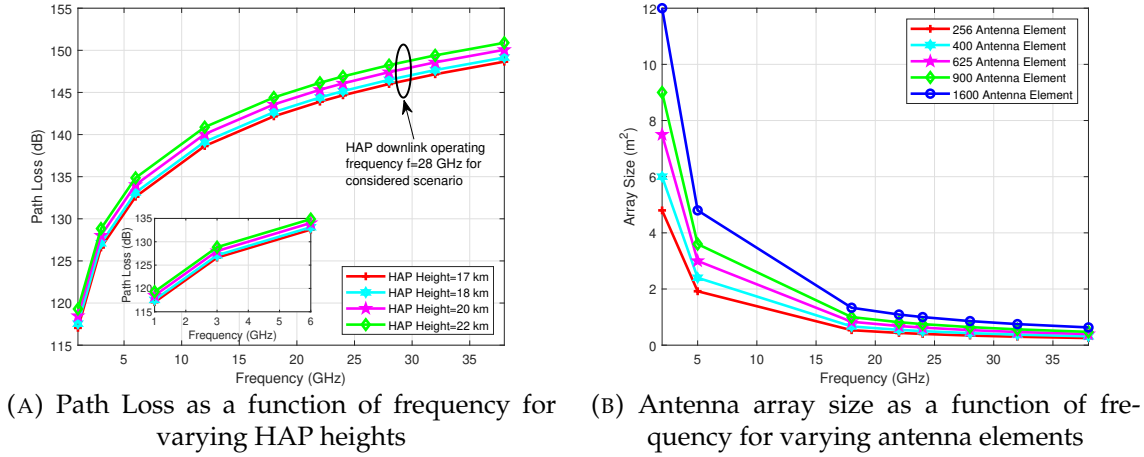


FIGURE 4.3: Effect of HAP height and frequency on Path loss and array size respectively

path loss and frequency. Increasing the HAP operating frequency will lead to an increased channel path loss due to the increasing distance between the HAP station and the vehicle UE. However, Fig. 4.3b shows that with the antenna array operating at higher mmWave frequencies, the antenna array can have a reduced form factor.

Similarly, increasing the HAP height increases the coverage radius at the Sub-Platform Point (SPP), with the active coverage radius defined as the maximum range within which the HAP provides coverage to a vehicle UE when the SNR or SINR exceeds a specified threshold χ [dB]. The beam coverage radius will clearly be determined by the HAP transmit power, antenna beamwidth, and HAP height.

$$AO = \max \left(AO \mid \left(P_{tx}, B_{\theta}, h \right) \geq \gamma [dB] \right). \quad (4.3)$$

Next, we present important fundamental concepts of benchmark characteristics of the phased array antenna in terms of the array factor and array gains. The radiation pattern of the antenna array will determine how much power is radiated from the antenna towards the steering direction. With the main lobe at boresight (i.e. $\theta = \theta_0$ and $\phi = \phi_0$) and $N = N_x M_y$ antenna elements, and with an appropriate windowing function, it is possible to steer the direction of the beam by adjusting the phase delay of the transmit signal from the separate antenna elements such that their contributions arrive at the same time in the desired direction and, therefore, add constructively.

For an antenna with M_x and N_y number of antennas elements in the horizontal and vertical directions, with an inter-element separation distance d_x and d_y , the array

factor AF is expressed as [183]:

$$\begin{aligned}
 AF(\theta, \phi) &= AF_x \times AF_y \\
 &= I_{m_x} \sum_{m_x=1}^{M_x} e^{j(m_x-1)\varphi_x} \times I_{n_y} \sum_{n_y=1}^{N_y} e^{j(n_y-1)\varphi_y}, \\
 &= \sum_{m_x=1}^{M_x} \sum_{n_y=1}^{N_y} w_{m_x n_y} e^{j[(m_x-1)(kd_x \sin \theta \cos \phi + \beta_x) + (n_y-1)(kd_y \sin \theta \sin \phi + \beta_y)]},
 \end{aligned} \tag{4.4}$$

where

$$w_{m_x n_y} = I_{m_x} I_{n_y},$$

and for beam steering in the desired direction, the phase excitation β_x and β_y between the antenna elements can be adjusted. This is expressed as:

$$\begin{aligned}
 \beta_x &= -k_a d_x \sin \theta_0 \cos \phi_0, \\
 \beta_y &= -k_a d_y \sin \theta_0 \sin \phi_0,
 \end{aligned} \tag{4.5}$$

where the azimuth and elevation angles are represented by $\phi = \phi_0$ and $\theta = \theta_0$, β_x , β_y is the phase shift between elements in both the horizontal and vertical directions respectively, $k_a = \frac{2\pi}{\lambda}$ is the wave number and λ represent the wavelength. $w_{m_x n_y}$ represents the amplitude of the antenna elements.

Therefore, the antenna gain $G_T(\theta, \phi)$ as a function of direction is given as:

$$\begin{aligned}
 G_T(\theta, \phi) &= |AF_x| |AF_y| G(\theta, \phi), \\
 &= |AF(\theta, \phi)|^2 G(\theta, \phi),
 \end{aligned} \tag{4.6}$$

where $G(\theta, \phi)$ is the gain pattern for a single element in the array and expressed as:

$$G(\theta, \phi) = \frac{4\pi d_x d_y}{\lambda^2} \eta \cos \theta. \tag{4.7}$$

and η is the antenna efficiency.

4.3.2 HAP Wireless Channel Propagation

As described in Section 2.2, the characterisation of an A2G channel in the mmWave band for a HAP-assisted vehicular network remains an open issue with limited measurements efforts due to the earlier mentioned constraints. Therefore, for the

HAP channel, we adopt a conservative assumption of signal propagation based on a free-space path loss model combined with a log-normal distributed shadowing similar to LoS path loss models in [184] and [185] with the following assumptions:

- the HAP is stabilised, and its quasi-stationary position is not unduly influenced by wind and other natural factors.
- there is a perfect beam alignment between the HAP transmitter and the vehicle UEs and no requirement for beam training.

Therefore, we express the path loss of the link between the HAP and vehicle UE as:

$$PL[dB](f_c, d) = 92.45 + 20 \log_{10}(d_l) + 20 \log_{10}(f_c) + X_{\sigma_{LOS}}, \quad (4.8)$$

where d_l is the distance in *km* between the HAP and vehicle UEs and f_c is the frequency in *GHz*. The shadow fading is represented by the log-normal distributed random variable, $X_{\sigma_{LOS}}(dB) \approx N(\mu_{LOS}, \sigma_{LOS}^2)$ with $\mu_{LOS} = 0$ dB and standard deviation σ_{LOS} , also in dB.

With the HAP operating at mmWave frequency, the quality of the communication link can be largely impaired by challenging propagation conditions with rain attenuation causing an absorption and scattering of the signal. As a result, it is important to consider this in the link budget analysis. Detailed modelling of the effect of rain effects is not the focus of this section. Rather we exploit a standard ITU-R model [186] to calculate the margins required to overcome rain attenuation in order to generate a specific link availability. The rain attenuation exceeded for 0.01% of an average year, in dB is expressed as [186]:

$$\begin{aligned} A_{0.01}[dB] &= \gamma_{rain} L_{eff}, \\ &= k_c R^{\alpha_c} L_{eff}, \end{aligned} \quad (4.9)$$

where $\gamma_{rain} = k_c R^{\alpha_c}$, is the specific rain attenuation in *dB/km*, k_c and α_c are constants that depends on frequency and rain polarization, obtained from [186], R is the rainfall rate (mm/hr). Because rainfall is not uniformly distributed along the propagation path, the effective length is determined by the slant path length L_S of the link and a path reduction factor r_p expressed as $L_{eff} = L_S \times r_p$. We obtain the path reduction factor r_p from [45]:

$$r_p = \frac{1}{0.477 L_S \times R_{0.01}^{0.073 \alpha_c} \times f_c^{0.123} - 10.579(1 - \exp^{-0.024 L_S})} \quad (4.10)$$

The slant path length L_S is computed as given in [187] for $\theta \geq 90^\circ$ and expressed as:

$$L_S = \frac{(h_R - h_S)}{\sin\theta} \tag{4.11}$$

where h_R is the rain height and h_S is the height above the sea level datum of the UE in km . The specific atmospheric attenuation due to oxygen, γ_o , [dB/km] and water vapour γ_w , [dB/km] along the slant path is also expressed as [187]:

$$\begin{aligned} A_{atm}[dB/km] &= (\gamma_o + \gamma_w)L_{eff} \\ &= \gamma_{atm}L_{eff} \end{aligned} \tag{4.12}$$

where $\gamma_{atm} = \gamma_o + \gamma_w$ is the specific attenuation. Therefore, an accurate description of the total path loss is a combined effect of (4.8) and (4.9) and expressed as:

$$PL_T[dB] = A_{0.01}(dB) + PL[dB](f_c, d)[dB]. \tag{4.13}$$

In Fig. 4.4, we show the total path loss with rain and atmospheric attenuation as a function of the slant path distance and at a frequency of 28 GHz, indicating the increasing effect of rain attenuation on the path loss.

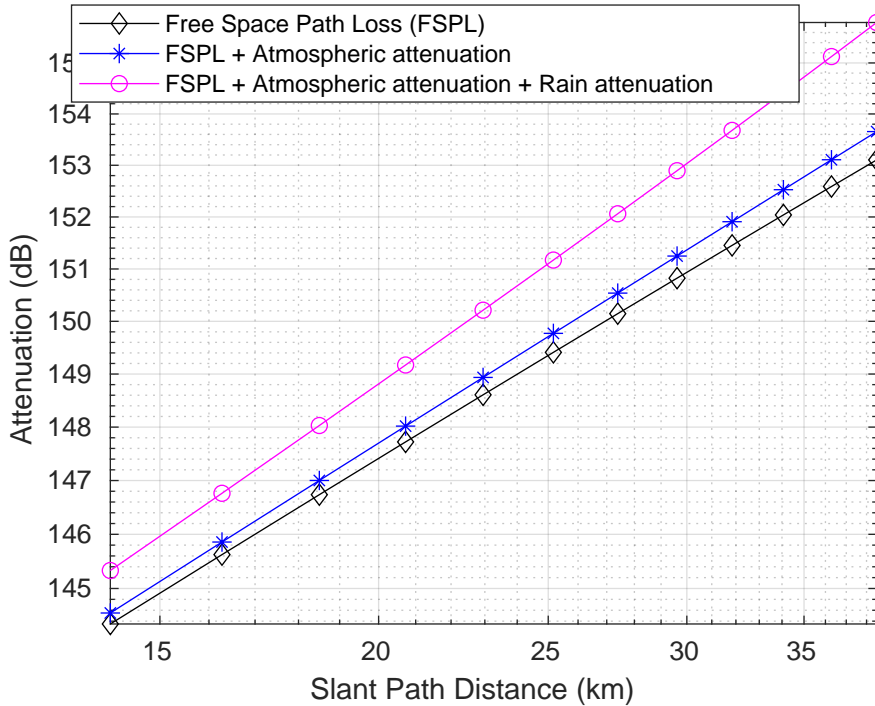


FIGURE 4.4: Total free space path loss at 28 GHz from the model in [188]

Considering the above losses, the received power $P_{rx}(dBm)$ is expressed as;

$$P_{rx}[dBm] = P_{tx}[dBm] + G_{rx}[dB] + G_{tx}[dB] - PL_T[dB], \quad (4.14)$$

where $P_{tx}[dBm]$ is the HAP transmit power, $G_{rx}[dB]$ is the vehicle UE gain, $G_{tx}[dB]$, is the HAP transmitter gain and $PL_T[dB]$ represents the other losses as expressed in 4.13. The link budget is as given in Table 4.1.

Additionally, vehicular mobility introduces Doppler, which is a linear function of the carrier frequency with the maximum Doppler frequency shift expressed as:

$$f_d = \frac{\pm v f_c}{c} \cos\theta \quad (4.15)$$

where f_c is the frequency, v is the relative velocity between the HAP and the vehicle UE, c is the speed of light, and;

$$\cos\theta = \frac{r}{\sqrt{r^2 + h^2}}. \quad (4.16)$$

is the angle of the velocity vector. For instance, the Doppler frequency shift for a vehicle UE at the edge of the coverage area is 8.9 kHz. This calculation is based on a worse case Doppler frequency shift for a vehicle UE that is travelling towards the quasi-stationary HAP from the edge of a 30 km coverage radius, at a UE velocity of 60 mph, HAP height = 20 km and, $f_c = 28$ GHz.

However, research in [189] and [190] have demonstrated that directional beams and the implementation of automated frequency control (AFC) loop in the receiver can compensate the Doppler frequency shift. As such, and in line with other works [191] and [192], we consider the effect of Doppler to be mitigated.

4.3.3 HAP Beamforming Gain

For beamforming, a fundamental component of the performance of a HAP system is the antenna payload on the HAP. Typically, the spatial power distribution of the signals is shaped such that a larger fraction of the signal power is directed towards the intended cluster. An inter-element spacing of a half-wavelength between the antenna element is used. The beamforming antenna system is depicted in the UPA of Fig. 4.1 and described in algorithm 4. The vehicle UE coordinates are mapped to spherical coordinates to obtain the azimuth and elevation angles and using (4.17) and the beamforming antenna gain is obtained using Equation (4.4) - (4.7).

In Fig. 4.5, we illustrate the normalised antenna gains and beam footprint contour gain for the SPP and for a 6 cluster scenario with a 30×30 antenna element array.

TABLE 4.1: System Parameters for HAP Model

Parameter	Value
Environment	Rural
HAP Height (km)	20
Channel Bandwidth (MHz)	200
Carrier Frequency (GHz)	28
HAP Transmit Power (dBm)	40 dBm
UE Antenna Gain (dB)	3 dB
Frequency Re-use	1, 3
Antenna Noise Temperature (K)	500 K
SNR/SINR Threshold χ (dB)	-5 dB
Thermal Noise Power (dBm) ¹	- 90
No. of Antenna Elements	[400],[625],[900],[1225],[1600]
User distribution	As per traffic model in Section 3.3

¹ Thermal Noise Power = kTB where k = Boltzman's Constant = 1.38×10^{-23} Joules/Kelvin, T = Antenna Noise Temperature, B = Noise Bandwidth, Hz

Algorithm 4 HAP Beamforming Antenna Gain

- 1: Map the UE Cartesian coordinates to spherical coordinates.

$$\begin{aligned}
 d &= (x_{HAP} - x_k)^2 + (y_{HAP} - y_k)^2 + (h_{HAP} - 0)^2, \\
 \theta_0 &= \pi - \arccos\left(\frac{h_{HAP}}{\sqrt{d}}\right), \\
 \phi_0 &= \arctan\left(\frac{y_{HAP} - y_k}{x_{HAP} - x_k}\right).
 \end{aligned} \tag{4.17}$$

where $[x_{HAP}, y_{HAP}, h_{HAP}]$, and $[x_k, y_k, 0]$ are the 3-D Cartesian coordinates for the HAP and cluster centroid UE respectively.

- 2: Obtain the phase shift β_x and β_y required to point the main beam to the cluster centroid using Equation (4.5).
 3: Generate Hann windowing coefficient [183]

$$w(n) = 0.5 \left(1 - \cos \left(2\pi \frac{n}{N} \right) \right), \quad 0 \leq n \leq N \tag{4.18}$$

- 4: Obtain total array factor using Equation (4.4).
 5: Obtain a single element gain pattern using Equation (4.7).
 6: Obtain total gain G_T from all antenna array elements using Equation (4.5). .
-

We observe higher gains are obtained at the SPP and cluster centers with a maximum normalised gain of 0 dB and a peak side-lobe level (SLL) of approximately -

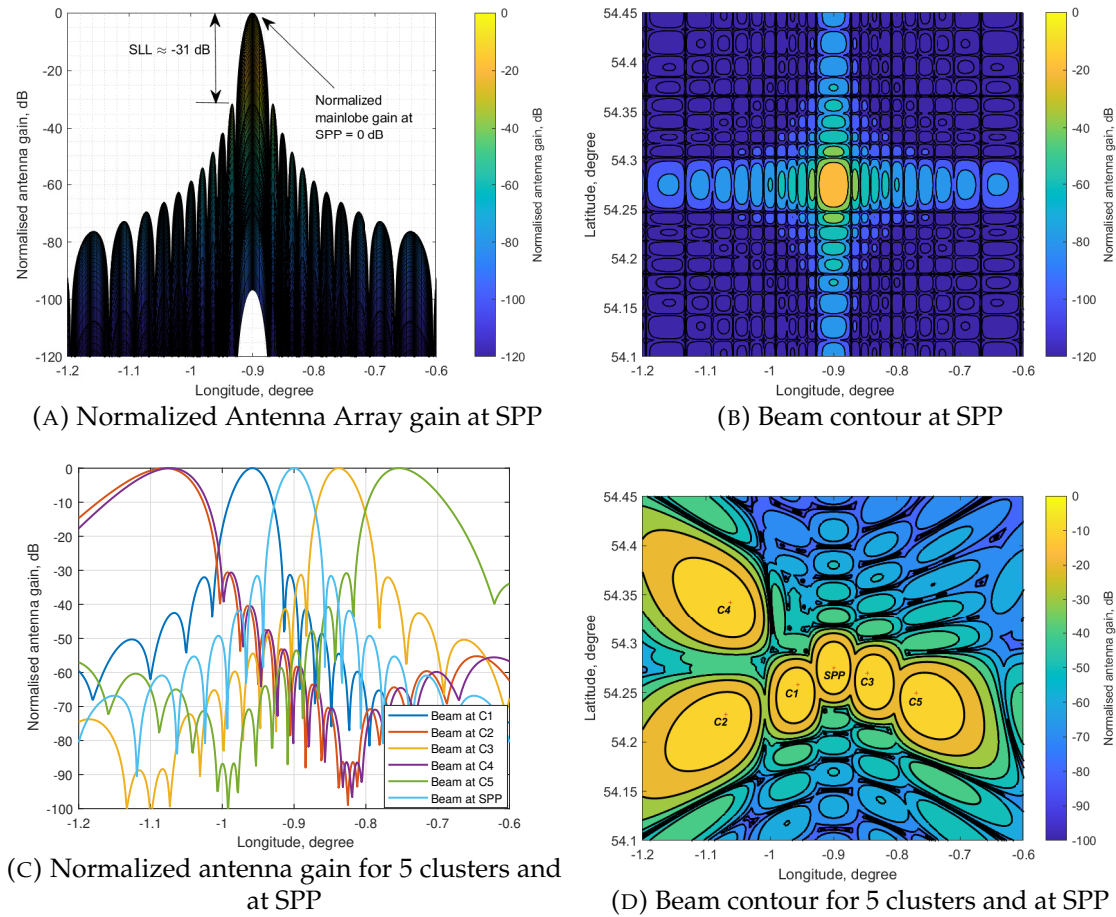


FIGURE 4.5: Antenna gains and contour plot for a 30×30 antenna element array

31 dB.

4.4 Performance Analysis Characterisation

Given clear LoS conditions, directional beams will be generated by the antenna array, thereby improving the link margin and reducing the interference level from the other beams in the coverage area. As such, the main lobe and side-lobe levels are critical to system performance. Therefore, an evaluation of the number of antenna elements per HAP antenna array that will form the beam footprint to provide adequate coverage is important for the communication link. As part of our analysis, we perform an evaluation of the performance metrics utilised in the characterisation of the system in terms of the coverage probability and achievable UE capacity for different numbers of antenna elements and clusters.

4.4.1 SNR and SINR Coverage Analysis

Without loss of generality, the vehicle UEs are distributed according to the traffic model discussed in Section 3.3.2 and the clustering model in Section 3.4. As an indication of the channel quality, we first consider the SNR γ_{h_i,k_i} between the HAP and the vehicle UE expressed in linear units as:

$$\gamma_{h_i,k_i} = \frac{P_{rx}}{N_p} \quad (\text{in linear units}) \quad (4.19)$$

where P_{rx} is the received power as obtained in (4.14) and N_p denotes the noise power. Similarly, the SINR $\tilde{\gamma}_{h_i,k_i}$ for a vehicle UE within the coverage area is expressed as:

$$\tilde{\gamma}_{h_i,k_i} = \frac{P_{rx}}{N_p + \sum_{j \in \mathcal{C}} P_I} \quad (\text{in linear units}) \quad (4.20)$$

where the summation term in the denominator represents the sum of the interference power from all the other HAP beams.

We define the SNR coverage probability $P_{c\gamma_{h_i,k_i}}$ as the probability that the received SNR of a vehicle UE in the beam coverage area is greater than a specified threshold χ_{SNR} [dB]. Mathematically, this is expressed as:

$$P_{c\gamma_{h_i,k_i}} = Pr\left(\gamma_{h_i,k_i}[dB] \geq \chi_{SNR}[dB]\right) \quad (4.21)$$

Similarly, the SINR coverage probability SINR $P_{c\tilde{\gamma}_{h_i,k_i}}$ is defined as the probability that the SINR of vehicle UEs in the beam coverage is greater than or equal to specified SINR threshold χ_{SINR} (dB) and expressed as:

$$P_{c\tilde{\gamma}_{h_i,k_i}} = Pr\left(\tilde{\gamma}_{h_i,k_i}[dB] \geq \chi_{SINR}[dB]\right) \quad (4.22)$$

Intuitively, the outage probability for Equation (4.21) and Equation (4.22) can be written as:

$$\begin{aligned} P_{o\gamma_{h_i,k_i}} &= Pr\left(\gamma_{h_i,k_i}[dB] < \chi_{SNR}[dB]\right) \\ &= 1 - P_{c\gamma_{h_i,k_i}} \end{aligned} \quad (4.23)$$

$$\begin{aligned}
 P_{o_{\tilde{\gamma}_{h_i,k_i}}} &= Pr\left(\tilde{\gamma}_{h_i,k_i}[dB] < \chi_{SINR}[dB]\right) \\
 &= 1 - P_{c_{\tilde{\gamma}_{h_i,k_i}}}
 \end{aligned} \tag{4.24}$$

$\forall t \in [t_1, t_2]$, and $t_2 - t_1 \geq t_m$.

In other words, a sufficient condition for a vehicle UE within the coverage area to be considered in an outage is that γ_{h_i,k_i} and $\tilde{\gamma}_{h_i,k_i}$ goes and stays below χ_{SNR} and χ_{SINR} for at least t_m where t_m is the minimum outage duration averaged over all snapshots.

4.4.2 Capacity Analysis

The channel capacity is defined as the upper bound of the theoretical data rate transmitted over a communication channel. If ρ_i is the physical data rate for a vehicle UE, then applying the Shannon capacity formula provides an upper bound on the capacity of the link as:

$$\rho_i = B_i \log_2(1 + \gamma_i), \tag{4.25}$$

where B_i is the bandwidth and, γ_i is SINR of the link. However, in practice, the transmission rate depends on the selected Modulation and Coding Scheme, determined by the maximum allowed Bit Error Rate (BER). Therefore, as in [193], we approximate the UE capacity by an attenuated and truncated Shannon bound (TSB), which is representative of the practical achievable vehicle UE capacity. This is expressed as [193]:

$$\rho_i = \begin{cases} 0, & \gamma_i(dB) < \gamma_{min}, \\ \alpha B_i \log_2(1 + \gamma_i), & \gamma_{min} \leq \gamma_i(dB) < \gamma_{max}, \\ \rho_{max}, & \gamma_i(dB) \geq \gamma_{max}. \end{cases} \tag{4.26}$$

where α is an attenuation factor representing the implementation loss of the link and is set to 0.65 [194]. This means that a lower limit of γ_{min} is set on γ_i below which link capacity is zero, link capacity is dependent on α if $\gamma_i \in [\gamma_{min} \quad \gamma_{max}]$ and capacity is maximum if $\gamma_i \geq \gamma_{max}$.

4.5 Simulation Results and Discussion

Simulation results are presented following the clustering scheme discussed in Section 3.4 and using the parameters presented in Table 4.1, with the vehicle UEs are

distributed according to the vehicular model outlined in Section 3.3. To evaluate the network performance, we characterise the performance of the UEs such that the HAP beam is directed to a UE with maximum gain and this will be the HAP beam boresight. UEs close to the beam boresight will also receive a higher signal gain. However, with increasing HAP beams, the system performance will be affected by interference from adjacent beams due to the signal power from the SLL of the adjacent beam radiation pattern. Therefore, the system is considered to be interference-limited and will therefore require the implementation of interference coordination measures to mitigate these effects. An investigation of the interference mitigation techniques lies beyond the scope of this thesis.

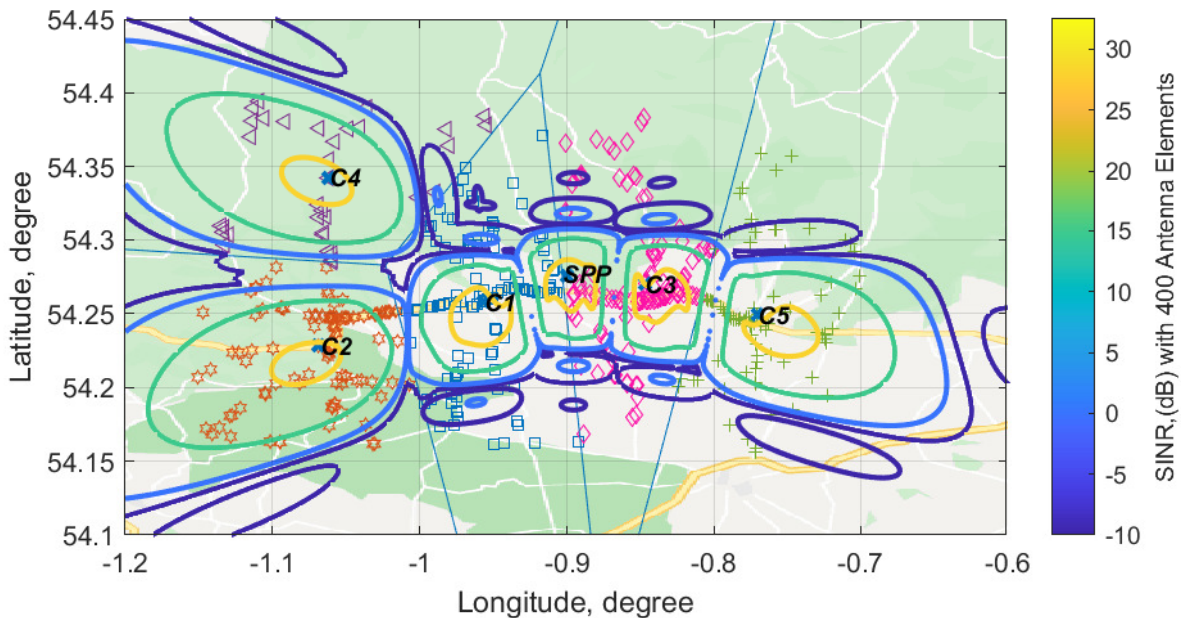


FIGURE 4.6: SINR contour with 6 clusters with a 40×40 antenna element array

4.5.1 Contour Footprint Performance

We begin the analysis by presenting a SINR contour footprint for a lower bound of 6 clusters and an upper bound of 100 clusters at a snapshot time $t=20$ s with a 20×20 antenna element array. This is as illustrated in Fig. 4.6, where vehicle UEs are grouped into clusters with markers of the same colour belonging to a clustered group of vehicle UEs and the cluster head vehicle denoted by an "x" symbol. Each contour line corresponds to a specific received SINR value. In Fig. 4.6, we observe that, with 5 clusters and 400 antenna elements, a SINR of 32.9 dB at the SPP. Evidently, as the difference between the user coordinates and the beam angle θ increases, the beam becomes increasingly elliptical, especially for vehicle UEs located farther away from the SPP. Also, we observe not all the vehicle UEs in the cluster

will be served by the beams as some UEs will fall outside of the beam coverage area.

Continuous coverage is provided to vehicle UEs in clusters across the longitude axis of coverage due to a continuous use-able overlap between the clusters. This is mainly due to the antenna main beam roll-off and the low SLL. Obviously, for a fewer number of clusters within the coverage area, each beam experiences low interference power from the other beams. As expected, we also observe that as the clusters are located further away from the SPP with a lower elevation angle, the beamwidth becomes increasingly elliptical, with the effective area of beam footprint increasing. Vehicle UEs closer to the cluster centroid have an SINR of ≈ 20 dB, which decreases as vehicle UEs are located farther away from the cluster centroid.

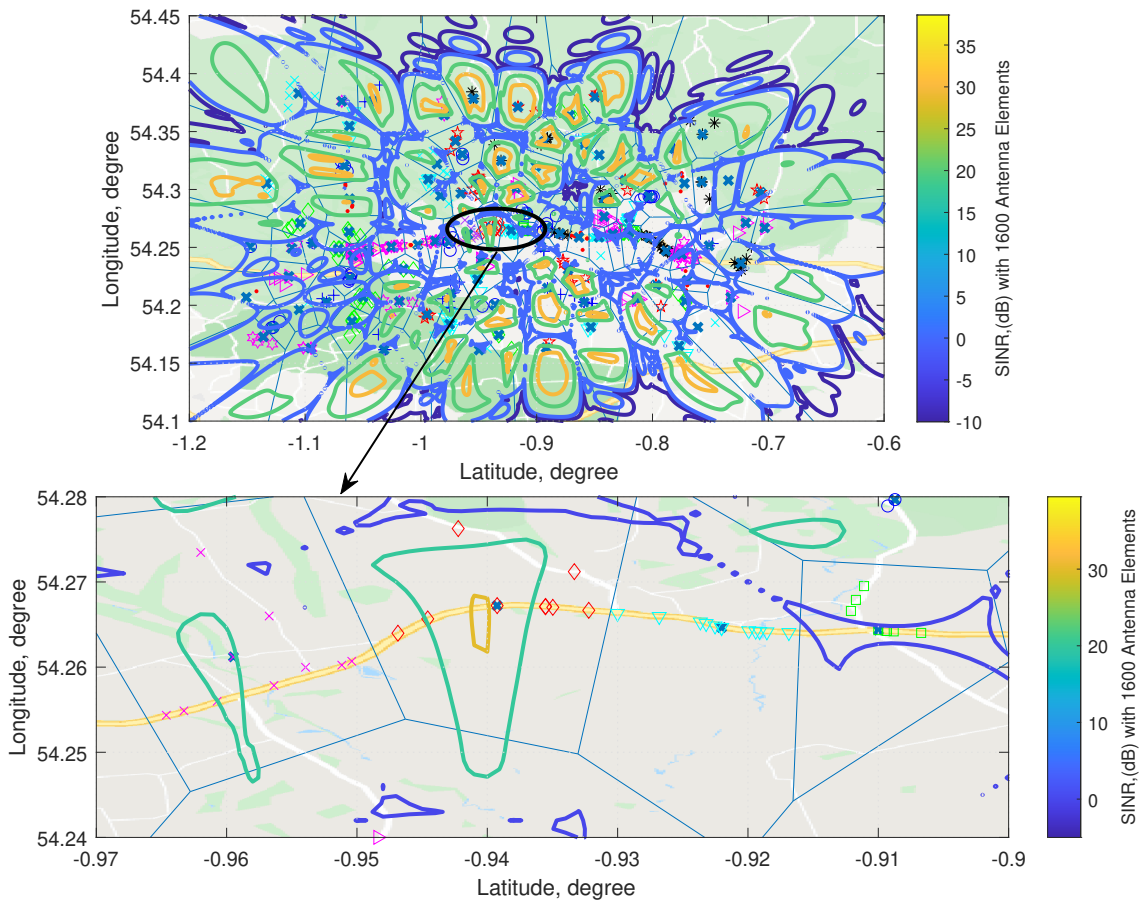


FIGURE 4.7: SINR contour with 100 clusters with a 40×40 antenna element array

Similarly, in Fig. 4.7, we increase the number of clusters and the number of antenna elements to 100 and 1600, respectively and show the SINR performance for the snapshot period. We observe an decrease in the SINR for the 100 cluster scenario as observed by the yellow contour lines. Specifically, the maximum UE SINR corresponds to a peak value of approximately 23 dB. This means as the main lobe

beam becomes narrower with an increase in the number of antenna elements, the main lobe gain with varying beam angle θ is higher when compared to the antenna array considered previously with 6 clusters and 400 antenna elements with a wider beamwidth. However, with an increase in the number of clusters, we can observe that interference dominates and the gap between the SINR performance for the 6 cluster scenario and 100 cluster scenario increases.

4.5.2 SINR Boxplot Distribution

To further analyse the distribution of link quality, we sample, in a box plot, the distribution of the link quality and present sample statistics of the median, upper and lower quartiles, the 5th and 95th percentiles across the longitude of coverage for the scenario considered in Fig. 4.9. The sampled distribution is derived from a two-dimensional grid coordinate of positions defined by a set $A_s = [s_1, s_2, \dots, S]$ containing all the sampled longitude of coverage in the two-dimensional grid where s is the sample points. As illustrated, the central red line in the box plot represents the median while the 25th and 75th percentiles are represented by the bottom and top edges of the box, respectively. The difference between these is the inter-quartile range (IQR). The dashed vertical lines represent the whiskers values that extend beyond both percentiles but are not considered as outliers, i.e., at 1.5IQR. The 5th and 95th percentile values are represented by a "*" that also extend above and below the whisker lines with the "+" representing the mean and the outliers marked with the "o" symbol.

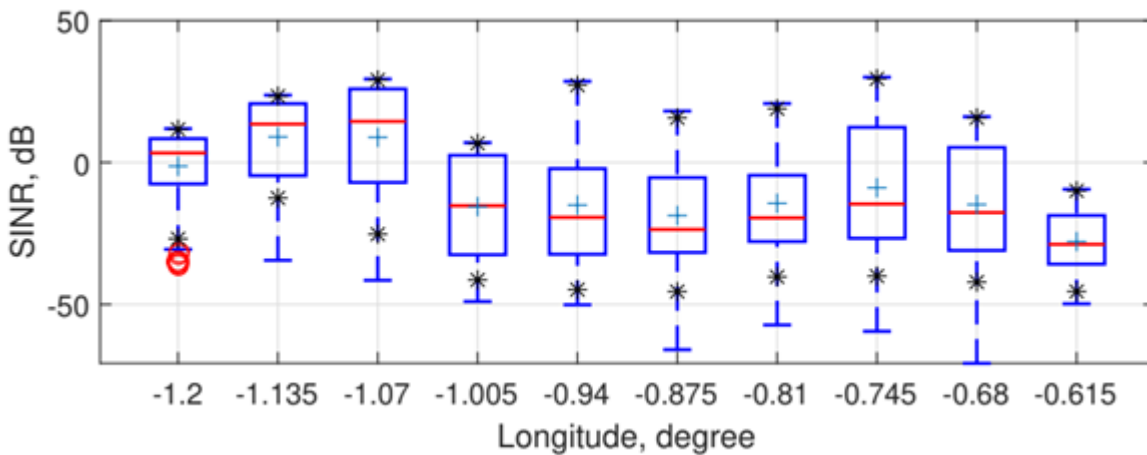


FIGURE 4.8: Boxplot of SINR - 6 clusters with a 20×20 Antenna element array

In Fig. 4.8, we observe, as in Fig. 4.6, link quality performance is higher with a fewer number of clusters. We observe that fewer outliers are obtained due to a larger main lobe beamwidth as most of the vehicle UEs fall within the HAP beam coverage.

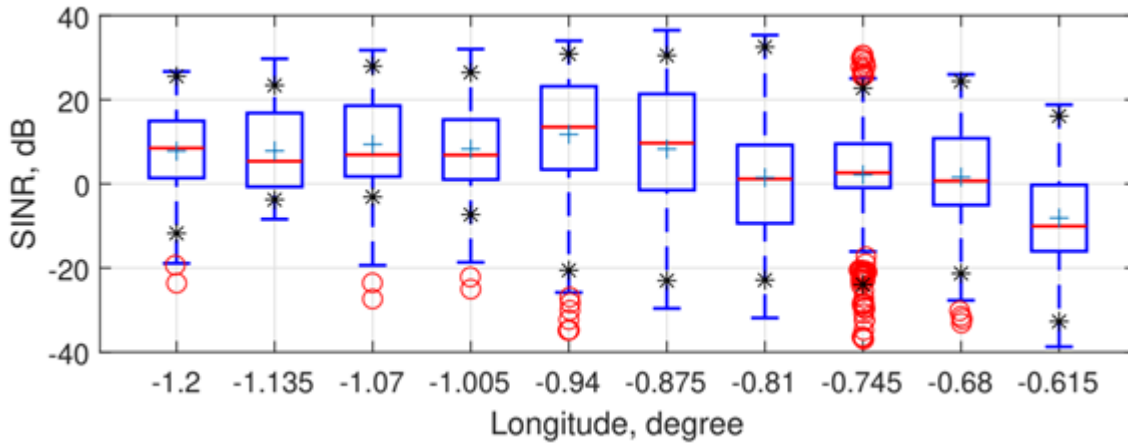


FIGURE 4.9: Boxplot of SINR - 100 clusters with a 40×40 Antenna element array

In Fig. 4.9, we observe an increased gap between the 6 cluster and 100 cluster scenarios, with UEs having a lower median SINR. However, with an increased density of clusters and much narrower beams due to an increased number of antenna elements, fewer UEs are served, and the effect of interference also becomes increasingly significant.

4.5.3 SINR Coverage Performance

We further present in Fig. 4.10 results for the SINR link quality analysis of the coverage probability with a varying number of clusters and different SINR thresholds. Firstly, we observe that the coverage probability reduces with an increase in the SINR threshold. As shown in the figure, a coverage probability of approximately 95% is obtained for SINR up to 0 dB. We also observe that the coverage probability is relatively constant between 30-50 clusters for SINR thresholds up to -5 dB. Beyond this threshold, the coverage probability begins to decrease. We also observe that in the 10 cluster scenario, the coverage probability falls rapidly for the range of SINR thresholds considered. This is because of a larger beamwidth which means a lower received main lobe gain due to coverage over a larger area. A lower main lobe gain will therefore result in a lower SNR coverage probability. The coverage probability will therefore depend on the coverage beamwidth and received gain which determines the received signal power.

Similarly, increasing the number of clusters results in higher interference from other clusters and consequently a lower coverage probability. Specifically, we observe that as the number of clusters increases, the coverage probability is initially high at about 95% at -5 dB but decreases as the SINR threshold increases. With a large number of clusters, we observe the increasing effect of the interference from other

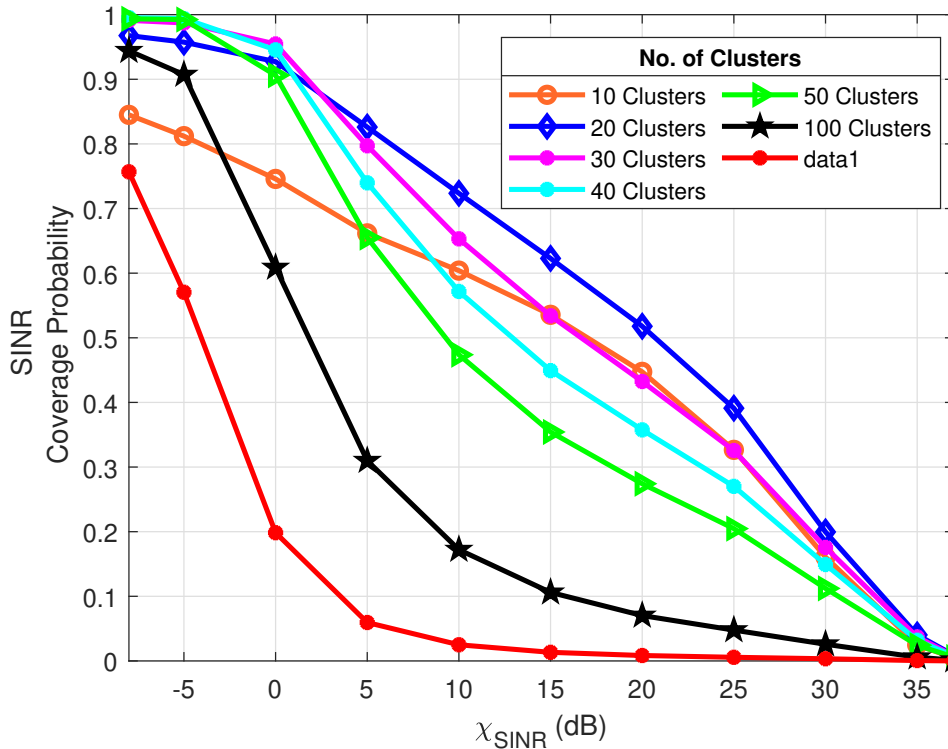


FIGURE 4.10: SINR coverage probability for different χ_{SINR}

main lobe beams within the coverage area. This leads to a decrease in the coverage probability, as shown with the 200 clusters scenario where the coverage probability drops to 0% for SINR thresholds above 10 dB.

From Fig. 4.10, we can deduce that there exists an SINR threshold and a corresponding number of clusters for which the worst-case coverage probability is maximised. Beyond this, interference becomes a significant degradation factor to the system’s performance, requiring effective interference management techniques to improve performance.

In Fig. 4.11, the coverage probability as a function of the average number of vehicle UEs per cluster is illustrated. Here, we observe that there is a maximum value of the number of vehicle UEs in the cluster, and correspondingly, the number of clusters at which the coverage probability is maximised. Beyond this, the coverage probability decreases with an increasing number of UEs. This trade-off is explicitly characterised and shows that as the number of vehicle UEs per cluster increases, the coverage probability initially increases, attains a maximum value at approximately 98.8% for 50 clusters, and then rapidly decreases.

Higher SINR thresholds and an increased number of clusters come at the expense of a poorer coverage performance and increased interference respectively. This is

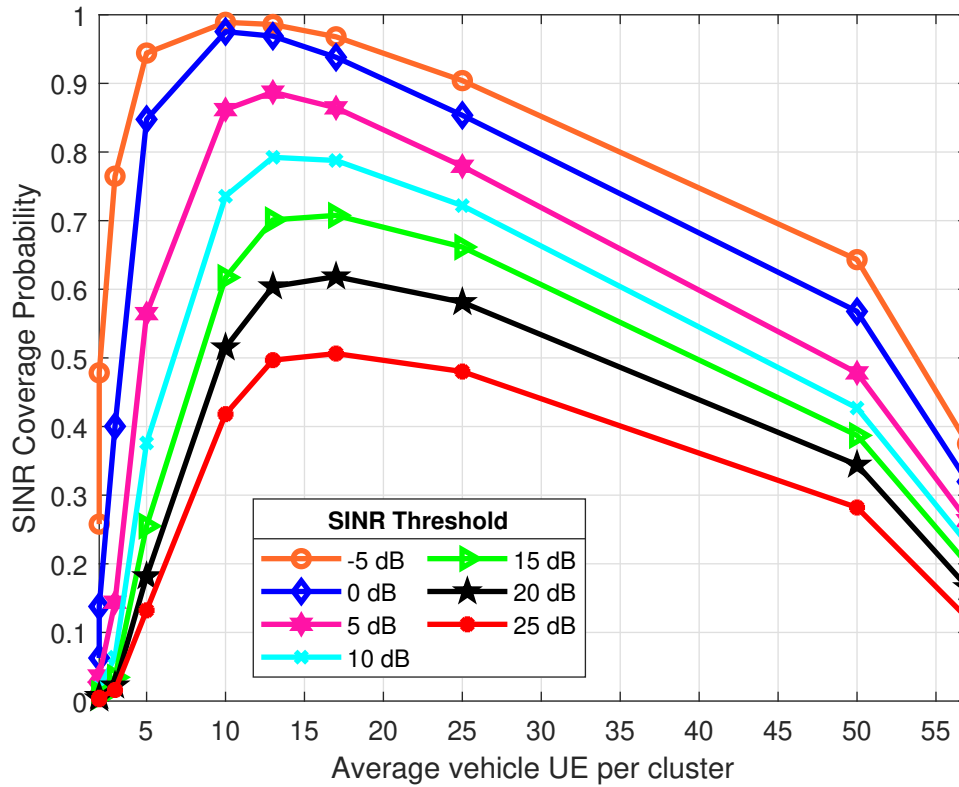


FIGURE 4.11: SINR coverage probability as a function of the average vehicle UE per cluster

shown by the poor coverage performance observed with a higher number of clusters for the range of SINR thresholds considered. Specifically, we observe that between -5 dB and 25 dB SINR thresholds and for 200 clusters and above, a coverage probability of 20% or less is achieved. This means that even with fewer UEs per cluster and a reduced SINR threshold, the coverage probability is still poor due to the increased interference from adjacent mainlobe beams.

Next, we investigate the SINR coverage probability for predetermined SINR thresholds. In NR-V2X, link adaptation is utilised to improve link reliability by adjusting the transmission's modulation and coding scheme (MCS) [195]. This depends on the link quality and channel conditions based on the channel quality indicator (CQI) reported by the vehicle UE. Therefore, if the link quality is poor, a lower modulation scheme and a lower code rate are employed. Using Tables 5.2.2.1-3 in [196] and similar to the work in [197], we consider a lower bound of the χ_{min} range corresponding to the lowest MCS and set $\gamma_{SINR} = -5$ dB, respectively. Accordingly, the SINR threshold reflects the minimum link quality requirement for the vehicle UE to be active and receive signals via direct transmission from the HAP. Otherwise, it is considered inactive.

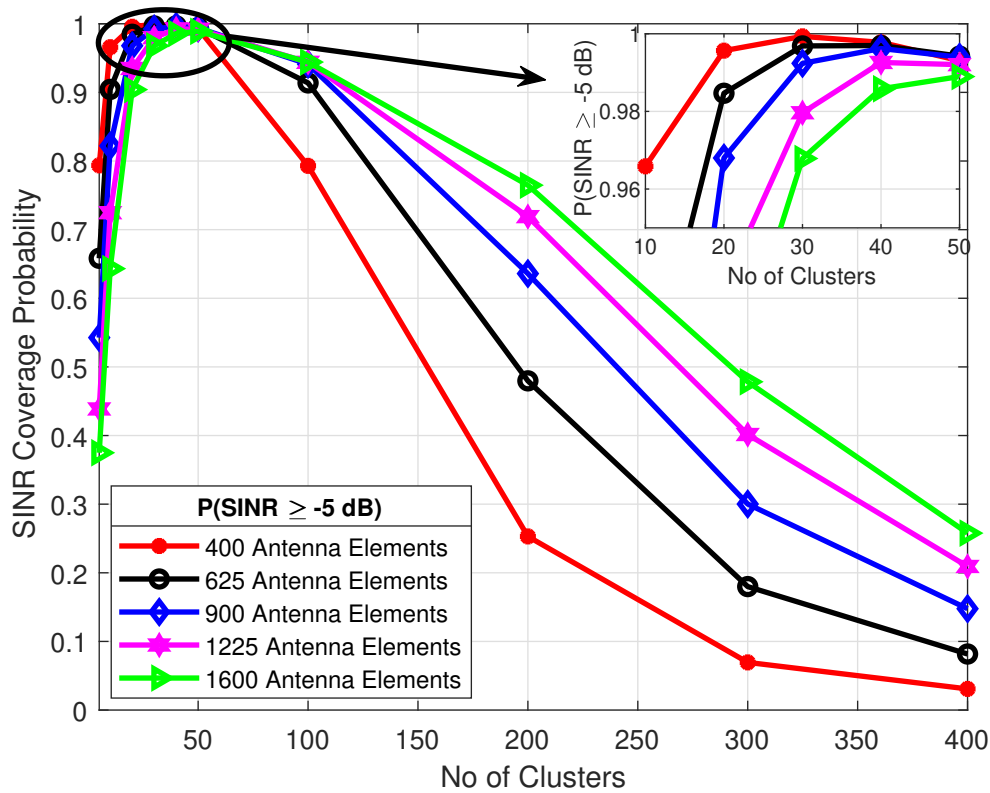


FIGURE 4.12: SINR coverage probability for a different number of clusters

The impact of a different number of HAP antenna elements on the SINR coverage performance is presented in Fig. 4.12 and Fig. 4.13 for different clusters and vehicle UEs per cluster respectively. Firstly, we observe that increasing the number of antenna elements with a corresponding increase in the number of clusters does not always improve the coverage performance. Specifically, in Fig. 4.12, we observe that when the number of clusters is relatively low, the coverage probability initially increases with the 400 antenna elements achieving a maximum coverage probability with a 30 cluster scenario as shown in inset figure of Fig. 4.12. However, the coverage performance begins to drop beyond 50 clusters which shows the increasing effect of the narrower beams on the coverage probability. We also observe a monotonically decreasing relationship of the coverage performance with an increasing number of clusters. The narrow beamwidth relationship on coverage is noticeable with the 1600 antenna elements. This is because as the beamwidth becomes narrower, fewer UEs are covered, and therefore the coverage probability decreases. In a similar vein, we observe that the lower the number of antenna elements, the higher the coverage performance. This effect can be explained from the perspective of the antenna beamwidth as this will produce a wider beamwidth, thereby improving the coverage performance. This effect is also observed with the 400 antenna elements having a higher coverage probability. We also note that there

exist a maximum number of clusters beyond which coverage probability begins to decrease irrespective of the number of antenna elements utilised.

Additionally, we observe that the coverage probability performance increases gradually attains a maximum value and then degrades monotonically with an increasing number of clusters. Beyond 50 clusters, interference becomes significant and begins to have a greater impact on the performance with a consequent decrease in coverage performance. Interestingly, we observe that with a fewer number of clusters (i.e., 5-50 clusters), the coverage probability performance is higher.

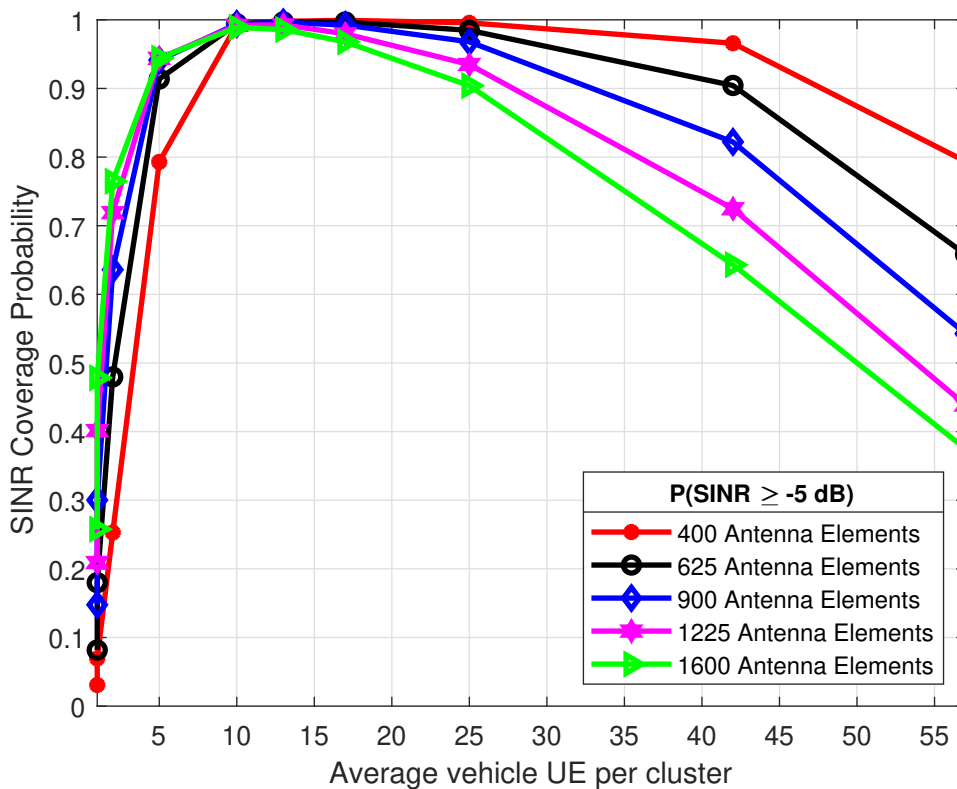


FIGURE 4.13: SINR coverage probability for different number of UEs

In Fig. 4.13, we show results for the SINR coverage performance as a function of the average number of vehicle UEs per cluster. We observe that coverage probability increases with an increasing number of vehicle UEs per cluster with a coverage probability of approximately 99% for the 400, 625 and 900 antenna elements with 10, 13 and 17 UEs per cluster, respectively. We observe that the 1600 antenna elements will achieve $\approx 88.7\%$ coverage for 13 vehicle UEs per cluster corresponding to a traffic scenario with 40 clusters which thereafter decreases with an increasing number of vehicle UEs.

To further analyse the coverage performance, we illustrate in Fig. 4.14 the SINR coverage performance for a varying number of clusters at a -5 dB threshold as a

function of a different number of HAP antenna elements. We observe that SINR coverage performance as shown in Fig. 4.14 and irrespective of the number of antenna elements, at least a 95% coverage is achieved with 30-50 clusters. Coverage performance decreases with increasing size of the HAP antenna array for the network scenario with 10 clusters. We also observe that as the number of clusters increases coverage performance increases with an increasing number of antenna elements. Specifically, this behaviour is observed with a 100 and 200 cluster scenario. Similarly, we observe that the 30, 40 and 50 clusters attain over 95% coverage irrespective of the number of antenna elements with a network scenario comprising 50 clusters performing marginally better at approximately 98%. Also, the 10 cluster scenario exhibits poorer performance with coverage probability decreasing with an increasing number of antenna elements. Between 30-50 clusters, the SINR coverage performance is above 95%. As we increase the number of antenna elements, coverage performance also increases. By examining Fig. 4.10 and Fig. 4.14, it is evident that at a threshold of -5 dB, a traffic scenario with 50 clusters can achieve at least a 88% coverage performance.

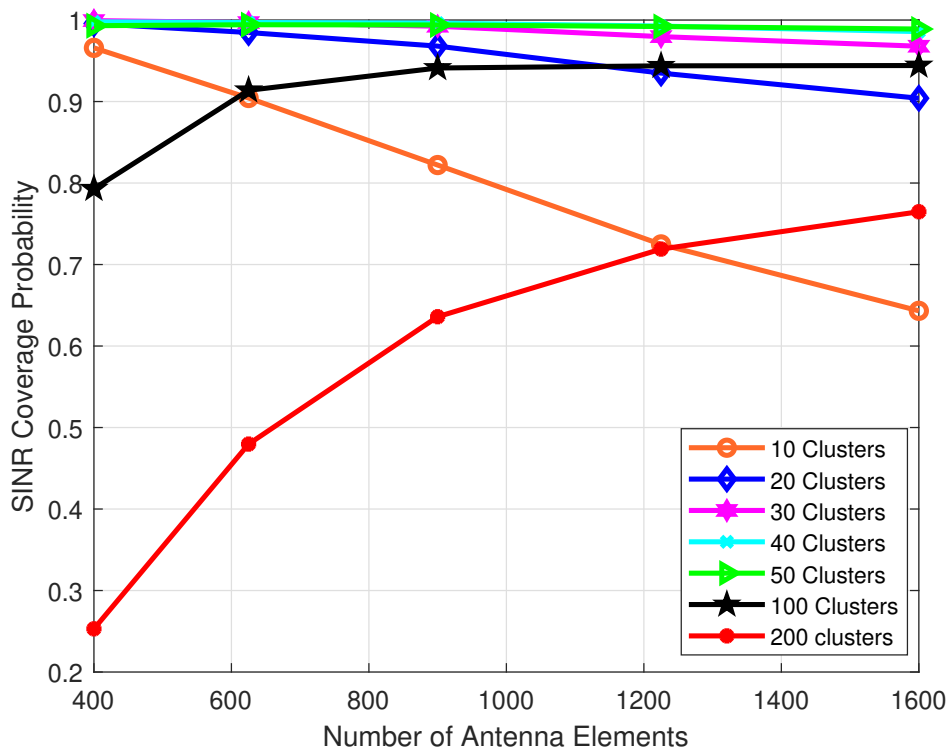


FIGURE 4.14: SINR Coverage probability for different number of clusters

4.5.4 CDF Distribution

We present the cumulative distribution function (CDF) for SINR link quality performance for 50 clusters in Fig 4.15 with the 5th percentile CDF used to represent UEs at the edge of the beam coverage. The CDF plot shows that the performance is generally poor for the 5th percentile UEs. The median SINR for the 400 antenna elements is 2 dB. We also observe the superiority of the 1600 antenna element, which has a higher SINR performance. This is not surprising as higher directionality can be obtained with signal power concentrated to the UE in the cluster. Clearly, by increasing the number of antenna elements, a higher main lobe gain is obtained which results in a higher SNR. Additionally, we observe that approximately 75% of the vehicle UEs achieve an SINR greater than 0 dB. Typically, it is expected that UEs at the edge of a cluster will have poor SINR performance. Taking the 400 antenna elements as a reference, we observe from the figure a mean SINR of approximately 0.4 dB for UEs at the edge of HAP beam coverage.

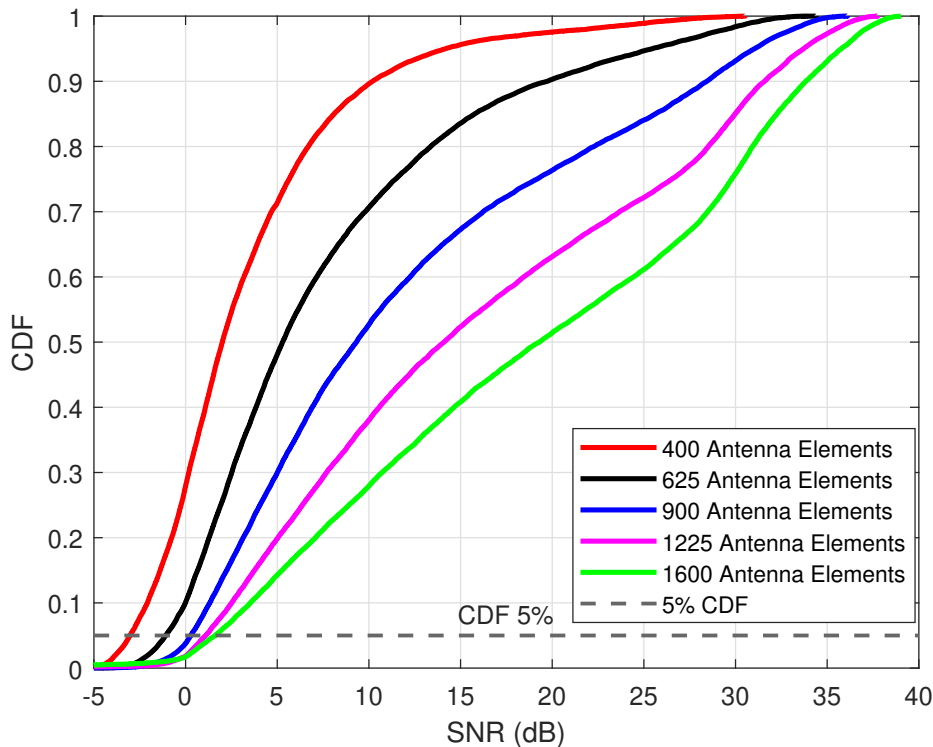


FIGURE 4.15: CDF of SINR for 50 clusters

4.5.5 UE Throughput Performance

The average UE throughput per cluster is defined as the ratio of the sum of the UE throughput to the total number of UEs in each cluster and is presented in Fig.

4.16 for a different number of antenna elements. We observe that the UE throughput increases as the number of clusters increase with the average user throughput remaining relatively constant for a network scenario of 10-20 clusters. Beyond this, increasing the number of HAP beams or clusters will increase the average UE throughput.

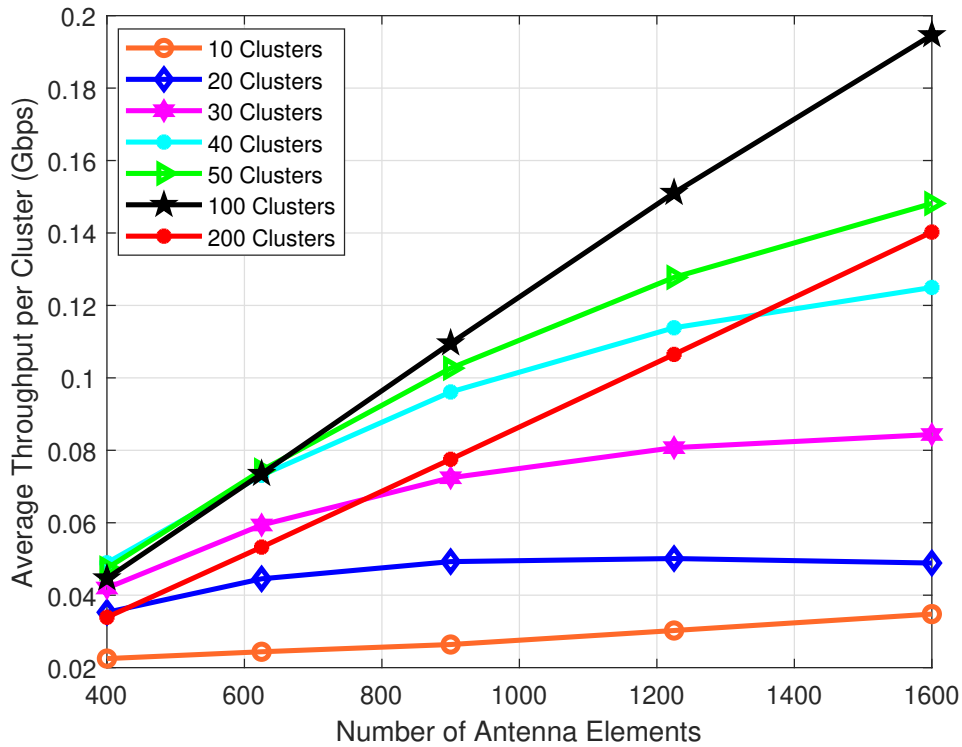


FIGURE 4.16: Average Throughput per cluster vs Number of antenna elements

For example, with a network scenario of 100 and 200 clusters, the average UE throughput increases with a maximum of approximately 0.19 Gbps and 0.14 Gbps with a 1600 antenna element array. We also observe the increased impact of inter-beam interference on the clusters with a lower average user throughput observed for all the cluster scenarios considered. This effect is particularly observed as the number of clusters increases. Specifically, we observe for the 200 cluster scenario, an average UE throughput of 140 Mbps for 1600 antenna elements and a median UE throughput of 82 Mbps. With an increasing number of clusters, the UE throughput is determined by the level of interference experienced in each beam and a function of the number of antenna elements with a much higher received signal power leakage in adjacent beams. We also observe that for the 10 and 20 cluster scenarios, the average UE throughput is approximately constant between 1225 and 1600 antenna elements. We attribute this to the fact that the average throughput of vehicle UEs

in the 10 cluster traffic scenario has throughput equal to the average throughput in the 20 cluster traffic scenario for the same number of antenna elements.

Fig. 4.17 depicts the average user throughput plot as a function of the average number of UEs per cluster. We observe that variations in the number of vehicle UEs in the cluster have an effect on throughput performance with the average user throughput decreasing as the number of vehicle UE increases. Surprisingly, with fewer UEs, throughput initially increases, but with an increasing number of clusters, the throughput degrades.

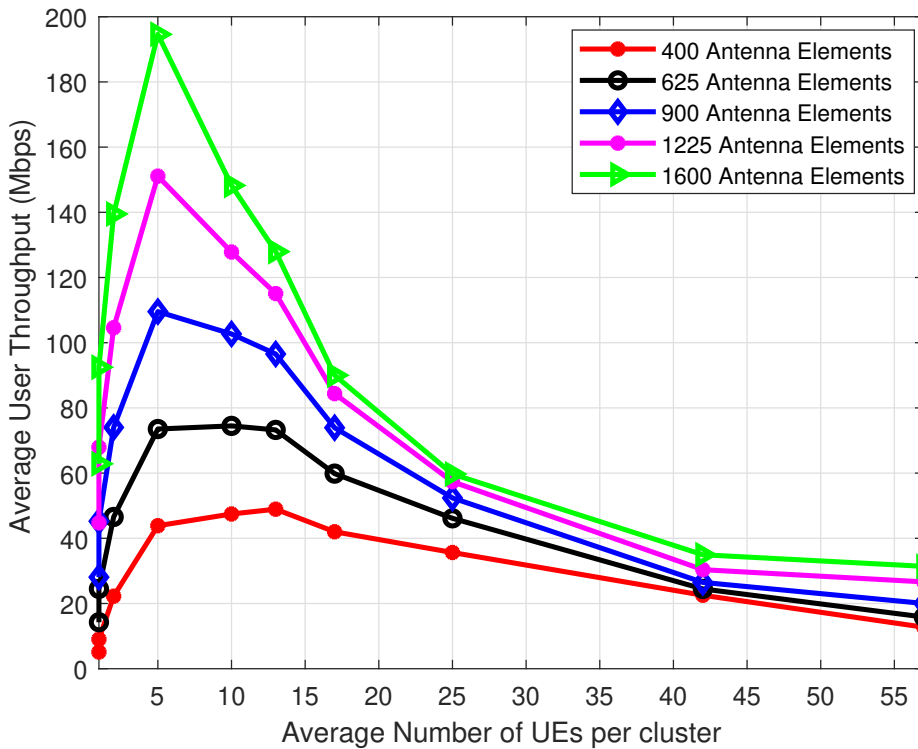


FIGURE 4.17: Average User throughput vs number of UEs per cluster

Next, we show in Fig 4.18, the cumulative distribution function (CDF) plot of the achievable UE throughput for varying numbers of antenna elements. We observe that the 1600 antenna element has a higher throughput performance with a minimum capacity of 10 Mbps. Obviously, as the number of antenna elements per HAP antenna array increases, the capacity also increases.

4.6 Coverage Probability and Throughput Performance under Ideal Interference Mitigation

For the typical system scenario considered, the full frequency reuse will cause inter-beam/ co-channel interference such that the ground UEs will have a degraded

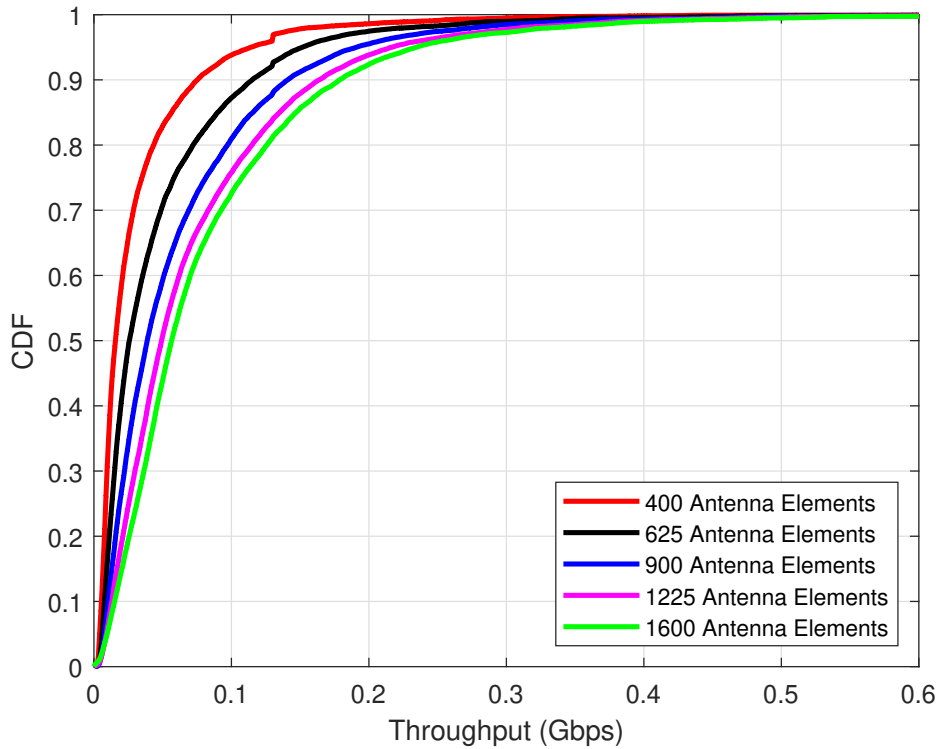


FIGURE 4.18: CDF of Capacity for different antenna elements

performance. However, with appropriate interference mitigation schemes such as coordinated multi-point (CoMP) or dynamic inter-cell interference coordination (ICIC) [198], inter-beam interference can be mitigated such that the system capacity and performance are constrained by the channel noise. In this situation, the system is considered to be noise-limited. Improved performance in terms the coverage probability and UE throughput can therefore be obtained. The performance improvement is as illustrated in Fig. 4.19. This shows that for a scenario with 30-100 clusters, coverage probability is greater than 95% for SNR thresholds up to 25 dB. Beyond this threshold, coverage probability reduces with coverage probability reducing to zero beyond 35 dB. In comparison to Fig. 4.10, we observe approximately a 20 dB difference in the SINR threshold compared to the SNR thresholds for between 40-100 clusters. employed.

Similarly, in Fig. 4.20, we illustrate the average throughput performance of the system when constrained by channel noise only. We observe again the significant performance improvement obtained when compared to Fig. 4.16 Taking the 200 cluster scenario as a reference, the results show an upper-bound performance of 0.92 Gbps with 1600 antenna elements and a lower-bound performance 0.8 Gbps with 400 antenna elements. In comparison, Fig. 4.16 shows that the SINR throughput performance achieves an upper bound of 0.14 Gbps and a lower bound average

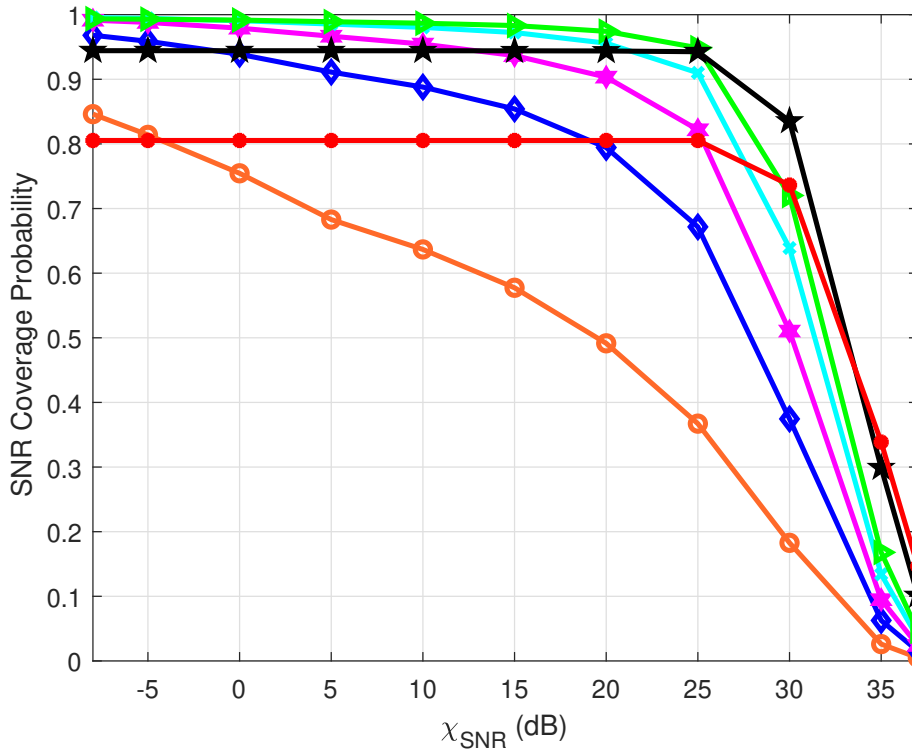


FIGURE 4.19: SNR coverage probability for different SNR thresholds

throughput per cluster of approximately 0.038 Gbps with 400 antenna elements. This shows an upper bound performance difference of 0.78 Gbps for the 1600 antenna elements and lower bound of 0.10 Gbps corresponding to a 147% difference in the average throughput per cluster between the SNR and SINR with 1600 antenna elements.

From Equation (4.26) and the preceding discussions, it is clear that for a fixed HAP transmit power, capacity is a function of coverage probability and a log function of the SNR or SINR thresholds. In other words, as the SNR or SINR threshold increases, the coverage probability decreases, whereas capacity increases. Specifically, the results from Fig. 4.17 and Fig. 4.11 show that a maximum average UE throughput is obtained in a traffic scenario with 100 clusters and a maximum coverage performance obtained with a lower bound of 30 clusters and an upper bound of 50 clusters. This clearly shows the conflicting impact of addressing both coverage and capacity objectives of the system at the same time, as capacity cannot be increased without sacrificing coverage performance, and vice versa. With the traffic scenario considered, one may argue that an appropriate solution to the capacity performance is one that balances the UE distribution across the beams. While this solution may be optimal for the network in an interference free scenario, it becomes

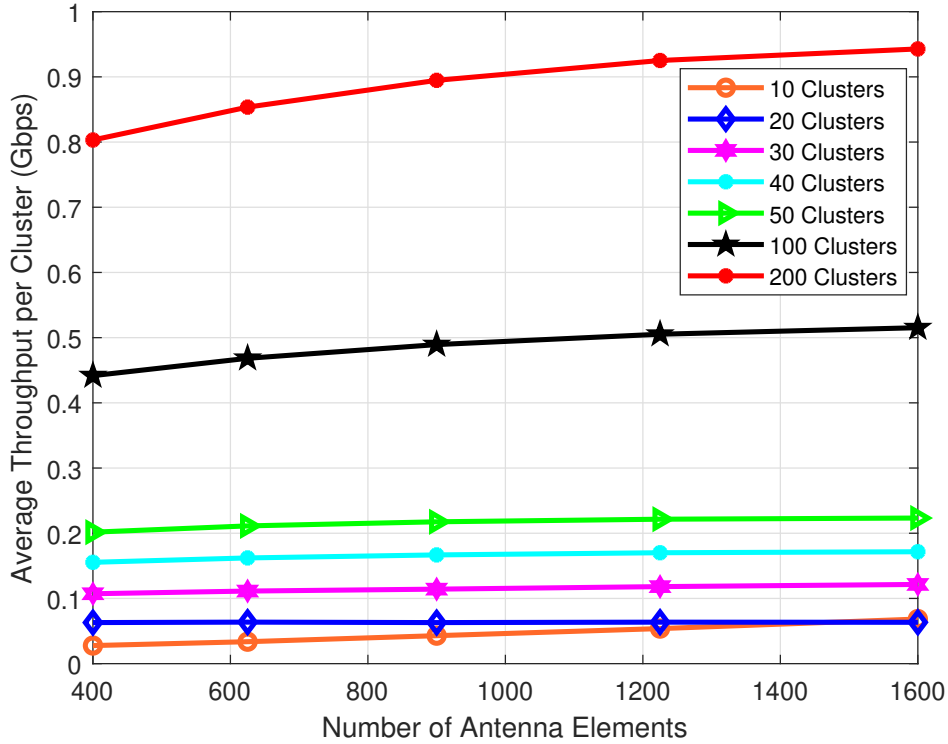


FIGURE 4.20: Average Throughput per cluster vs Number of antenna elements

a challenge in a scenario with significant interference due to the increased interference with a large number of HAP beams.

4.7 A Dynamic Fractional Frequency Reuse (D-FFR) Scheme

To efficiently utilize the available bandwidth and mitigate the inter-beam interference, frequency reuse schemes higher than 1 can be utilized between the clusters to deliver an improved SINR and spectral efficiency. In the traditional reuse-1 scheme employed in Sec. 4.5, all of the available bandwidth is reused in adjacent clusters and this causes interference, especially for clusters that are close to one another. The SINR and UE capacity are significantly affected by the inter-beam interference, particularly for UEs at the edge of coverage. This will result in an increased outage probability and lower UE capacity. To improve the signal quality, a Dynamic Fractional Frequency Reuse scheme (D-FFR) is employed with the available bandwidth divided into a full-reuse and partial-reuse sub-bands based on the number of UEs at the centre and edge of the cluster, respectively. The UEs at the cluster centre are determined based on their received signal power being higher than a threshold value P_{thr} and can utilize the full reuse bandwidth, otherwise, they are considered as cell-edge UEs. If the available bandwidth is not utilized by UEs at the cell-edge,

they may be utilized by the cluster centre UEs and a higher power allocated to the edge UEs to counter the reduced SINR and UE capacity. Similarly, a re-use distance is employed in the partial re-use sub-band to maximize the distance between each sub-band. We have used the D-FFR scheme in this work as it offers significant improvements in the spectral efficiency of cell-edge UEs, has low computational complexity and does not require precise knowledge of the receiver channel state information (CSI). Therefore, with an adequate knowledge of the receiver CSI obtained from the UE position information, we exploit D-FFR to improve the SINR and increase the UE capacity at the centre and at the edge of the HAP coverage. This will also offer also offer significant improvement in the the spectral efficiency of UEs at the edge of coverage. We depict in Fig. 4.21 an illustration of the D-FFR scheme with full and partial reuse at the centre and edge areas of coverage, respectively.

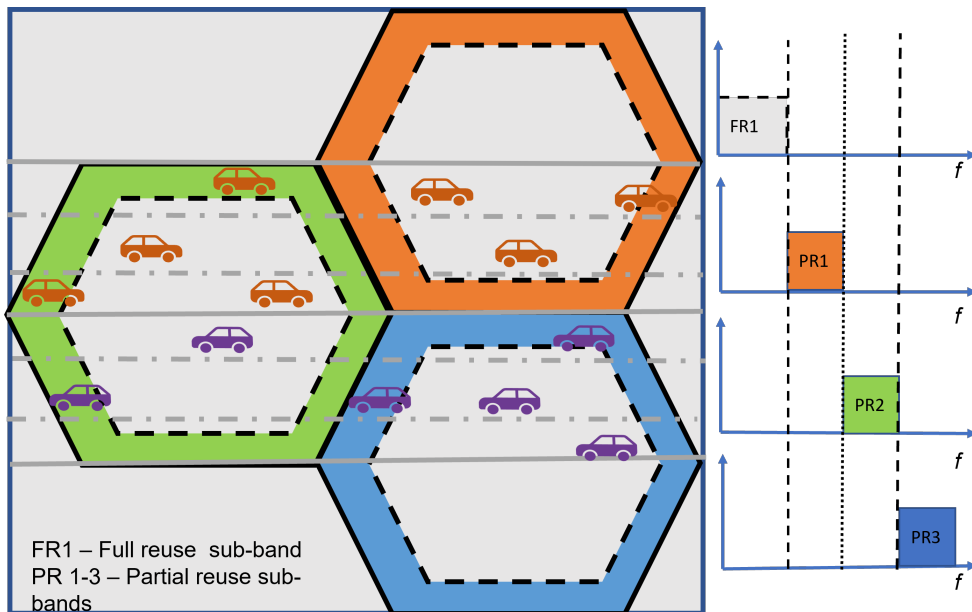


FIGURE 4.21: Geometry of Dynamic Fractional Frequency Reuse (D-FFR)

The total bandwidth BW_T is therefore expressed as:

$$\begin{aligned}
 BW_T &= BW_{FR1} + BW_{PR}, \\
 BW_{PR} &= BW_{PR1} + BW_{PR2} + BW_{PR3}, \\
 &= \frac{1}{3} (BW_T - BW_{FR1})
 \end{aligned} \tag{4.27}$$

For each vehicle UE in the cluster, the highly dynamic UE movement means that the interference changes depending on the position of the vehicle UE. This changes the effect of interference for each set of adjacent beams considered, making it complex to analyse the performance of the entire system. Therefore, for simplicity, we

consider a 5-cluster scenario and evaluate the performance of the UEs in the cluster with and without D-FFR based on the averaged instantaneous snapshots which represent copies of the network at different time periods.

We show in Fig. 4.22 the CDF of the SINR performance with and without the D-FFR scheme. We observe that in the scenario without D-FFR, the UEs experience significant interference which degrades the SINR with approximately 48% of UEs experiencing an SINR performance below zero. Specifically, for the UEs at the cell edge (represented by the dashed line in Fig. 4.22, i.e., the 5th percentile CDF of SINR), we observe that the SINR performance is poor with the interference power significantly higher than the received signal power especially for UEs at the cell edge. The high interference degrades the performance of the system and affects the overall system throughput. However, with the D-FFR scheme (as observed with the red curve), we observe a significant reduction in the interference due to the influence of the different frequency sub-bands. This leads to an increase in the propagation distance between adjacent interfering beams and therefore, the inter-beam interference decreases.

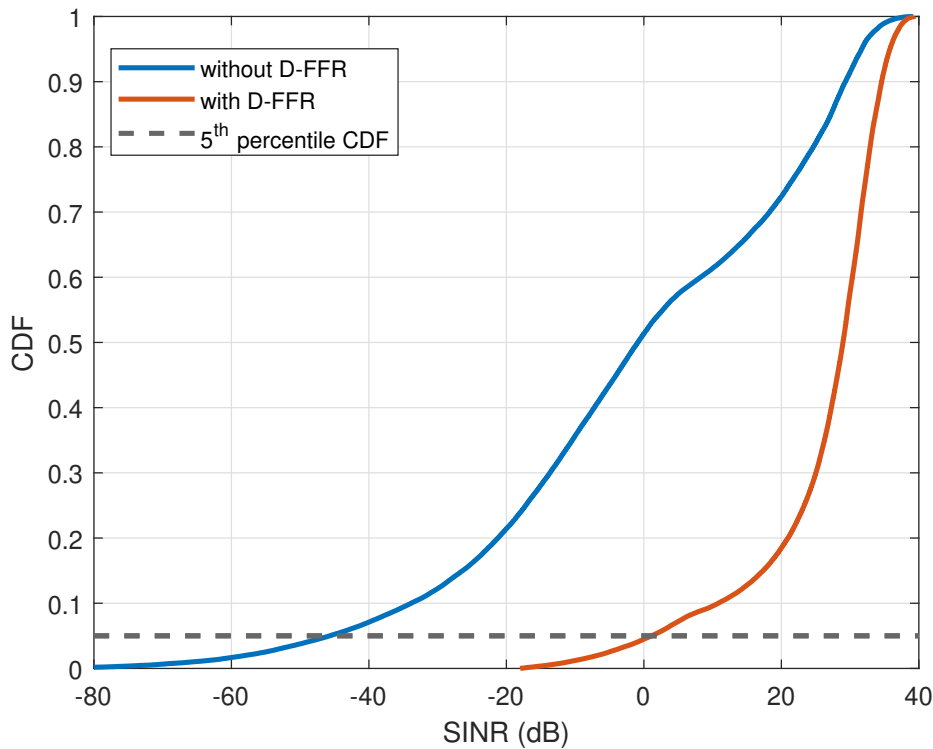


FIGURE 4.22: CDF of SINR with and without D-FFR

In Fig. 4.23, we illustrate the CDF of UE capacity for UEs above a -5 dB SINR threshold with D-FFR scheme and without D-FFR. We can easily observe a significant performance improvement in the UE capacity due to the a reduction in the

inter beam interference with more UEs having an SINR greater than -5 dB threshold. This means the SINR of the UEs is effectively increased which shows that the system benefits from the D-FFR scheme as opposed to without D-FFR.

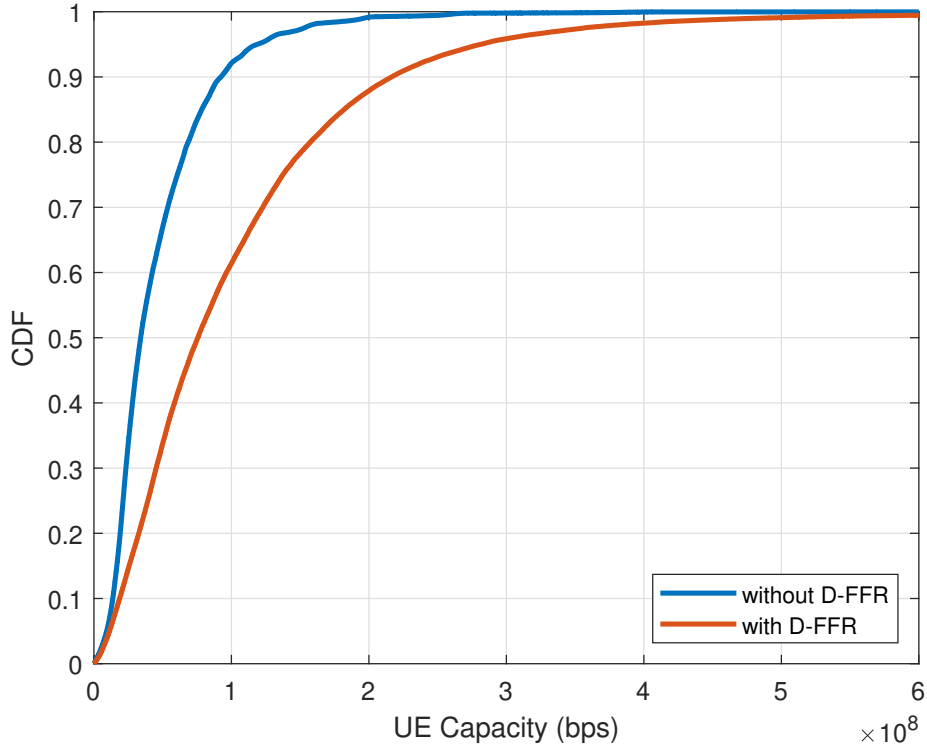


FIGURE 4.23: CDF of UE capacity with and without D-FFR

4.8 UE Trajectory Performance

In the following discussion, we investigate the performance of arbitrarily selected vehicle UEs in the clusters considered over the vehicle trajectory. For this, we illustrate scenarios for 30, 40 and 50 clusters which as shown in Fig.4.14 achieves an average coverage probability of at least 95%. Here, our goal is to investigate from a user-centric perspective how dynamic changes in position and direction of the vehicle UE over time impacts the link quality for a varying number of clusters. We remark that the small subset of arbitrarily chosen vehicle trajectories is not necessarily representative of the link quality for the entire set of vehicles considered; nonetheless, it gives an insight about the link quality for vehicles travelling in the simulation area and offers an idea of the SNR and SINR link quality that is attainable by other vehicles.

We select two UEs: a UE with a North to South heading (magenta curve) and East to West heading (cyan curve), which we hereafter refer to as veh_{id7} and veh_{id9} respectively and show in Fig. 4.24 the pair of vehicle trajectories. For our analysis,

we utilise a 1 s snapshot interval to better capture the vehicle performance over time and present the SNR and SINR performance for veh_{id7} and veh_{id9} from $t_{initial}=0$ sec to $t_{final} = 1659$ secs and 2258 secs respectively. Given the vehicle trajectories, we also investigate the throughput performance of the selected vehicle over the trajectory.

We begin by illustrating the contour snapshots of the SNR and SINR link quality trajectories in Fig. 4.25 for a 30, 40 and 50 cluster traffic scenario utilising 1600 antenna elements. A visual comparison of these plots show, as expected, the good performance is obtained within the SNR regions with veh_{id9} experiencing a significantly better SNR performance gain to the vehicle veh_{id7} . Based on the vehicle velocity and depending on the current position of the vehicle UE, we observe increased interference for veh_{id9} , which increases with increasing distance from the HAP.

Specifically, we observe an approximate peak SNR of 39 dB for the SNR scenario. For the SINR scenario, we observe that the resulting SINR contours exhibit considerable distortions as the number of beams increases. This is due to increased interference from neighbouring beams, which causes the mainlobe beam to be pushed away from the intended beam centre.

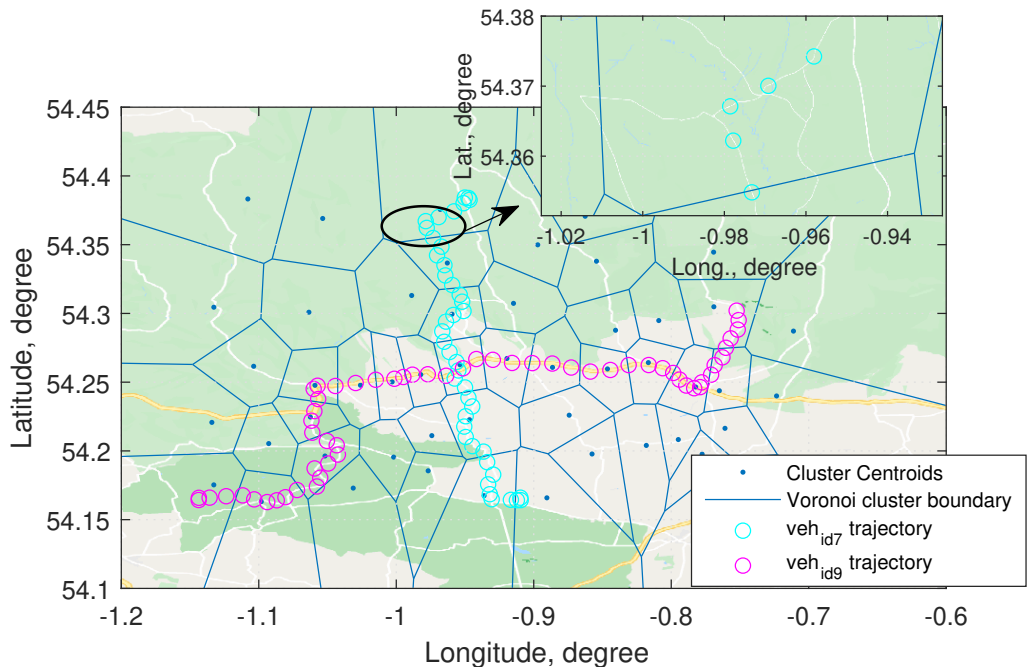


FIGURE 4.24: Coverage Map of vehicle trajectory

An illustration of the SNR and SINR trajectory for the vehicle UE in the contour plots depicted in Fig. 4.25 is presented in Figs. 4.26, 4.27 and 4.28. For the vehicle trajectory over time, an instantaneous outage will likely occur depending on the

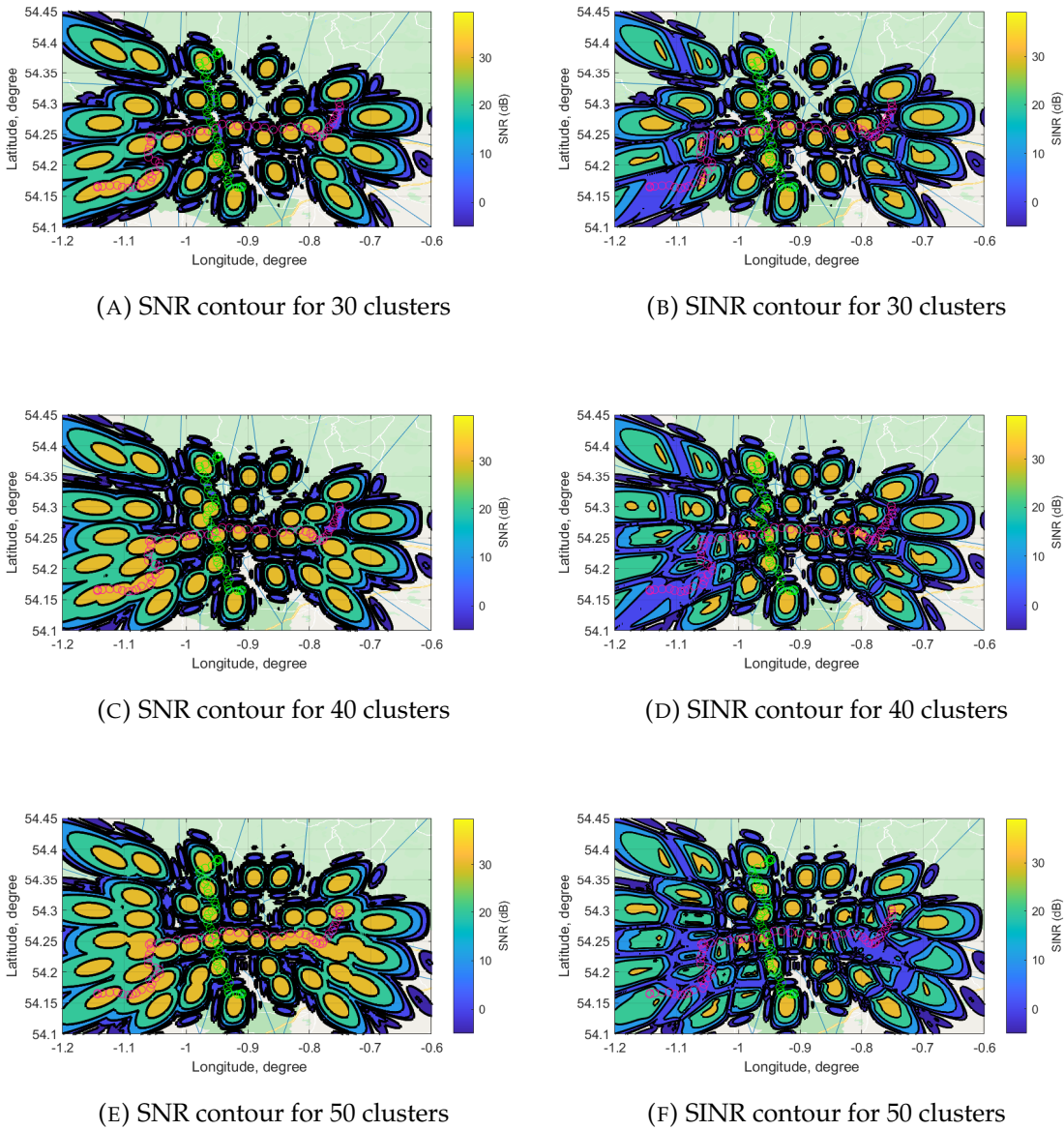


FIGURE 4.25: SNR and SINR Vehicle Trajectory

signal quality experienced by the vehicle UE. This momentary drop of the signal below the minimum threshold may not have a significant effect on the outage performance of the system. However, the duration of the outage becomes significant. In other words, the average duration of the time period at which the UE stays below the minimum χ_{SNR} and χ_{SINR} threshold and frequency of outage determines the outage performance.

In Fig. 4.26, veh_{id7} initially experiences a peak SNR/SINR between at different times with a maximum of 37 dB. This is due to the vehicle travelling within contours of

high SNR/SINR indicated by the yellow contour regions. The vehicle UE also experience momentary dips in the SNR/SINR at various times over its travel trajectory. The decrease in link quality occurs over a total period of 180 s, accounting for approximately 11% of the total travel time. This decrease is mainly due to inadequate beam coverage for the 30 cluster traffic scenario due to an increase in the coverage holes. Therefore, seamless coverage is not guaranteed for veh_{id7} in the 30 cluster traffic scenario. A further observation from Fig.4.26 is that the SINR performance of the vehicle UE closely tracks the SNR, which indicates a reduced effect of interference for the vehicle UE. This is observed from the contour plots of Fig. 4.25a and Fig. 4.25b respectively. We note that such SNR/SINR degradation observed over long periods with veh_{id7} will be challenging for mmWave vehicular networks as the benefits of beamforming will not be achieved due to poor link reliability.

For veh_{id9} in Fig. 4.26, we observe that the link quality performance is significantly improved with an increased peak SNR/SINR over the vehicle trajectory. Specifically, we observe regions of higher SNR/SINR contours due to a continuous, usable beam overlap for the vehicle UE with a maximum SNR and SINR of approximately 39 dB and 38 dB, respectively. Coverage for the vehicle UE is achieved for 99% of the vehicle trajectory. Also, we observe a dip in SNR/SINR occurs for approximately 15 s between $t = 2032$ s and $t = 2047$ s of the vehicle trip, corresponding to a 0.66% outage duration of the vehicle travel time. This means veh_{id9} experiences fewer outages compared to veh_{id7} .

For the 40 cluster traffic scenario in Fig. 4.27, we observe that similar to Fig.4.26 for veh_{id7} , the SINR performance closely tracks the SNR performance with an average outage of 8.08%. We observe again the impact of coverage holes and interference on performance due to an increased number of clusters. Performance degradation in the link quality is observed for veh_{id9} between $t = 2032$ s to $t = 2045$ s corresponding to 0.58% outage duration. For the SINR link quality, we also observe the increased effect of interference due to an increased number of clusters, particularly between $t=1$ s and $t= 1065$ s.

In Fig. 4.28, we present the performance of veh_{id7} and veh_{id9} with a 50 cluster traffic scenario. An increase in SNR and SINR performance is observed for both vehicle UEs compared to the 30 and 40 cluster traffic scenarios. For instance, for veh_{id7} , the frequency of the momentary outages over the vehicle travel period due to outages is observed to be approximately 99%. Also, we observe a maximum outage duration of 16 s from $t = 359$ s to $t = 374$ s. The total outage duration is obtained at 34 s, corresponding to an average outage probability of 2%. This means that SINR and SNR performance drops below the threshold for less than 2% of the time, with the vehicle UE experiencing a coverage probability of approximately 98%. For veh_{id9} , we observe the link quality performance is consistently above the -5 dB threshold

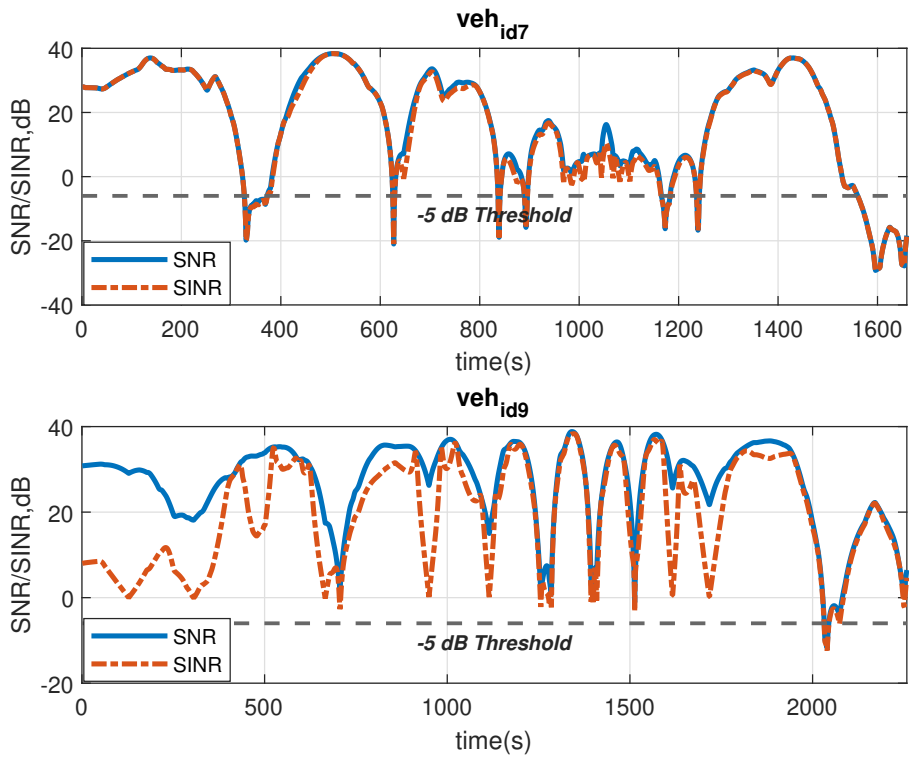


FIGURE 4.26: 30-cluster SNR/SINR trajectory

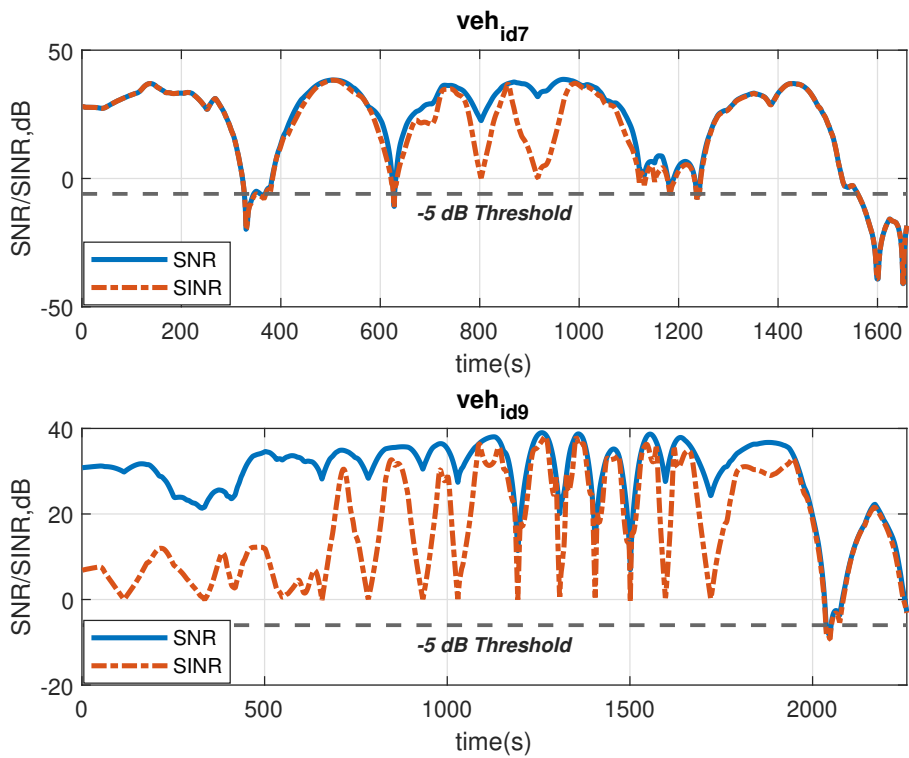


FIGURE 4.27: 40-cluster SNR/SINR trajectory

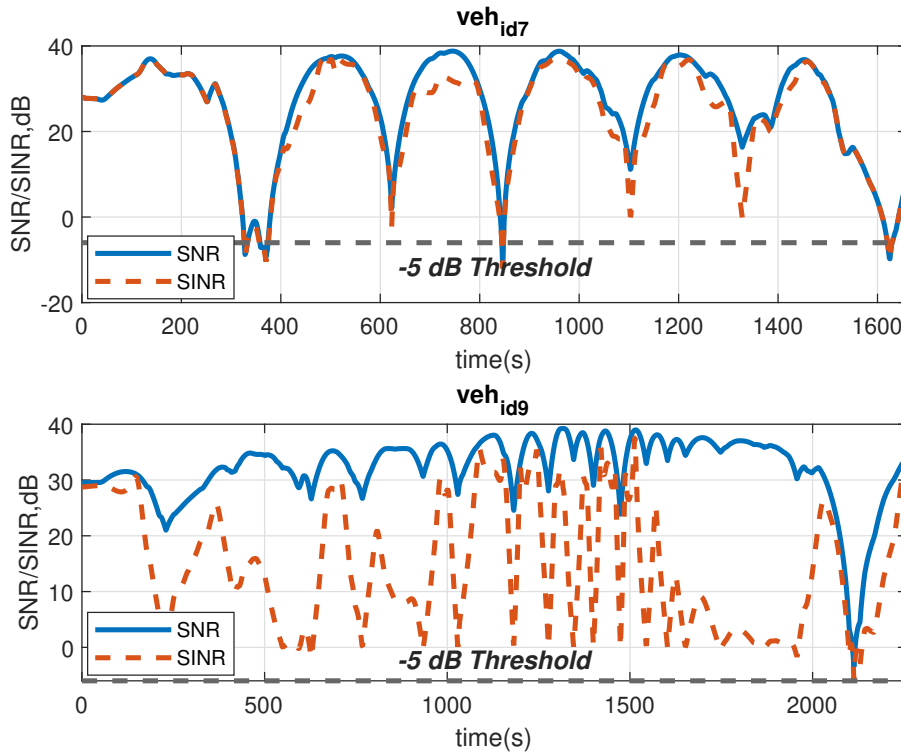


FIGURE 4.28: 50-cluster SNR/SINR trajectory

for the duration of the vehicle travel time. The figure also shows the worst-case performance for the vehicle UE occurs between 1500 s to 1890 s with SINR decreasing to approximately 0 dB.

4.9 Throughput Trajectory Scenario

In Fig. 4.29, Fig. 4.30 and Fig. 4.31, we present the throughput plots for both the SNR and SINR performance over the vehicle trajectory for veh_{id7} and veh_{id9} for a 30, 40 and 50 cluster scenario. The spatio-temporal channel conditions of the vehicle UEs is also reflected in the throughput variation since the UE distance from the HAP determines the path loss and, consequently, the link quality. We observe that the maximum throughput for veh_{id7} is approximately 228 Mbps. It is also worth noting that similar to the SNR and SINR performance in Fig. 4.26, the throughput performance of Fig. 4.29 follows a similar trend with both SNR and SINR throughput performance approximately equal. The variation in SNR throughput and SINR throughput for veh_{id7} in Fig. 4.29 is observed to decrease to a minimum of 0 Mbps which can also be observed from the SNR and SINR trajectory in Fig 4.28 between $t = 330$ s and $t = 374$ s. This occurs when the SNR and SINR performance decreases below the -5 dB threshold, for a total outage duration of 34 s, corresponding to approximately 2% outage duration for the vehicle UE.

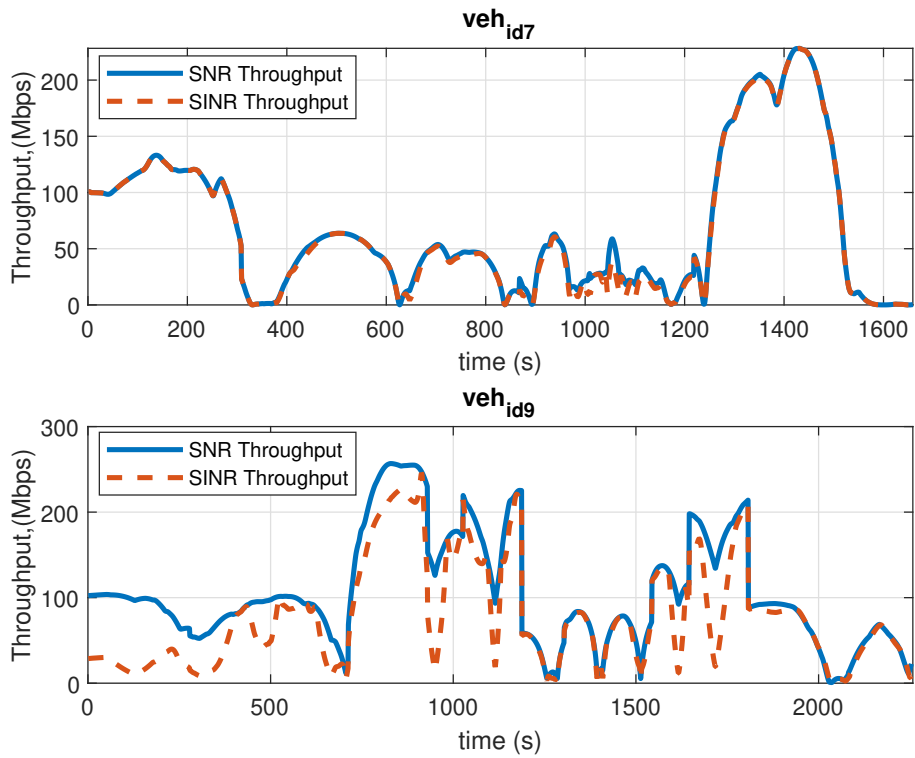


FIGURE 4.29: 30-cluster SNR/SINR Throughput

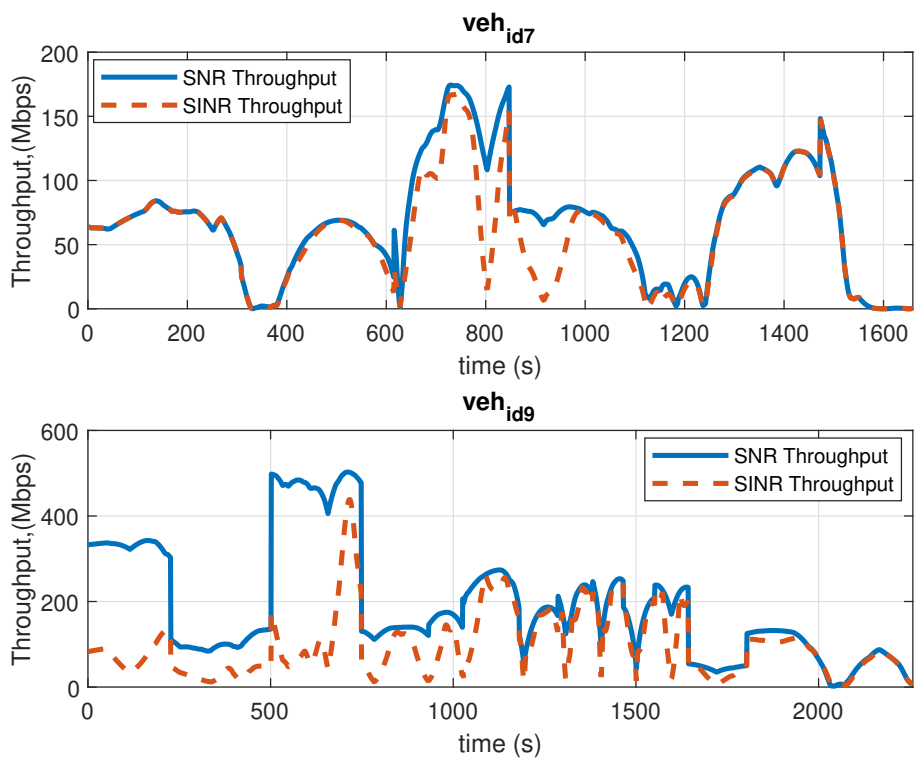


FIGURE 4.30: 40-cluster SNR/SINR Throughput

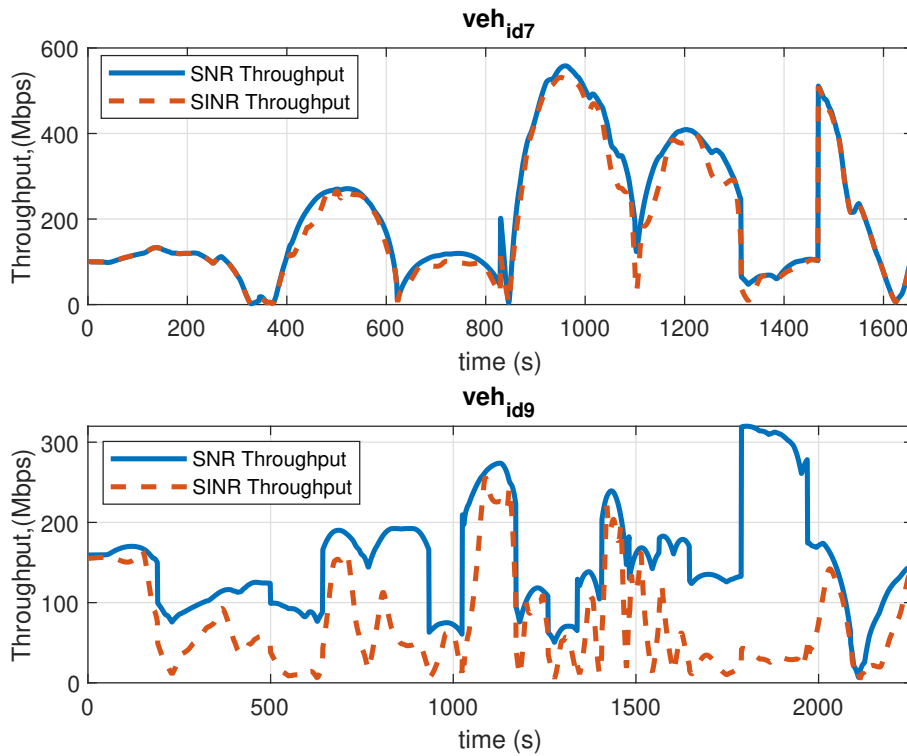


FIGURE 4.31: 50-cluster SNR/SINR Throughput

From Fig. 4.27, we can observe the SNR and SINR link performance drops below the -5 dB threshold at $t = 2032$ s, with UE throughput also reducing to zero in Fig. 4.30. This observation indicates that the UE cannot decode information successfully from the HAP as the UE SNR and SINR is below the threshold. The figure also reveals an upper bound SNR throughput performance of 174 Mbps for veh_{id7} and 512 Mbps for veh_{id9} . In Fig. 4.31, the throughput performance for a 50-cluster traffic scenario is presented. We note that the degradation of throughput performance is more severe in the worst-case SINR throughput, particularly for veh_{id9} . From this figure, we also observe a peak SNR throughput performance at 558 Mbps for veh_{id7} and 310 Mbps for veh_{id9} . The figure also shows that due to high interference generated in the network for an increased number of clusters, the SINR throughput performance drops to as low as 5 Mbps for veh_{id9} with an increased performance gap observed between the SNR and SINR throughput performance.

4.10 Conclusion

This chapter has investigated the impact of different number of antenna elements per HAP array on different clusters and their effect on the coverage probability, downlink SINR and the achievable user throughput. The trade-off between the coverage probability and the achievable user throughput for a different number of

clusters has been illustrated. Results have shown that increasing the number of clusters will decrease the downlink SINR. We have shown that with an increasing number of clusters, the interference degrades performance with interference coordination techniques required to achieve the required quality of service (QoS). Furthermore, we have shown the coverage probability performance for a different number of clusters and a different number of antenna elements. Additionally, we have also investigated the coverage probability and UE throughput performance when system performance is constrained by the channel noise only. We have also characterised the trade-off between the number of vehicle UEs and coverage probability with results showing the coverage and UE throughput performance for a traffic scenario with varying clusters and utilising a different number of HAP antenna elements. A characterization of the coverage-capacity trade-off behaviour for a varying number of clusters and various number of antenna elements has also been investigated as well as a UE-centric throughput performance for selected vehicle UEs. Given a particular traffic scenario, our investigation may be used to arrive at a good approximation to the appropriate number of beams and achievable UE capacity with a projected coverage probability requirement which can provide significant insight for vehicular content delivery in a rural geographical area based on prior information about the traffic demand.

Chapter 5

Optimal Relay Selection for a HAP-assisted Vehicular Network

5.1 Introduction

This chapter investigates an optimal relay selection scheme in an emerging area of research known as cooperative vehicular networking (CVN) [199]. CVN enables neighbouring vehicles to share information at different network layers via multiple transmission alternatives, thereby enhancing the transmission rate of UEs with poor channel conditions, and as a result, the network coverage. CVN leverages the broadcast nature of wireless communication; that is, when a source (a vehicle UE or the infrastructure) broadcasts a message, other vehicles in the network with good channel link quality can assist in relaying the message to its destination. As the vehicles cooperate with each other directly or via the infrastructure, CVN provides spatial diversity and improved network connectivity [199]. The vehicle UE that aids in data transmission is commonly referred to as the *relay UE*.

5.1.1 Cooperative Relay Transmission Protocol

Typically, UEs will associate with the link that provides the maximum SNR or SINR to achieve a higher network coverage and capacity. For a relay link, there is a need to select a first-hop link with good channel quality to maximize the reliability and throughput performance of the network. In the literature, several relay selection approaches based on the link quality, direction of travel, traffic density, received signal power [200], e.t.c., have been proposed. However, an important consideration for the evaluation of the performance of the relay selection is the choice of the the cooperative relay transmission protocol. Primarily, the two main transmission protocols are: (1) *amplify and forward (AF)* and (2) *decode and forward (DF)* [201].

In AF, the received signal at the relay is amplified and forwarded to the destination UE with the SNR at the destination UE expressed as:

$$\gamma_{AF} = \frac{\gamma_{SR}\gamma_{RD}}{\gamma_{SR} + \gamma_{RD} + 1} \quad (5.1)$$

where γ_{SR} and γ_{RD} are the SNR at the source to relay and relay to destination link respectively.

In DF, the relay UE decodes and re-encodes the received signal before it is forwarded to the destination UE. The link performance is dependent on the decoding complexity of the relay. The equivalent SINR at the destination UE is given by:

$$\tilde{\gamma}_{DF} = \min \left\{ \tilde{\gamma}_{SR}, \tilde{\gamma}_{RD} \right\} \quad (5.2)$$

where $\tilde{\gamma}_{SR}$ and $\tilde{\gamma}_{RD}$ are the equivalent SINR for the source to relay and relay to destination links, respectively. Regardless of the relay transmission protocol utilized, a proper selection of a relay UE is critical to improving the link reliability and the overall performance of the network. A scenario where information from the source (i.e., the HAP) is relayed to destination UEs via a relay UE is envisaged. Our goal is to determine the best relay UEs by formulating the relay selection as an optimization problem for all relay-destination pairs, with the aim of maximizing the data rate of the destination UEs. We illustrate this scheme with a simple scenario as shown in Fig. 5.1. Specifically, the HAP UE denotes the set of all possible UEs that are served by the HAP and which satisfy an SINR constraint. Vehicle UEs from this set are selected as relay UEs in a situation where a direct link from the HAP is unavailable.

By leveraging a cooperative communication link, destination UEs can increase their transmission rate and extend the network coverage. A possible solution to the relay selection can be obtained via an exhaustive search among all candidate relay UEs. However, this will incur a high computational complexity with an increasing network size which makes it infeasible for practical applications. Therefore, in this chapter, we propose a multi-UE relay selection algorithm that strikes a trade-off between performance and complexity. The proposed algorithm operates under the following constraints: (a) each destination UE can only be assisted by at most one relay UE which has a good channel quality link to the HAP, (b) each relay UE can only select at most one destination UE. The algorithm aims at maximizing the data rate of the destination UEs and offers the benefit of a lower computational complexity compared to the exhaustive search approach.

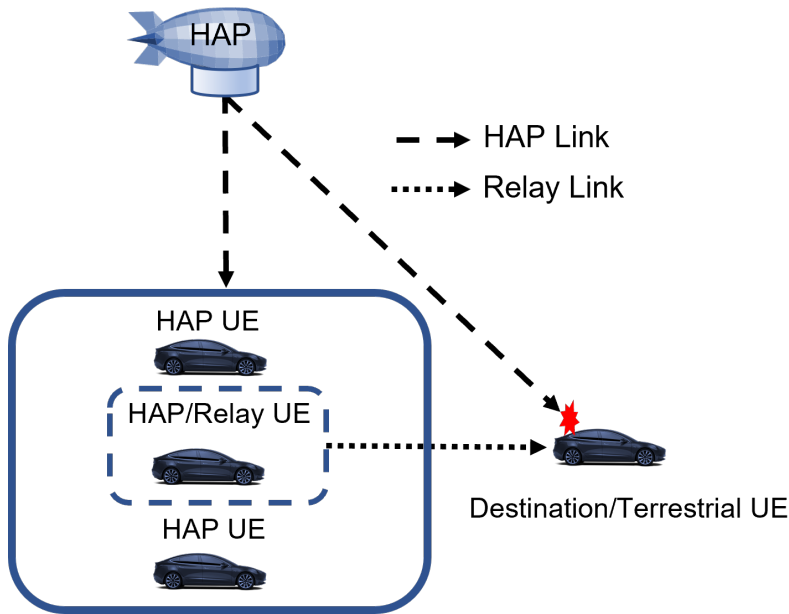


FIGURE 5.1: A V2V relay assisted communication

5.2 Related Work

In the literature, there exists a rich body of studies on the relay selection schemes [202], [122]. The results of these studies have demonstrated that the selection of relay UE is one of the most effective ways to improve the link reliability and enhance the performance of the network.

In the terrestrial domain, studies in [203], [200] have investigated relay selection techniques to enhance data dissemination to vehicular networks when outside the coverage area of an RSU. Specifically in [200], a multi-hop bi-directional relay selection scheme was investigated where relay UEs were selected based on a link estimation algorithm. Their study investigated varying network densities by using three types of V2V broadcast messaging: broadcast packets, application messages, and some additional background traffic. Their results showed performance improvement in packet delivery ratio and the end-to-end delay, especially for dense vehicular networks.

In [204], the authors investigated a relay assignment scheme aimed at maximizing the total capacity of the cooperative network. In this scheme, they present a system model where a relay UE is assigned to multiple destination UEs, otherwise termed a one-to-many relay assignment. Their investigation showed that this method could result in a sub-optimal relay assignment, whereas an optimal assignment would assign at most one relay UE to at most one destination UE, in other words, a one to one assignment. The approach used in this chapter is similar to a one-to-one relay assignment.

In [205], the authors considered the use of parked vehicles as relay UEs. Based on the current traffic conditions for moving vehicles, they proposed the use of selected parked vehicles to work dynamically as relay UEs in an energy efficient manner. By dividing multiple traveling vehicles into clusters, and selecting parked vehicles between the clusters as relay nodes, they were able to show that their algorithm achieved a higher rate of information exchange and increased connectivity between the vehicles.

A multi-metric relay selection scheme was evaluated in [206] where a mobility metric and received signal strength were utilized for relay selection. Using performance metrics of routing overhead, packet delivery ratio and end-to-end delay, they compared their proposed algorithm with a modified ad-hoc on-demand routing protocol (AODV) with results showing improved routing performance of their proposed algorithm. A nearest-first relaying scheme was evaluated in [207] where the nearest UEs are selected as relay UEs based on messages broadcast to all vehicle UE within a communication range.

In the context of an aerial platform vehicular relaying scheme, the authors in [208] formulated the relay selection problem as an interference-aware multi-objective optimization problem where the link transmission rate, communication handover and transmit power were the objective functions. The proposed relay selection scheme was compared with state-of-the-art UAV-assisted relay selection scheme in the literature in terms of data delivery ratio, end-to-end delay and throughput with an improvement in performance observed compared to the other schemes. The authors in [209] investigated a scheme where the relay selection problem was formulated as a multi-objective function of the link quality of service (LQoS) and the UE node forward capacity (NFC), respectively. Based on the defined utility function, they were able to show that the proposed relay selection problem improved the message delivery ratio for the network.

Although the existing studies have investigated relay selection schemes to improve data delivery ratio and throughput, among others, none of the surveyed works have investigated the relay selection for a HAP-assisted vehicular network as most of the work have been focused on the terrestrial and UAV domain. However, due to their distinct differences, models developed for the latter may not be specifically applicable to the former. For instance, due to the constraints of the HAP such as power requirements, the antenna payload characteristics (antenna size, mutual coupling and antenna polarity), optimizing the relay selection approach for the communication scenario can improve improve the quality of the overall system for content delivery. Moreover, in the work by [209], a derivative of the Random Way-point model was used for the traffic model which is not representative of realistic vehicular movements as this may bias the results obtained.

Motivated by the aforementioned discussion, we aim to present a relay selection scheme for the HAP network which can improve the reliability of connectivity and transmission rate performance of the destination UEs thereby improving the network performance.

5.2.1 Contributions and Organization

In this chapter, we investigate a relay selection scheme for the HAP-assisted vehicular network. The performance of the relay selection schemes is evaluated using the criteria of outage probability (OP) and achievable UE throughput.

Our main contributions are as follows:

- We examine a cooperative relay assignment problem for the HAP-assisted vehicular network, which seeks to maximize the total capacity of all relay-destination pairs.
- propose an optimal relay selection scheme by formulating the relay selection problem as an optimisation problem. Using graph theory concepts, we represent the network as a weighted bipartite graph and solve the maximum weighted matching of the graph using the Kuhn-Munkres algorithm from which the relay UE assignments which provide the maximum capacity among all relay assignments is determined.
- Based on the relay assignment solution, we investigate the performance of the proposed scheme based on the successful transmission probability, outage probability and achievable UE throughput. The algorithm is evaluated against three commonly adopted relay selection schemes, namely; a threshold-based relay assignment scheme (TBRA) - which considers the channel quality and selects a relay vehicle with a maximum link threshold, a link lifetime relay selection scheme (LLRS) - which is based on a weighted distance and UE link stability metric, and a random relay assignment scheme (RRA) which selects a random relay vehicle. Finally, we evaluate the performance of the system with and without cooperative relaying.

This chapter is organised as follows. In the next section (Section 5.3), we present the system model. In Section 5.4, we present the problem formulation and in Section 5.5, the proposed relay selection scheme is presented. Section 5.6 presents the performance metric used in the evaluation of the proposed relay selection scheme with simulation results presented in Section 5.7. Finally, we present our conclusions in Section 5.8.

5.3 System Model

The system model of the envisioned network architecture is described in this section and a visual illustration of the proposed relaying scheme is depicted with an example given in Fig. 5.2. We consider the scenario where a UE can receive data from the HAP and cooperatively transmit it to the destination UEs that cannot be served by the HAP. Therefore, we distinguish between three types of vehicle UEs:

- HAP UEs: UEs that are served directly by the HAP, i.e., meet a SNR or SINR threshold criteria. We denote this of UEs by \mathcal{H} .
- Terrestrial UEs: destination UEs with poor channel conditions that cannot be served by the HAP. We denote the UE set by $\mathcal{T} = \{t_{r_1}, t_{r_2}, \dots, t_{r_n}\}$
- Relay UEs: \mathcal{M} denotes candidate relay UEs, which are vehicle UEs in \mathcal{H} , $\mathcal{M} = \{k_{r_1}, k_{r_2}, \dots, k_{r_n}\}$. The set \mathcal{R} represents the set of relay UEs where $\mathcal{R} = \{r_1, r_2, \dots, r_n\}$. In other words, $\mathcal{M} \in \mathcal{R}$.

For a relay UE, we denote it by $k_i \in \mathcal{R}$. This means that \mathcal{M} is a subset of \mathcal{H} and \mathcal{R} is a subset of \mathcal{M} . Therefore,

$$\mathcal{M} = \{k_i \in \mathcal{H} : \gamma_{h_i, k_i} \geq \chi\}, \quad (5.3)$$

For the V2V transmission rate, we denote it by r_{k_i, t_i} . Unless otherwise stated, the definition of notations used and simulation parameters is as given in Table 5.1.

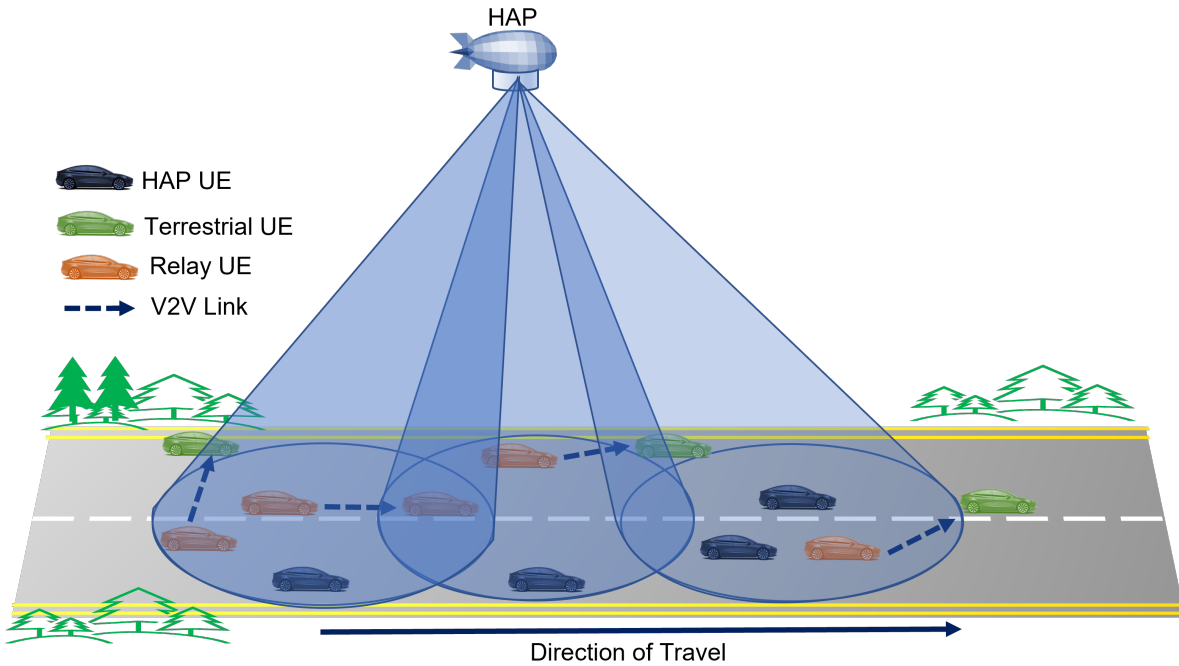


FIGURE 5.2: Network Architecture of relaying scheme

The proposed relay selection scheme selects from the candidate set of vehicle UEs in \mathcal{H} , optimal relay UEs \mathcal{R} to extend coverage and connectivity to the set of terrestrial UEs in \mathcal{T} via cooperative V2V links. We assume that all vehicle UEs are aware of the time-stamped information of position, speed and moving direction of other vehicles in its immediate neighbourhood and denote the total number of vehicle UEs by $\mathcal{N} = \{1, 2, \dots, \mathcal{N} - 1\}$.

5.3.1 Outage Probability of the HAP Link

For the direct transmission between the HAP and the vehicle UE, an outage occurs if γ_{h_i, k_i} and $\tilde{\gamma}_{h_i, k_i}$ falls below χ_{SNR} and χ_{SINR} for at least t_m . This is represented by:

$$\begin{aligned} P_{o_{\gamma_{h_i, k_i}}} &= Pr\left(\gamma_{h_i, k_i}[dB] < \chi_{SNR}[dB]\right) \\ P_{o_{\tilde{\gamma}_{h_i, k_i}}} &= Pr\left(\tilde{\gamma}_{h_i, k_i}[dB] < \chi_{SINR}[dB]\right) \end{aligned} \quad (5.4)$$

We recall also from section 4.3.2 that the HAP has a dedicated spectrum with SNR and SINR obtained as (4.19) and (4.20). The link quality of the vehicle UE decreases with an increasing distance from the HAP particularly for UEs at the edge of HAP coverage. The 5th percentile throughput is used to represent this set of vehicle UEs. A CDF plot of the capacity for this set of users is illustrated in Fig. 5.3.

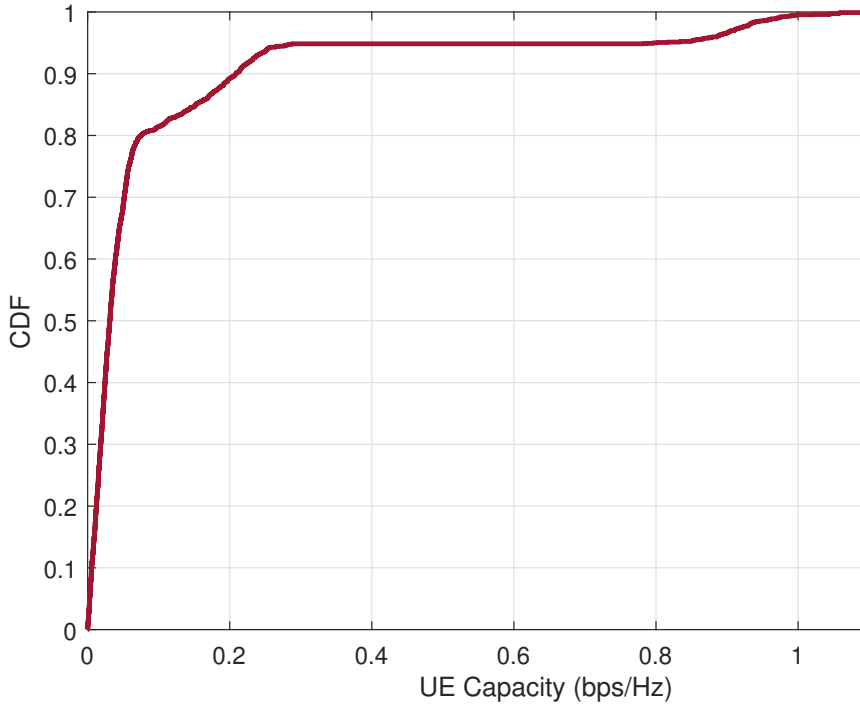


FIGURE 5.3: CDF of 5th percentile UE Capacity

5.3.2 Channel Propagation Model

For a vehicle UE in \mathcal{N} , recall that the received SNR γ_{h_i, k_i} and SINR $\tilde{\gamma}_{h_i, k_i}$ from the HAP to a UE $k_i \in \mathcal{H}$, $\mathcal{R} \subseteq \mathcal{H}$ is given in Equation(4.19) and Equation (4.20) as:

$$\begin{aligned}\gamma_{h_i, k_i} &= \frac{P_{rx}}{N_p} \\ \tilde{\gamma}_{h_i, k_i} &= \frac{P_{rx}}{\sum_{j \in \mathcal{C}} P_I + N_p}\end{aligned}\quad (5.5)$$

For a given pair of adjacent vehicles, we assume a connectivity requirement is conditioned on the UEs being within a communication range R_{max} . The probability of connectivity P_c is therefore expressed as:

$$P_c = \begin{cases} 1 & d_{k_i, t_i} \leq R_{max} \\ 0 & \text{otherwise} \end{cases}\quad (5.6)$$

where R_{max} is the maximum transmission range. For the cooperative V2V link, the received SNR and SINR between UE $k_i \in \mathcal{R}$ and $t_i \in \mathcal{T}$ is:

$$\gamma_{k_i, t_i} = \frac{P_{k_i, t_i} g_{k_i, t_i}}{N_p}\quad (5.7)$$

$$\tilde{\gamma}_{k_i, t_i} = \frac{P_{k_i, t_i} g_{k_i, t_i}}{\sum_{\substack{j \in \mathcal{N}, \\ i \neq j}} P_{k_j, t_j} g_{k_j, t_j} + N_p}\quad (5.8)$$

where P_{k_i, t_i} is the transmit power between k_i and t_i , g_{k_i, t_i} denotes the channel gain and N_p represents the noise power.

Equation (5.8) is used as a metric for the successful transmission probability between the relay and terrestrial UE. This is satisfied if (4.22), (5.6) and $\tilde{\gamma}_{k_i, t_i}$ is greater than or equal to a predefined threshold γ_{th} , expressed as:

$$\tilde{\gamma}_{k_i, t_i} \geq \gamma_{th}\quad (5.9)$$

This will be further discussed in Section 5.6.

For a two-hop transmission, the equivalent SINR at $t_i \in \mathcal{T}$ is:

$$\tilde{\gamma}_{k_i} = \min \left(\tilde{\gamma}_{h_i, k_i}, \tilde{\gamma}_{k_i, t_i} \right)\quad (5.10)$$

Therefore, for a UE $t_i \in \mathcal{T}$ aided by a relay $k_i \in \mathcal{R}$, where $\mathcal{R} \subseteq \mathcal{M} \subseteq \mathcal{H}$, the achievable data rate r_{t_i} for a DF protocol is expressed as:

$$r_{t_i} = B \log_2 \left(1 + \tilde{\gamma}_{k_i, t_i} \right) \quad (5.11)$$

Substituting (5.10) into (5.11),

$$r_{t_i} = B \log_2 \left\{ 1 + \min \{ \tilde{\gamma}_{h_i, k_i}, \tilde{\gamma}_{k_i, t_i} \} \right\} \quad (5.12)$$

where B is the channel bandwidth. Equation (5.12) can now be expressed as:

$$\begin{aligned} r_{t_i} &= B \min \left\{ \log_2(1 + \tilde{\gamma}_{h_i, k_i}), \log_2(1 + \tilde{\gamma}_{k_i, t_i}) \right\} \\ &= B \min \left\{ \log_2 \left(1 + \left(\frac{P_{h_i, k_i} g_{h_i, k_i}}{\sum_{\substack{j \in \mathcal{C}, \\ i \neq j}} P_{h_j, k_j} g_{h_j, k_j} + N_p} \right) \right), \log_2 \left(1 + \frac{P_{k_i, t_i} g_{k_i, t_i}}{\sum_{\substack{j \in \mathcal{N}, \\ i \neq j}} P_{k_j, t_j} g_{k_j, t_j} + N_p} \right) \right\} \end{aligned} \quad (5.13)$$

Therefore, using (5.8) and (5.13), we can characterise the link quality and achievable data rate performance of the system. For the case where a relay is not used, the transmission rate r_{t_i} is that obtainable when the UE is served directly by the HAP as given by (4.26) and therefore, $\mathcal{R} = \emptyset$.

5.4 Problem Formulation

We denote the relay selection result by a matrix $\mathbf{S}_{P \times Q}$, where each entry in \mathbf{S} indicates whether a relay UE is selected or not. Then, let $s_{i,j}$ represent each entry of the matrix, where:

$$s_{k_i, t_i} = \begin{cases} 1, & \text{if a relay UE is assigned to a terrestrial UE} \\ 0, & \text{otherwise} \end{cases} \quad (5.14)$$

Our objective is to find the optimal set of relay UEs \mathcal{R} that maximise the minimum transmission rate of the terrestrial UEs in \mathcal{T} . Therefore, the relay solution should address the following:

- What are the constraints for the selection of a relay UE?
- How do we characterize the impact of interference power from adjacent relay UEs?
- Does the relaying outperform the direct transmission by the HAP?

In consideration of the above, we formulate the relay UE selection problem as an optimization problem to maximize the transmission rate r_{t_i} of the terrestrial UE. We express this as follows:

$$\max_{\rho_i, r_{t_i}} s_{k_i, t_i}(r_{t_i}) \quad (5.15a)$$

$$\text{s.t.} \quad \sum_{k_i \in \mathcal{R}} B \min \left\{ \log_2(1 + \tilde{\gamma}_{h_i, k_i}), \log_2(1 + \tilde{\gamma}_{k_i, t_i}) \right\} \geq R_{th} \quad (5.15b)$$

$$\frac{P_{h_i, k_i} g_{h_i, k_i}}{\sum_{\substack{j \in \mathcal{C}, \\ i \neq j}} P_{h_j, k_j} g_{h_j, k_j} + N_p} \geq \chi_{SINR} [dB] \quad (5.15c)$$

$$\frac{P_{k_i, t_i} g_{k_i, t_i}}{\sum_{\substack{j \in \mathcal{C}, \\ i \neq j}} P_{k_j, t_j} g_{k_j, t_j} + N_p} \geq \gamma_{th} [dB] \quad (5.15d)$$

$$0 \leq P_{h_i, k_i} \leq P_{h_i} \forall k_i \in \mathcal{H} \quad (5.15e)$$

$$0 \leq P_{k_i, t_i} \leq P_{k_i} \forall k_i \in \mathcal{R} \quad (5.15f)$$

$$s_{k_i, t_i} \in \{0, 1\} \forall k_i \in \mathcal{R}, t_i \in \mathcal{T} \quad (5.15g)$$

where the objective as given by (5.15a) is to maximise the minimum data rate of terrestrial UEs, constraint (5.15c) ensures that only HAP UEs with an SINR above the threshold are assigned as relay UEs, constraint (5.15d) ensures the successful transmission probability between the relay and terrestrial UE, constraint (5.15e) and constraint (5.15f) ensure that transmit powers of the HAP and relay UEs are not higher than the allotted transmit powers. s_{k_i, t_i} is a decision variable that specifies if a relay UE is assigned or otherwise.

For the relay selection problem of (5.15a), an additional challenge is the characterisation of the interference introduced by other simultaneously transmitting relay UEs. This level of this interference is unknown and therefore the relay selection should adequately address this effect to avoid performance degradation of the system.

5.4.1 Interference Characterisation

Our first challenge is to characterise the interference from simultaneous transmissions from other relay UEs in adjacent clusters which will cause significant interference to terrestrial UEs. To mitigate this impact, we propose a dual-mode selection solution for the characterization of the V2V interference as follows:

- a mode where for the transmitting relay UEs in the same cluster, available resources are orthogonally assigned. In other words, by dividing the available frequency band (or time slots) into separated channels, interference does not exist for simultaneous transmissions from relay UEs in the same cluster.
- a reuse mode where the the terrestrial UE is located outside an interference region such that the potential interference is below a pre-defined threshold I_{th}

A typical interference scenario is as shown in Fig. 5.4.

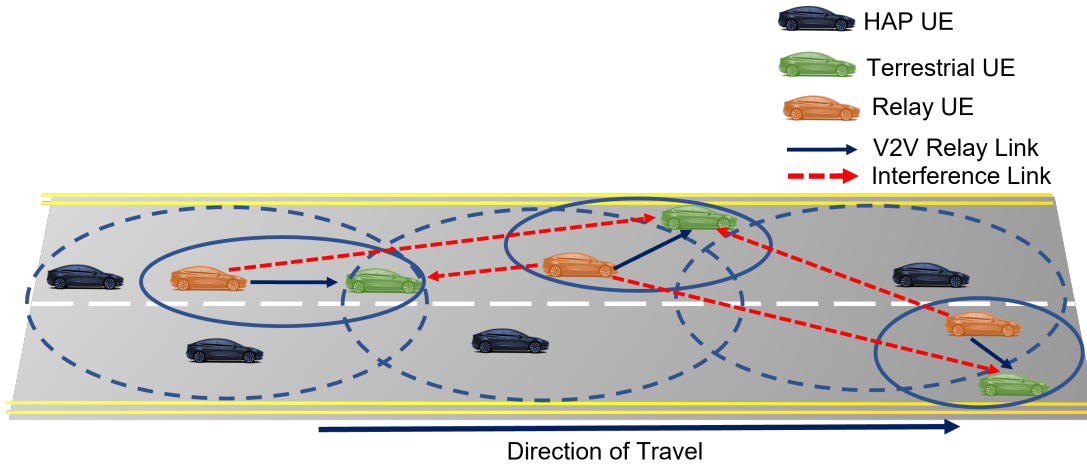


FIGURE 5.4: Interference scenario for relay selection

For terrestrial UEs with dominant interference, the interference power is considered to be much greater than the noise power, i.e.,

$$\sum_{\substack{j \in \mathcal{N}, \\ i \neq j}} P_{k_j, t_j} g_{k_j, t_j} \gg N_0$$

This means that (5.8) can be expressed as:

$$\tilde{\gamma}_{k_i, t_i} \approx \beta_{k_i, t_i} = \frac{P_{k_i, t_i} g_{k_i, t_i}}{\sum_{\substack{j \in \mathcal{N}, \\ i \neq j}} P_{k_j, t_j} g_{k_j, t_j}} \quad (5.16)$$

5.5 Relay Selection Scheme

By inspecting the optimisation problem in (5.15a), we observe that the objective function is a non-linear logarithmic expression of the transmission rate with combinatorial binary variables. These properties causes (5.15a) to be a non-convex mixed integer nonlinear programming (MINLP) optimisation problem. This problem is

an NP-hard optimisation problem which can be difficult to solve. An exhaustive search is only feasible with a small network size which will therefore require a small number of output combinations for all possible assignment pair. However, the computational complexity grows with increasing network size. In lieu of an exhaustive search, we therefore tackle this problem by formulating the solution to (5.15a) as a maximum weighted bipartite matching problem and exploit the *Kuhn-Munkres* Algorithm [210] to solve the maximum weighted matching. The function of the Algorithm is therefore, to choose a relay pair that maximises r_{t_i} .

Kuhn Munkres Algorithm

The Kuhn-Munkres Algorithm, also called the *Hungarian Algorithm* [210], transforms the problem of finding the maximum weighted matching of an optimization problem into a combinatorial problem of finding a perfect match by combining the weights assigned to the edges of a weighted bipartite graph. The algorithm requires a task to be assigned to exactly one agent and is typically used to solve one-to-one assignments. As a starting point and to provide clarity, we revisit some key graph-theoretic terms [211]:

(a) Bipartite Graph

Given a graph $G = (V, E)$ where V is a set of vertices and E is the set of edges, a bipartite graph is one whose vertices can be divided into two disjoint subset V_1 and V_2 such that no edge can connect to vertices of the same subset and every edge that can connect to vertices of a different subset forms part of the graph, i.e $i \in V_1, j \in V_2, i, j \in V$. Therefore, no two vertices in the same subset are adjacent. G is complete if every vertex $i \in V_1$ and $j \in V_2$.

(b) Weighted Bipartite and Maximum Weighted Matching

A bipartite graph is said to be weighed if each edge is assigned a weight vector $w(i, j)$. By setting the weight for each matching M , the weighted bipartite graph can be obtained. If a non-negative weight $w(i, j)$ is assigned to each edge $e \in E$, the objective is to find a feasible labelling of maximum cost where the cost of matching is $c(M) = \sum_{e \in M} w(e)$. In other words, assign a vertex $k_i \in \mathcal{M}$ with a vertex $t_i \in \mathcal{T}$ as a one-to-one matching to obtain an upper bound of the cost function. A necessary condition for solving the matching problem is that $|\mathcal{M}| \geq |\mathcal{T}|$ and the graph is symmetric when the cardinality of UEs in \mathcal{M} and \mathcal{T} are equal, $|\mathcal{M}| = |\mathcal{T}|$.

(c) Vertex Label and Equality sub-graph For a label ℓ assigned to each vertex, the label is said to be feasible if it satisfies:

$$w(i, j) \geq \ell(i) + \ell(j) \forall (i, j) \in E \quad (5.17)$$

If $G = (V, E_\ell)$ is a sub-graph of G , i.e., G_ℓ contains all the vertices from G , then G_ℓ is an equality sub-graph of G if:

$$E_\ell = \{(i, j) : \ell(i) + \ell(j) = w(i, j)\} \quad (5.18)$$

Subsequently, our objective is three-fold:

1. construct the weighted bipartite graph
2. solve the maximum weighed matching problem with edges weighted according to the transmission rate of vehicle UE.
3. optimise the V2V relay pairs by updating (1) and (2) until an optimal UE pairing that maximises (5.13) is achieved.

We proceed to provide a description of the KMRA Algorithm for the vehicular scenario as follows:

The network is modelled as a graph $G = (V, E)$. Recall that we represented the set of candidate relay UEs by \mathcal{M} and the set of terrestrial UEs by \mathcal{T} . The vertices are the set of vehicle UEs, i.e., $\mathcal{M}, \mathcal{T} \in V$ and the weights of edges represent the transmission rate r_{t_i} of vehicle $k_i \in M$ when serving UE $t_i \in T$. Therefore, \mathcal{T} and \mathcal{M} will form two independent set of the bipartite graph. The weighted bipartite graph $G = (V, E)$ is formed where $V = \mathcal{T} \cup \mathcal{M} \forall k_i t_i \in V$.

If a maximum matching M exist, then M is a perfect matching, and ℓ is a feasible labelling. Therefore, M and ℓ are optimal if and only if $M \subseteq E_\ell$, in other words, each edge in M is also found in the equality sub-graph E_ℓ .

Theorem 1 *If ℓ is feasible and M is a perfect matching in E_ℓ , then M is a maximum weighted matching. The proof is provided in Appendix C.*

A depiction of an 8 vehicle weighted bipartite graph is presented in Fig. 5.5. The vehicles represent the vertices with $|\mathcal{M}| \geq |\mathcal{T}|$. In this example, there are 4 relay UEs in the set \mathcal{M} and 4 terrestrial UEs in the set \mathcal{T} . Each edge has an associated weight w corresponding to whether a UE in \mathcal{M} can provide service to a UE in \mathcal{T} via V2V relaying links. The aim is to obtain a reasonable weight for each edge such that a larger weight is assigned to an edge that connects the terrestrial UE with poor channel conditions to a relay UE with more resources. Therefore, in the final matching decision, there exists at most one link corresponding to the maximum weighted matching between each relay and terrestrial UE. The maximization of the sum of the weight between edges $k_i \in M$ and $t_i \in T$ corresponds to a solution to the objective function in (5.15a). This is represented by the solid line in Fig. 5.5 with a global maximum of weighted sum given by $k_1 t_1 + k_2 t_3 + k_3 t_4 + k_4 t_2 = 20$. The dotted lines

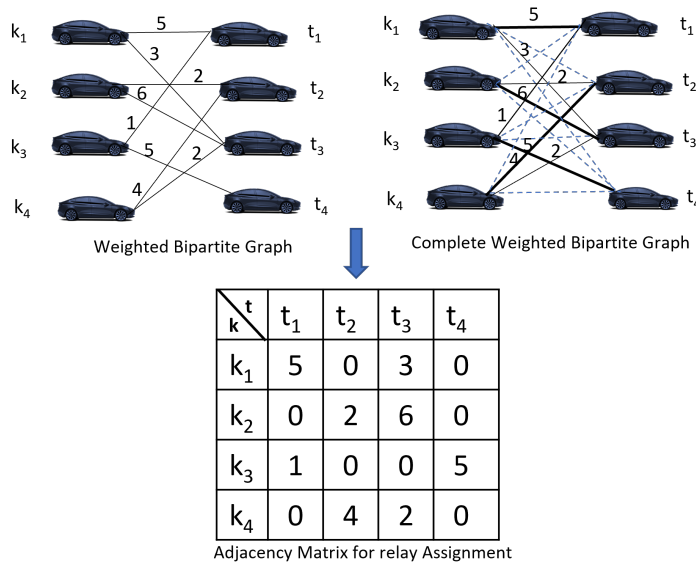


FIGURE 5.5: Bipartite Matching Graph for relay assignment and adjacency matrix

are assigned weight value of zero to ensure symmetry. For clarity, the algorithm is outlined in Algorithm 5. We note that for the network example depicted above, the relay selection can be solved via an exhaustive search by considering the best combination of the relay selection that maximizes the overall data rate. This means the search will need as many as RN possible combination of the relay assignment. This will increase the increase the computational complexity especially with an increasing number of vehicles.

In the following discussion, we describe the algorithm in detail.

The aim of the relay selection algorithm is to choose for each UE pair, a relay UE that provides the maximum transmission rate (5.15a). Initially, arbitrary vertices with an edge weight of 0 are added to each edge to make the graph symmetric and complete (line 1). Next, labels are assigned to the each vertex of the graph to determine the equality sub-graph as given by (5.18) ((line(2) of Algorithm (5)). The algorithm traverses across each relay and terrestrial UE pair for $V \in (\mathcal{M}, \mathcal{T})$ at each iteration, it selects a UE pair that maximizes (5.15a). A perfect matching M is obtained if for every $v \in (\mathcal{M}, \mathcal{T})$, there is an associated edge weight $w(e) \in M$. If a perfect match is found in the equality sub-graph G_ℓ , then M_ℓ is a maximum weighted matching, otherwise we relax the label (line 15), add and update vertex and equality subgraph to create a new feasible matching (lines(16-18)) for edges that were not initially feasible. These edges now becomes feasible edges and a perfect matching in the sub-graph can be obtained.

Algorithm 5 Kuhn-Munkres Relay Assignment (KMRA)**Input:** Weighted Bipartite Graph $G = (\mathcal{M}, \mathcal{T}, w)$ **Output:** Optimal perfect match M corresponding to relay assignment $k_i \leftrightarrow t_i$

- 1: Add vertices and edges with $w = 0$ to G to obtain a complete bipartite graph
- 2: Assign an arbitrary feasible vertex labelling ℓ for every vertex in G G_ℓ .
- 3: **for each** $k_i \in \mathcal{M}$ **do**
- 4: $\ell(t_i) = \max_{t_i \in \mathcal{T}}(w(k_i, t_i))$.
- 5: **for each** $t_i \in \mathcal{T}$ **do**
- 6: $\ell(k_i) = 0$
- 7: **end for**
- 8: **end for**
- 9: Obtain equality sub-graph from (5.18).
- 10: Determine maximum cardinality matching M
- 11: **if** M is perfect **then**
- 12: Delete vertices and edges with $w = 0$
- 13: **return** M
- 14: **else**
- 15:
$$\alpha_\ell = \min_{t_i \in \mathcal{M}} \{ \ell_{k_i} + \ell_{t_i} - w(k_i, t_i) \} \quad (5.19)$$
- 16: Update vertex labels
- 17: Update equality sub-graph
- 18: Determine new feasible matching
- 19: **end if**

5.6 Performance Metrics

In this section, outage probability, transmission success probability and achievable transmission rate are used to evaluate the performance of the relay selection scheme.

5.6.1 Outage Probability and Transmission Success Probability

The outage probability P_{out} is the probability that the transmission rate r_{t_i} is lower than a predefined threshold R_{th} . With a slight abuse of notation, we drop the subscript in (5.8) and (5.7) and denote the outage probability as [212]:

$$B \log_2(1 + \gamma) < R_{th}, \quad (5.20)$$

where γ represents the SINR, and R_{th} denotes the transmission rate of UE t_i respectively. Therefore, P_{out} is written as:

$$\begin{aligned}
\gamma &< 2^{R_{th}} - 1 \\
&= \mathbb{P}(\gamma < 2^{R_{th}} - 1) \\
&= \mathbb{P}(\gamma < \tilde{\gamma}_{th})
\end{aligned} \tag{5.21}$$

where $\tilde{\gamma}_{th} = 2^{R_{th}} - 1$ is the SINR threshold.

Similarly, the terrestrial UE can successfully decode the information from both the HAP and the relay UE only if the SINR at the relay and terrestrial UE exceeds a predetermined threshold, i.e., $\tilde{\gamma}_{h_i, k_i} \geq \chi_{SINR}$, and $\tilde{\gamma}_{k_i, t_i} \geq \gamma_{th}$. Therefore, for the terrestrial UEs assisted by the relay UEs, the probability of successful transmission is expressed as:

$$\begin{aligned}
&\mathbb{P}(\tilde{\gamma}_{h_i, k_i} \geq \chi_{SINR}[dB])\mathbb{P}(\tilde{\gamma}_{k_i, t_i} \geq \beta_{SINR}[dB]) \geq \tilde{\gamma}_{th}^T \\
&= \left(\frac{P_{h_i, k_i} g_{h_i, k_i}}{\sum_{j \in \mathcal{C}} P_{h_j} g_{h_j, k_j} + N_p} \right) \left(\frac{\gamma_{k_i, t_i}}{\sum_{\substack{j \in \mathcal{N}, \\ i \neq j}} \gamma_{k_j, t_j} + N_p} \right) \geq \tilde{\gamma}_{th}^T
\end{aligned} \tag{5.22}$$

where $\tilde{\gamma}_{th}^T = 2^{2R_{th}} - 1$

For a successful transmission probability, the V2V link contact duration for communication must satisfy:

$$C_{k_i, t_i} = \begin{cases} \frac{d_{k_i, t_i}}{v_{rel}}, & d_{k_i, t_i} \leq R \\ 0, & \text{otherwise} \end{cases} \tag{5.23}$$

where d_{k_i, t_i} and v_{rel} is the Euclidean distance and relative velocity respectively.

5.7 Simulation Results

The simulation parameters are given in Table 5.1. The path loss model is also given in the table with $PL(d_0)$ denoting the reference distance path-loss, γ the path-loss exponent, and χ_δ is a Gaussian distributed variable with mean 0 and standard deviation δ . For the simulation, the parameters $\sigma = 1.61$, $PL(d_0) = 57.6$ and $\chi_\delta = 5.49$ are adopted from [213].

The performance of the KMRA algorithm is compared with with three benchmark algorithms outlined below.

- **Threshold Based Relay Assignment (TBRA)** In this relay selection scheme, the criterion for selecting the relay UEs to be used is based on a threshold SINR of the HAP-relay link. In other words, the relays are selected by comparing the

TABLE 5.1: V2V Simulation Parameters

V2V Link Parameter	
Parameter	Value
Carrier frequency	5.9 GHz
Transmit Power	20 dBm
Noise Power	-101 dBm
Bandwidth	10 MHz
SINR threshold	-5 dB
R_{th} threshold	1 bps/Hz
Number of vehicles	80
Traffic Model	
Scenario	Rural traffic demand as in Sec. (3.3)
Mobility Model	SUMO Traffic Model
Path Loss Model	
V2V link [214]	$PL(d) = PL(d_0) + 10\gamma \log_{10}(\frac{d}{d_0}) + \chi_\sigma$

SINR of the source-relay link with a threshold value. Relays are assigned to terrestrial UEs based on the maximum link SINR, i.e.,

$$\mathcal{R} = \max(k_i \in \mathcal{M}) \mid \tilde{\gamma}_{k_i, t_i} \geq \chi_{SINR} \quad (5.24)$$

This scheme is similar to the relay selection presented in [122].

– Link Lifetime Relay Selection (LLRS)

Due to the UE mobility characteristics, the communication link between the vehicle UE in \mathcal{M} and \mathcal{T} are prone to frequent link disconnect as they move out of the transmission range of each other. Therefore, the duration of the link between UE pairs need to be long enough to avoid a frequent link re-establishment. The link lifetime is expressed as [215]:

$$LLT_{k_i, t_i} = \frac{\sqrt{(\alpha^2 + \gamma^2)R^2 + (\beta\alpha - \delta\gamma)^2} - (\delta\alpha + \beta\gamma)}{\alpha^2 + \gamma^2} \quad (5.25)$$

where $\delta = x_{k_i} - x_{t_i}$, $\beta = y_{k_i} - y_{t_i}$, $\alpha = v_{k_i} \cos \theta_{k_i} - v_{t_i} \cos \theta_{t_i}$ and $\delta = v_{k_i} \sin \theta_{k_i} - v_{t_i} \sin \theta_{t_i}$ and, $0 < \theta_{t_i} < 2\pi$ and $0 < \theta_{k_i} < 2\pi$ denotes the angle of the vehicle with the road. The stability metric of the link is also expressed as [216]:

$$\tilde{s}_{k_i, t_i} = 1 - \exp^{-2 \frac{LLT_{k_i, t_i}}{a}} \quad (5.26)$$

where $a = \min(LLT_{k_i, t_i})$. The inter-vehicular distance metric $\tilde{\Phi}_{t_i, k_i}$ between pair of vehicles now defined as:

$$\tilde{\Phi}_{k_i, t_i} = \frac{\cos(\theta_{k_i} - \theta_{t_i}) \cdot d_{k_i, t_i}}{R} \quad (5.27)$$

where $d_{k_i, t_i} = \sqrt{(x_{t_i} - x_{k_i})^2 + (y_{t_i} - y_{k_i})^2}$, θ_{t_i} and θ_{k_i} denotes the angle vector between pair of vehicles. Hence, by combining Equation (5.26) and Equation (5.27), the link connectivity ν as a weighted sum of both the inter-vehicular distance metric and the link stability metric is given as:

$$\nu = w_0 \tilde{s} + (1 - w_0) \tilde{\Phi}, \quad (5.28)$$

where w_0 is a weighing factor, $w_0 \in [0, 1]$. This approach is similar to a weighted relay selection approach presented [157].

– Random Relay Assignment (RRA)

In this assignment, relay assignment is done randomly from the set \mathcal{M} of candidate relay UEs. In other words, we randomly assign a relay UE to a terrestrial UE and repeat until all terrestrial UEs have corresponding relay UEs.

In Fig. 5.6, we plot the probability of successful message transmission against the average link contact duration with a minimum link distance of 150 m. As expected, when the link contact duration increases, the probability of the information being successfully decoded increases. This also increases with an increase in the transmit power which shows that the message will be decoded correctly with a high transmit power and higher link contact duration.

In Fig. 5.7, we show the probability of a successful message transmission for terrestrial UEs with varying link distance. We first remark that with an increasing link distance, the UEs become disconnected which reduces the transmission success probability. This is particularly observed with the random relay assignment with a 0% transmission success when the link distance is greater than or equal to 350 m. For shorter link distances, an increased number of UEs can exchange high quality links and therefore maximize the SINR and achievable transmission rate. We observe that the performance of the proposed scheme is almost identical to the threshold based and link-lifetime relay selection especially at shorter link distances. This is because the number of UEs that are available for relaying increases which increases the connectivity of the network. Moreover, shorter link distances results in a higher average SINR and therefore a higher probability of a successful message transmission.

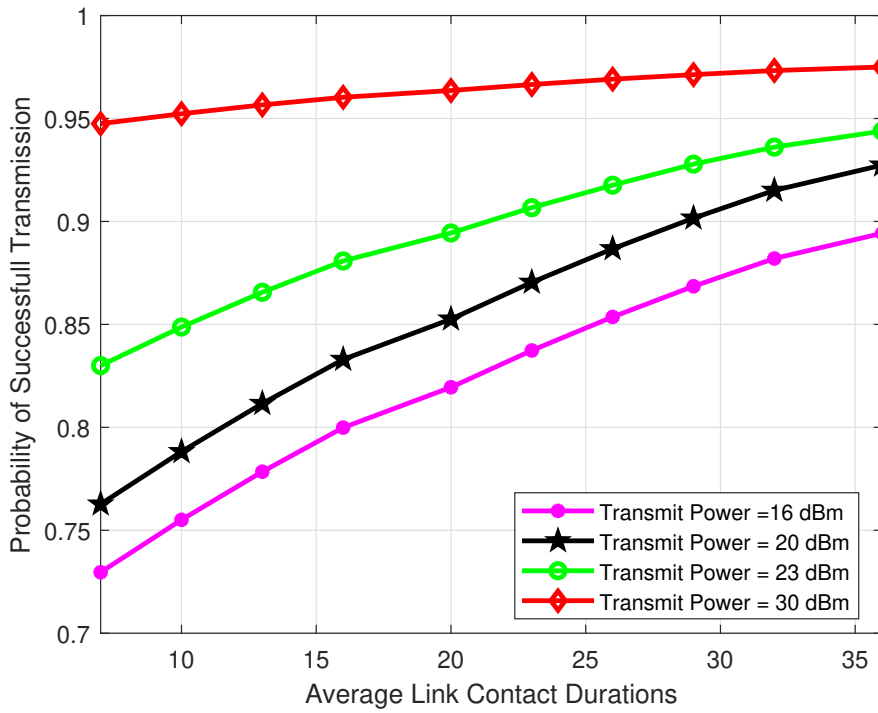


FIGURE 5.6: Transmission success probability vs Average Link Contact Durations

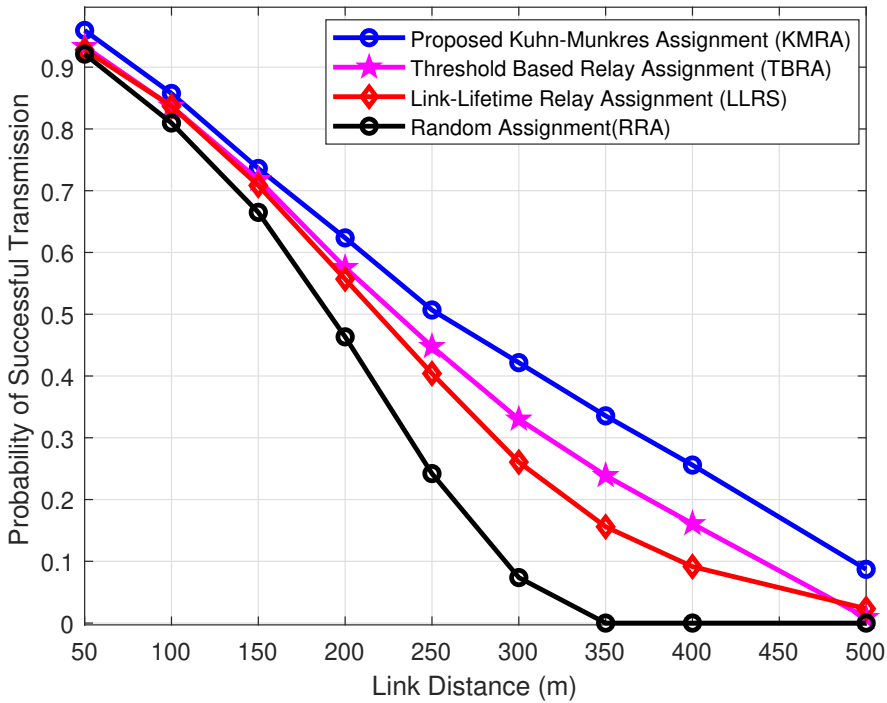


FIGURE 5.7: Transmission success probability vs V2V Link distance

Fig. 5.8 shows the transmission success probability of our proposed algorithm against the other considered algorithms as a function of an increasing UE speed. Obviously, the time interval for the message to be successfully decoded by the UEs decreases with an increasing speed. As the UE speed increases, the advantage of the proposed approach can be clearly seen: the proposed algorithm achieves a lower bound transmission success probability of 85% for an average UE speed of 91 km/h. The RRA scheme exhibits the lowest probability with increasing UE speed.

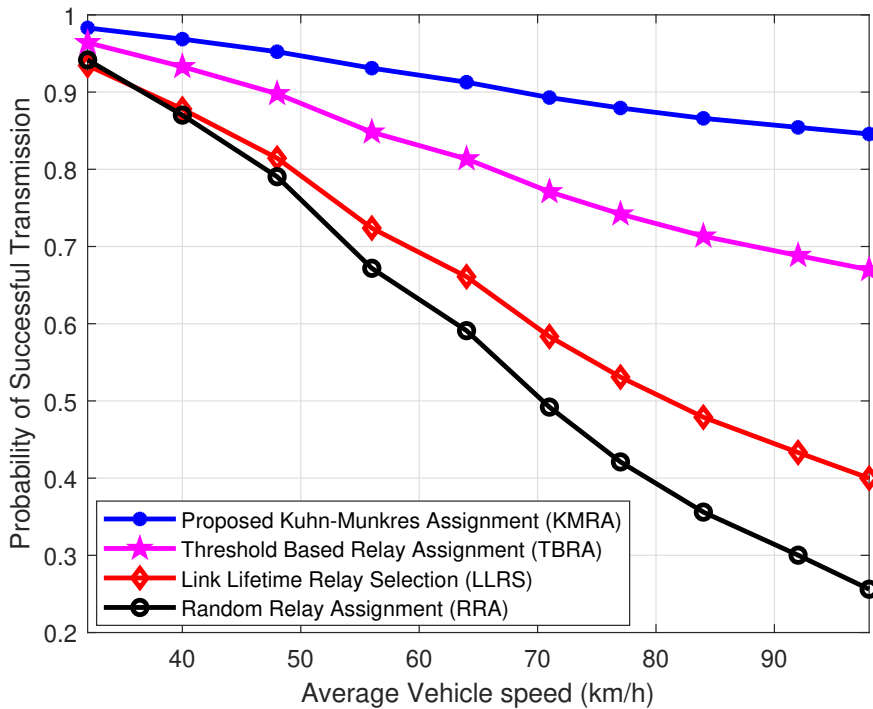


FIGURE 5.8: Transmission success probability vs Average Vehicle Speed

In Fig. 5.9, we depict the outage performance of the KMRA and benchmark relaying schemes. Unsurprisingly, we observe that as the SNR increases, the outage probability reduces. The KMRA algorithm is observed to have the best outage performance while the RRA performs worst with an outage probability consistently close to 1. We also observe that, compared to TBRA and LLRS, the outage performance of KMRA is not significant especially at low SNRs. However, the superiority of the KMRA becomes obvious at higher transmit SNR. Evidently, the KMRA scheme can realise an outage probability approaching zero for higher transmit SNRs.

Next, we consider the effect of the outage probability on the average tolerable interference thresholds as shown in Fig. 5.10. As the noise power increases, the outage probability also increases. This means that a tolerable interference threshold exist beyond which the the system the rate falls below r_0 and the system is in outage. In particular, with a tolerable interference power below the noise power, we observe a

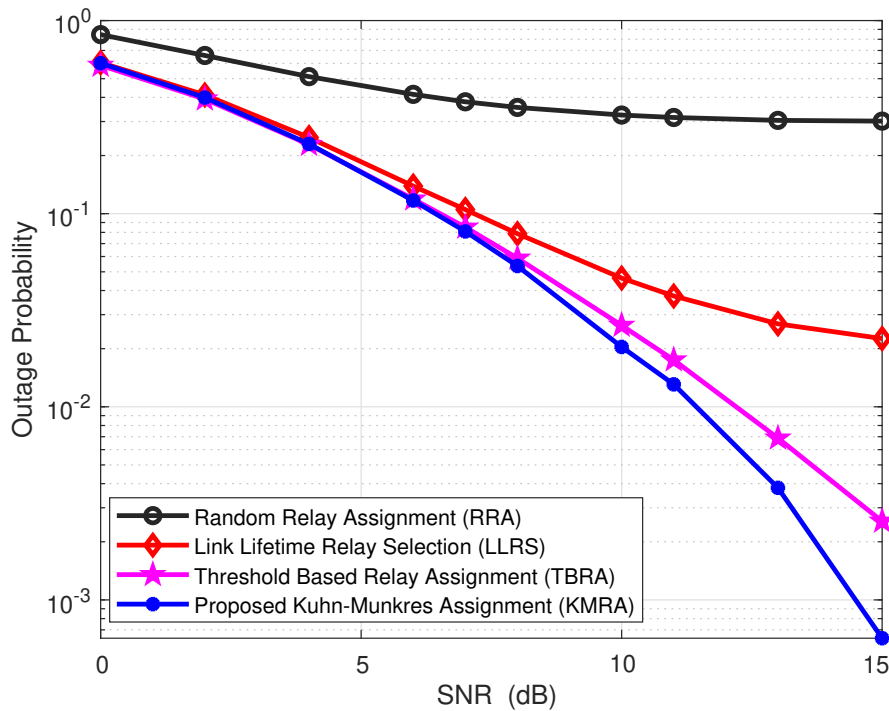


FIGURE 5.9: Outage Probability vs SNR

significant decrease in outage probability for KMRA compared to the three benchmark schemes considered which illustrates the superiority of the relaying scheme.

In Fig. 5.11, we present the CDF transmission rate at the terrestrial UE for the various schemes considered. We observe the benchmark schemes exhibit an almost identical throughput performance. For comparison, the throughput performance of our proposed relaying scheme is compared with throughput obtained via a direct transmission, i.e. with no relaying. It can be observed that relays can be used to enhance the throughput performance of the terrestrial UE compared to the direct transmission, i.e., no relaying. The KMRA algorithm provides the best performance followed by TBRA which exhibits an almost identical performance to the LLRS and RRA. Specifically, we observe that the maximum achievable transmission rate for the terrestrial UEs without relay is approximately 1.2 bps/Hz. A percentage difference of approximately 82.4% is observed as compared to the KMRA scheme with a 3.6 bps/Hz maximum data rate. This shows that the proposed scheme offers a significant improvement in the UE transmission rate compared to direct transmission.

5.8 Conclusion

This chapter has focused on investigating a relay selection scheme to maximise the transmission rate and minimise the outage probability of vehicle UEs with poor

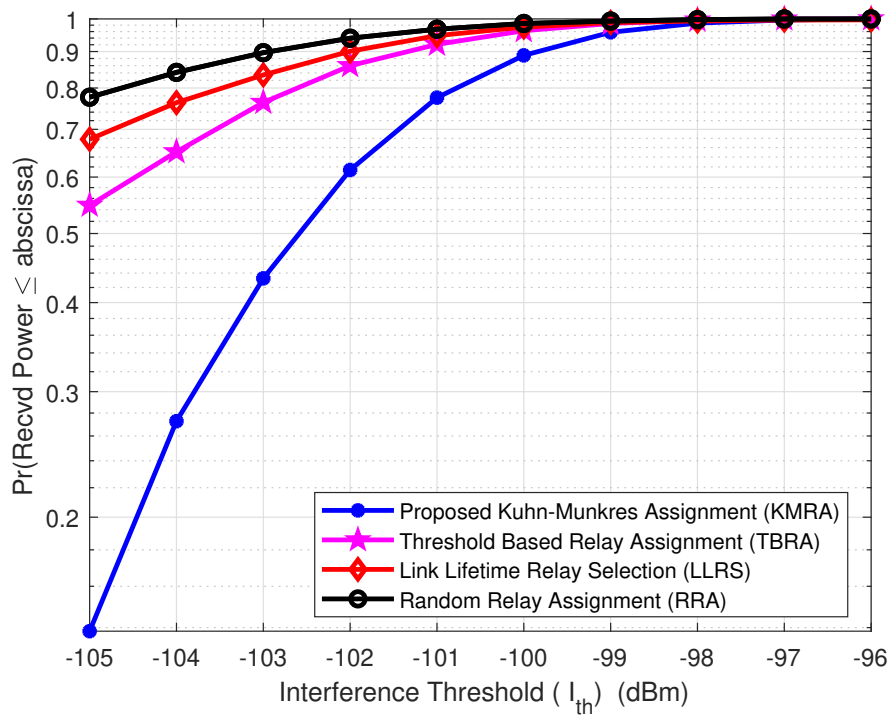


FIGURE 5.10: Outage Probability Vs Interference Threshold of UE

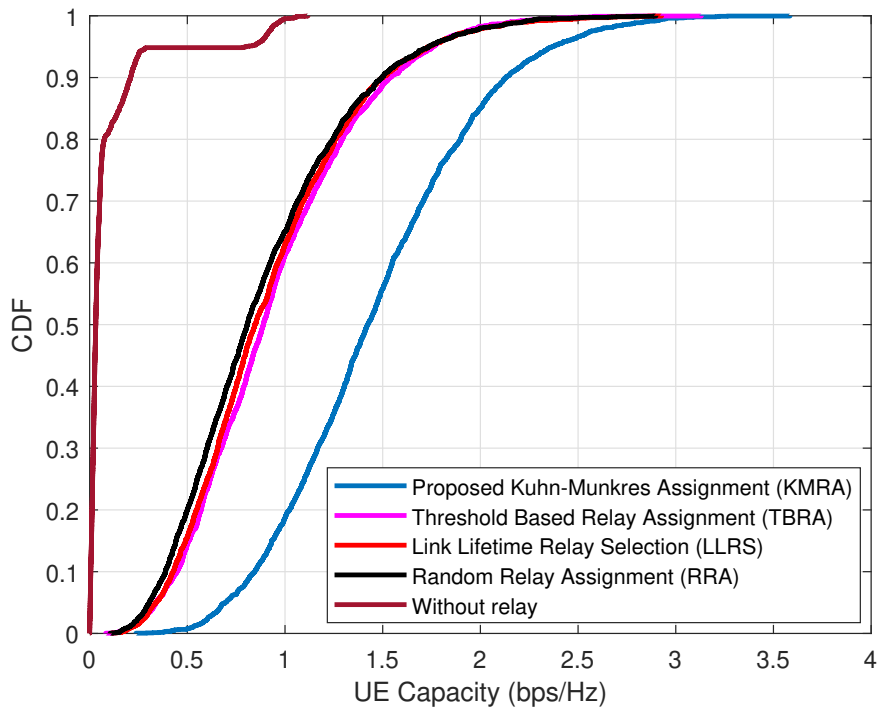


FIGURE 5.11: CDF plot of UE Throughput

channel conditions, as a way of improving overall performance compared with the HAP connectivity alone. Relays are employed to improve the link quality of UEs and provides improved data transmission. This was formulated as an optimisation problem where the selection of UE pairs that will maximise the minimum data rate of the vehicle UEs was the objective function. The relay selection was then formulated into a weighted bipartite matching problem and the KMRA algorithm was proposed to solve the problem. The performance was evaluated in terms of the transmission success probability, outage probability and achievable UE capacity. The proposed relay selection scheme was also evaluated against benchmark relay selection schemes in the literature with results showing that proposed KMRA algorithm achieves an improved transmission success probability, a lower outage probability, and an improved transmission rate. Specifically, the KMRA scheme provided a performance improvement of approximately 82% in the achievable transmission rates when compared to the direct transmission from the HAP which shows the effectiveness of our proposed approach.

Chapter 6

Conclusion and Future Work

6.1 Chapter Summary and Conclusion

The work presented in this thesis is motivated primarily by the fact that despite the expectation of ubiquitous wireless connectivity with next-generation wireless networks, significant gaps still exist today, notably for rural roads which are characterized by significantly poor or non-existent coverage. Furthermore, the explosive growth and increased demand for a diverse range of vehicular network services and applications, i.e., infotainment services, is expected to place an increased burden on current vehicular network architectures, significantly stretching their capacity limits. Due to these challenges, a paradigm shift away from the traditional network architectures is required.

Therefore, in this thesis, we have investigated the hypothesis that a HAP operating in the mmWave frequency band and equipped with a large number of antenna elements per HAP antenna array can be exploited to provide vehicular communications in an unserved or under-served rural area. In such a scenario, the HAP can provide directional and high-gain LoS spot-beams to ground UEs with a high probability and capacity for extended coverage which might not be achievable with the traditional vehicular networking architectures. Additionally, the performance could be further improved via relaying to provide connectivity to UEs not served by the HAP. Despite the potential of the proposed architecture, the propagation behaviour and characteristics of the HAP operating at the mmWave band, i.e., increased atmospheric absorption and path loss, may pose challenges to the system performance. However, these effects can be mitigated with adequate link budget provisioning coupled with the possibility of exploiting antenna beamforming with small form factor antenna arrays.

The following are detailed conclusions of the work in this thesis:

Chapter 1 presents the principal motivation for the work in this thesis. A brief research background of the ITS ecosystem was introduced. In Chapter 2, we presented a comprehensive literature review of relevant state-of-the-art research and important fundamental concepts related to the work presented in this thesis. An overview of the mmWave A2G channel propagation, the HAP antenna array, vehicular traffic demand and clustering models was presented.

In Chapter 3, we presented a technique for grouping vehicle UEs into clusters from the generated traffic demand for the study area. To enhance the beam pointing direction, ensure spatial reuse of the available bandwidth and improve network scalability, we proposed a simple clustering approach based on a CVT k-means++ clustering. By leveraging the UE behaviour in terms of the position and mobility information, the algorithm groups neighbouring UEs into clusters and selects a cluster head UE to which the HAP beams are directed. The silhouette coefficient (SC) was utilized as a measure of cluster quality to evaluate the quality of the clustering approach. With an average SC of 0.51, the results indicated that a reasonable intra-cluster similarity and cohesion can be achieved. To improve the clustering performance and due to the limitations of the k-means++ clustering, we extended the clustering problem and formulated it as a multi-objective optimization problem which was solved using an ant colony clustering algorithm. Unlike the k-means++ clustering, which requires a fixed number of clusters, the ant colony clustering can effectively adapt to varying network density since the ant agents can interact and self-organize to find optimal clusters. This approach provides a distinct advantage in terms of improving cluster stability. Simulation results show the effectiveness of the proposed scheme in creating stable clusters as it provided the best performance in terms of cluster head and cluster member stability compared to the k-means++ algorithm and comparable heuristic clustering algorithms in the literature.

In Chapter 4, the vehicular trace data obtained from the traffic demand and clustering model in Chapter 3 was used to investigate the performance of the HAP equipped with a large number of antenna elements per HAP antenna array providing service to UEs in the rural area of study. It presents an investigation of the HAP-assisted vehicular network in terms of the coverage probability and achievable UE throughput. The impact of various combinations of number of antenna elements and clusters, SNR and SINR thresholds on the coverage probability and achievable UE throughput was investigated. By exploiting the antenna array beamforming on the HAP, the coverage and capacity trade-off required to characterize the system performance is presented. Results show the upper bound and lower bounds of the coverage probability and achievable UE throughput for the representative traffic scenario. Finally, and to provide an insight into the user-centric performance, we investigate the best and worst-case throughput performance of selected UEs within

the study area.

To enhance the network performance and provide adequate service to vehicle UEs that cannot be served by the HAP, Chapter 5 proposes an optimal relay selection scheme to enhance the minimum data rate of these set of users, otherwise called terrestrial UEs. Specifically, we adopt graph theory concepts in the proposed relay selection scheme and represent the network as a weighted bipartite graph. Using the *Kuhn-Munkres* algorithm, we determine the optimal relay UEs that maximize the minimum achievable data rate of the terrestrial UEs. The proposed scheme effectively determines the selection of optimal relay UEs from the set of HAP UEs with good channel conditions. Using performance metrics of successful message transmission probability, outage probability and UE throughput, we evaluate the performance of the proposed algorithm against benchmark relay selection schemes in the literature. We show that the proposed algorithm can achieve a lower outage probability while maximizing the UE throughput. Compared to the benchmark algorithms in the literature, the proposed algorithm was also shown to achieve better performance. Furthermore, the results also demonstrate that the proposed algorithm significantly improve the achievable UE throughput with an 82.4% difference observed for the vehicle UE when the relaying scheme is implemented compared to without relaying.

6.2 Research Hypothesis Revisited and Summary of Original Contributions

The central hypothesis that has influenced the research work presented in this thesis is that:

"A HAP, operating at the mmWave frequency band and deployed with a large number of antenna elements per HAP antenna array can provide adequate wireless coverage and capacity for vehicular users specifically in rural scenarios where the terrestrial network infrastructures are inadequate or unavailable.

Evidence from the models and results presented in this thesis supports our hypothesis.

6.3 Future Work

In this thesis, the investigation of a HAP system with a large antenna array as a viable option for rural vehicular communication has been presented. Our model captures the salient trade-offs between the capacity and coverage requirements of

the HAP-assisted vehicular network. Furthermore, the thesis has also presented an investigation into an optimal relay selection scheme to extend the coverage and capacity of UEs with poor radio conditions. However, there are numerous areas for future research that might be explored to extend the investigation presented in this thesis.

Future work could focus on improving the traffic demand model within a virtualized network architecture, intelligent beamforming approaches, an energy management scheme, a learning scheme for the clustering weights, interference coordination and consideration of uplink. These suggestions are discussed in more detail in the subsections below.

6.3.1 A Heterogeneous Traffic Model with Network Virtualization

The traffic model presented in Section 3.3.2 is made up of homogeneous traffic with the vehicle UEs exhibiting identical average behaviour. However, actual traffic flows are made up of traffic heterogeneity, each exhibiting different characteristics and travel behaviour. This is exemplified by the different car-following behaviours between vehicle UEs, trucks and buses. As a result, future work should consider investigating a heterogeneous traffic scenario with a diverse mix of vehicle types. Furthermore, a heterogeneous traffic demand will increase the demand for a wide range of vehicular network services and applications. As a result, additional research into a HAP-Network function virtualization (HAP-NFV) architecture to deploy and manage service provisioning for the network is warranted. This will enable a cost-effective and flexible network and ensure that future vehicular services and applications can be easily deployed, scaled, and managed.

6.3.2 Intelligent beamforming

Generally, it has been established that the high path-loss of the mmWave HAP system can be mitigated with a large number of antenna elements with a smaller form factor. The large antenna arrays can concentrate signal power in a specific direction, thereby mitigating the severity of the channel loss. For the mmWave HAP system, this brings into focus the requirement of beam alignment considering the quasi-stationary HAP and the highly dynamic conditions of the vehicular network. In the literature, various research has investigated efficient beam alignment solutions [80], [83]. However, most approaches have been tailored towards the terrestrial and UAV domains. Therefore, a potential future direction for the HAP beamforming scheme presented in this thesis is to investigate an intelligent and predictive beamforming algorithm that can predict and adapt the beam pattern based on previous knowledge of the beamforming angles. Using historical data from the snapshots of the UE trajectory over time, historical angle data between the HAP beam and the

centroid UE can be predicted using deep-learning algorithms such as a recurrent neural network (RNN). It will be helpful to investigate how such algorithms can effectively exploit this historical data and adaptively steer the beamforming vectors based on the predicted angles, thereby improving the reliability of the link.

6.3.3 Energy Management of the HAP Antenna Payload

The maximization of the energy utilization of the HAP payload plays an important role in determining the deployment costs and is an important consideration for a network operator. Considering the spatio-temporal variation in vehicular traffic density, a possible consideration for improving the energy efficiency for the HAP antenna payload is a scheme that investigates the possibility of switching off some of the antenna array elements without significantly penalizing the antenna radiation patterns. This is important to preserve the resource (power consumption) and extend the life cycle of the HAP system. Obviously, each antenna element can only take on two states: on or off. However, the computational complexity and time required for switching increases with increasing antenna elements. Therefore, considering the vehicular traffic density, efficient optimization and artificial intelligence algorithms could be implemented to reduce the computational complexity and determine the optimal combination of antenna elements for switching.

6.3.4 Local Search method and Learning for clustering weights

As discussed in Section (3.4.3), applying ACO for clustering can improve the network's performance in terms of cluster stability. The clustering algorithm can be further improved by optimizing the weighting factors used in the objective functions. Recall the normalized weighted sum method was used to assign weights to the objective function such that:

$$w_{i,j} = \begin{cases} 1, & \text{if a vehicle UE } i \text{ is assigned to a cluster } j \\ 0, & \text{otherwise} \end{cases} \quad (6.1)$$

Recall also that the linear weight coefficient was arbitrarily chosen as $w_1 = w_2 = 0.5$, corresponding to the relative importance of the objective function of the clustering metric in (3.22). However, with the Pareto front for the clustering optimization unknown, it is difficult to determine the specific weights required to obtain Pareto optimal solutions. Similarly, selectively varying the weights may not necessarily result in an optimal solution. Therefore, to improve the clustering process for the ACO, an adaptive weight selection approach that will dynamically alter the weight parameter based on the quality of solutions found could be investigated. An algorithm for a 2-step adaptive search process could be implemented where a local

search for either of the objective functions (Φ_1, Φ_2) is evaluated, and the solution to this phase is used for determining the weighting factors. Similarly, a learning method using reinforcement learning (RL) could also be investigated for dynamically tuning the weights.

6.3.5 Worst-case Interference control with Link adaptation

To illustrate the effect of the inter-beam interference on system performance, we show in Fig. 6.1 the CDF of the downlink HAP interference to noise ratio (INR) at a thermal noise power of -120 dBW. A first obvious interpretation is that the interference increases with an increasing number of clusters, and the system becomes increasingly biased towards operating in an interference-limited region.

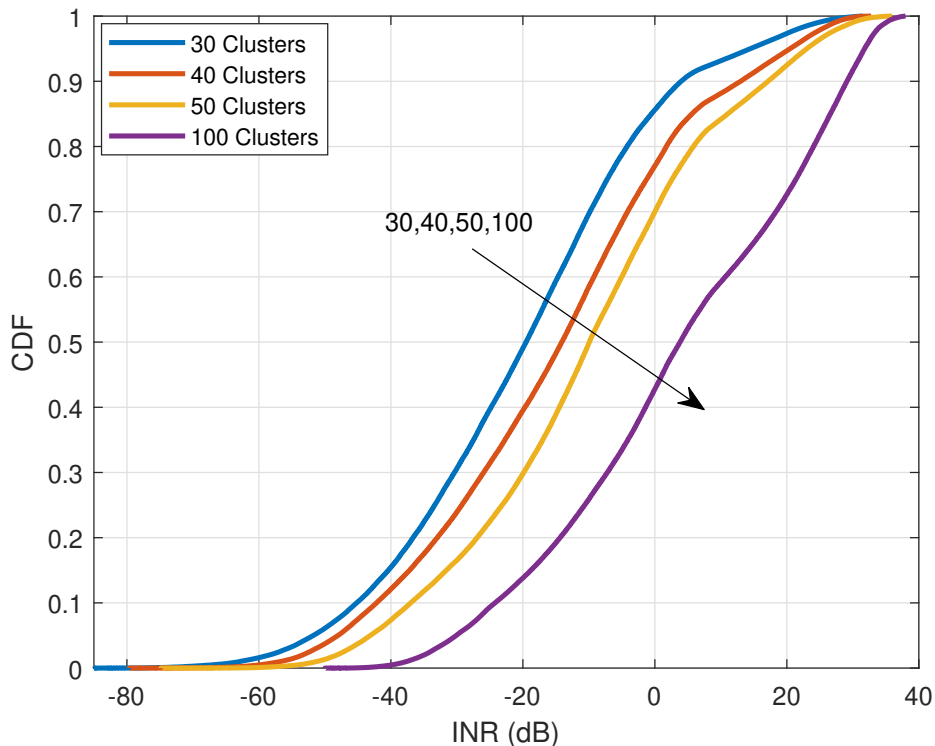


FIGURE 6.1: Interference to Noise ratio (INR) for different number of clusters

The increased interference results in degraded network performance, and implementing effective interference coordination to mitigate this impact is vital.

Interference mitigation techniques such as coordinated multi-point (CoMP) and dynamic inter-cell interference coordination (ICIC) can be employed to mitigate this scenario. In the former, and based on the channel state information (CSI) reported at the HAP, vehicle UEs that require CoMP assistance due to high interfering signals can be grouped into a CoMP set and CoMP assistance provided to this set

of users by implementing a cluster-specific muting for severely interfering clusters based on the threshold SINR. In the latter, UEs at the edge of coverage with poor channel conditions can be allocated orthogonal bandwidth to mitigate the effect of the adjacent beam interference.

6.3.6 Consideration of Uplink

For the investigations in this thesis, a downlink performance analysis of the vehicle UE and the HAP is considered. However, combining an analysis of both the downlink and the uplink will provide a comprehensive and in-depth analysis of the system performance and complement the existing work. Similarly, an investigation into uplink power allocation schemes from the aspect of power efficiency of the HAP is an area of future research worth investigating. This is important because such power allocation schemes can help to determine the optimal power required for each sub-carrier (resource), thereby improving the efficiency. With the HAP being power-limited, the radio resource allocation is important in creating maintaining the direct link between the HAP and ground UEs.

6.3.7 Resource Division and Transmit Power Control

Our investigation considered that the bandwidth is reused in each beam with a fixed transmit power. With an increase in the number of beams, interference management mechanisms become important, without which the throughput performance degrades. As consideration for future work, a scheme for splitting the bandwidth resource based on the prevailing traffic conditions is also an area of further research worth exploring. By splitting the bandwidth, UEs at the edge of coverage with poor channel conditions and which require additional resources can be dynamically allocated additional bandwidth. Additional transmit power can compensate for the beams with a reduced spectrum resource. Depending on the traffic conditions, the available transmit power and the bandwidth resource, a dynamic resource split and transmit power control scheme could be implemented.

6.3.8 Constellation of Inter-connected HAPs

A network constellation of inter-connected HAPs could also be investigated to provide increased coverage and enhance the network resiliency. In this context, a performance evaluation of such a system architecture that can exploit directional antenna arrays on the HAP in terms of the constellation design, achievable capacity, coverage and interference characterization

Appendix A

Study Area

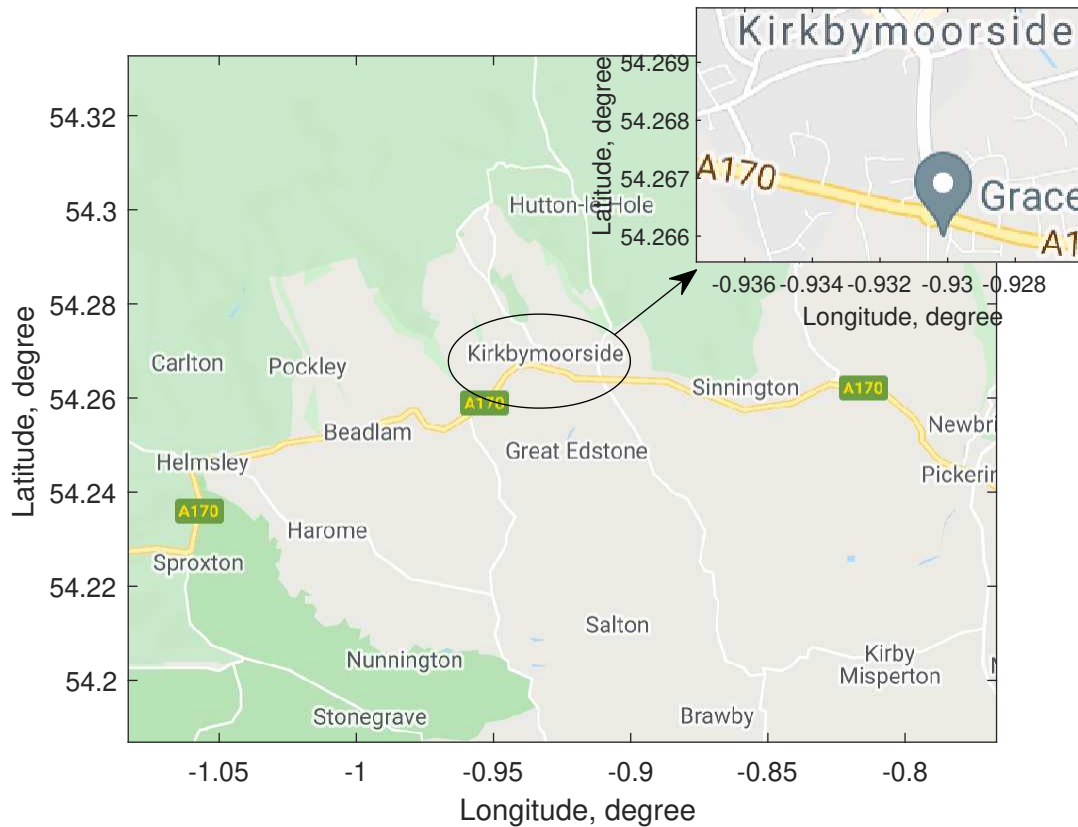


FIGURE A.1: Study Area comprising rural road way of North Yorkshire-Kirkbymoorside and Helmsley

Appendix B

Simulation Snapshot

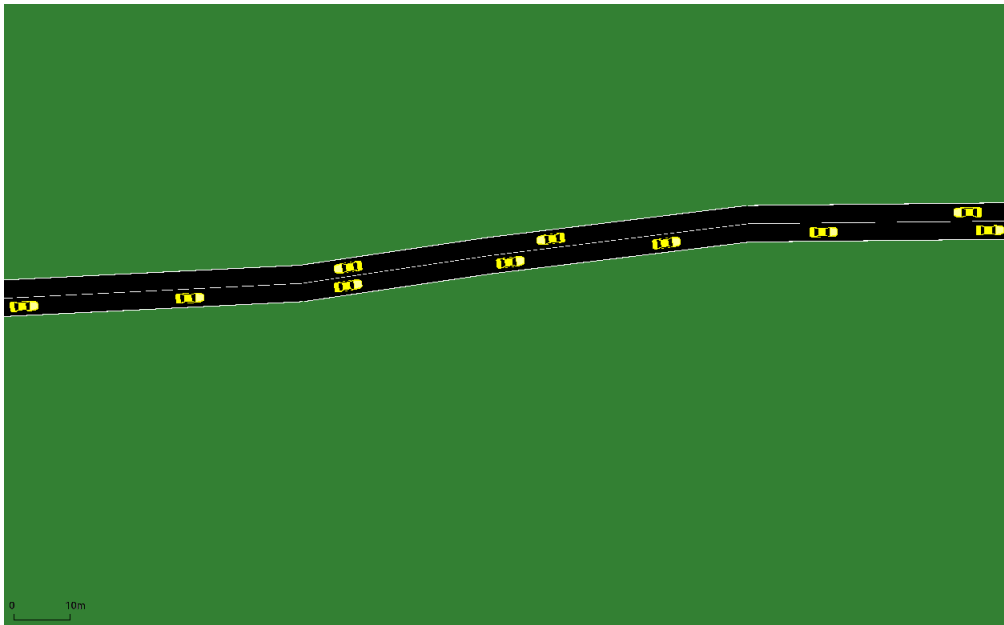


FIGURE B.1: A SUMO simulation snapshot at $t=20$ s

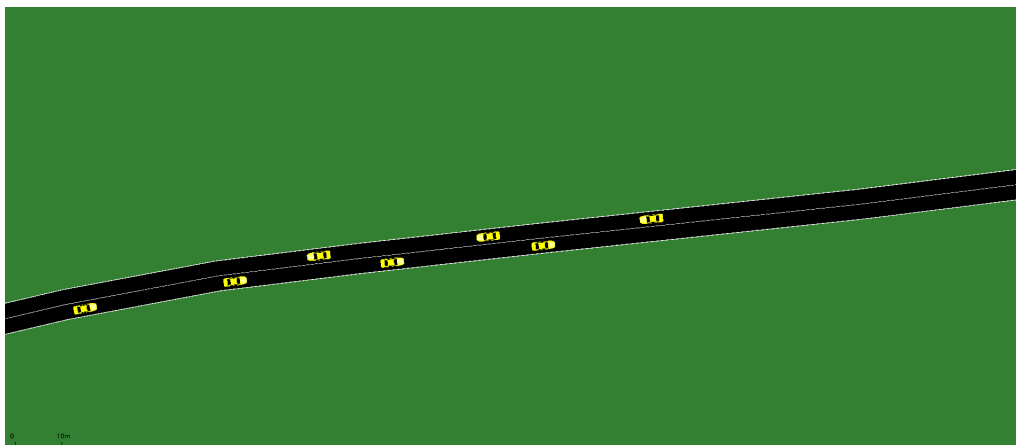


FIGURE B.2: A SUMO simulation snapshot at $t = 30$ s

Appendix C

Proof of Theorem 1

Let the graph of the network be represented by $G = (V, E)$ where $\mathcal{M}, \mathcal{T} \in V$. Let the edge $e \in E$ be denoted by $e = (w_{k_i}, w_{t_i})$.

Let M' be any perfect matching in G .

Every $v \in V$ is covered exactly once by M (the maximum weighted matching), therefore, the expression for the weight of the perfect matching is expressed as:

$$\begin{aligned} w(M') &= \sum_{e \in M'} w(e) \leq \sum_{e \in M'} \{ \ell(w_{k_i}) + \ell(w_{t_i}) \} \\ &= \sum_{v \in V} \ell(v) \end{aligned} \tag{C.1}$$

Therefore, $\sum_{v \in V} \ell(v)$ is the upper-bound on the utility cost of the perfect matching.

If M is a perfect matching in E_ℓ , then

$$w(M) = \sum_{e \in M} w(e) = \sum_{v \in V} \ell(v), \tag{C.2}$$

Therefore,

$$w(M') \leq w(M) \tag{C.3}$$

and, therefore, M is optimal. \square

Bibliography

- [1] Cisco, U, *Cisco annual internet report (2018–2023) white paper*. 2020.
- [2] U. Nissan. “Humandrive.” (2021), [Online]. Available: <https://humandrive.co.uk/nissan-leaf-completes-the-uks-longest-and-most-complex-autonomous-car-journey/> (visited on 09/21/2021).
- [3] C. for Connected and A. Vehicles(CCAV). “Multi-car collision avoidance (mucca).” (2021), [Online]. Available: <https://mucca-project.co.uk/> (visited on 09/21/2021).
- [4] J. B. Kenney, “Dedicated short-range communications (dsrc) standards in the united states,” *Proceedings of the IEEE*, vol. 99, no. 7, pp. 1162–1182, 2011.
- [5] U. D. of Transport (USDOT). “Broad agency announcement (baa) no. 693jj3-20-baa-0002 amendment 001 “its v2x spectrum testing”.” (2020), [Online]. Available: <https://sam.gov/api/prod/ops/v3/opportunities/resources/files/6d38fc4c72e44cf384f7a1a1fa8b922e/download?&status=archived&token=> (visited on 09/21/2021).
- [6] F. C. C. (FCC). “Use of the 5.850-5.925 ghz band.” (2020), [Online]. Available: <https://www.fcc.gov/document/fcc-modernizes-59-ghz-band-improve-wi-fi-and-automotive-safety-0> (visited on 09/22/2021).
- [7] M. Gonzalez-Martín, M. Sepulcre, R. Molina-Masegosa, and J. Gozalvez, “Analytical models of the performance of c-v2x mode 4 vehicular communications,” *IEEE Transactions on Vehicular Technology*, vol. 68, no. 2, pp. 1155–1166, 2018.
- [8] K. Kiela, V. Barzdenas, M. Jurgo, *et al.*, “Review of v2x-iot standards and frameworks for its applications,” *Applied Sciences*, vol. 10, no. 12, p. 4314, 2020.
- [9] N. Cheng, F. Lyu, J. Chen, *et al.*, “Big data driven vehicular networks,” *IEEE Network*, vol. 32, no. 6, pp. 160–167, 2018.
- [10] H. Qin, B. Cao, W. Chen, X. Xiao, and Y. Peng, “Wifi-assisted control traffic offloading in vehicular environments,” *IEEE Transactions on Vehicular Technology*, vol. 69, no. 4, pp. 4542–4547, 2020.
- [11] A. Al-Hilo, D. Ebrahimi, S. Sharafeddine, and C. Assi, “Revenue-driven video delivery in vehicular networks with optimal resource scheduling,” *Vehicular Communications*, vol. 23, p. 100 215, 2020.

- [12] G. Noh, J. Kim, S. Choi, N. Lee, H. Chung, and I. Kim, "Feasibility validation of a 5g-enabled mmwave vehicular communication system on a highway," *IEEE Access*, vol. 9, pp. 36 535–36 546, 2021.
- [13] Autotalks. "C-v2x implementation considerations." (2020), [Online]. Available: <https://www.auto-talks.com/wp-content/uploads/2020/12/C-V2X-implementation-considerations-final.pdf> (visited on 09/22/2021).
- [14] G. T. 38.801, *Study on new radio access technology: Radio access architecture and interfaces*, 2017.
- [15] M. Mohorcic, D. Grace, G. Kandus, and T. Tozer, "Broadband communications from aerial platform networks," in *IST Mobile Summit*, Citeseer, 2004.
- [16] P. Sudheesh, M. Magarini, and P. Muthuchidambaranathan, "Multiple-high altitude platforms aided system architecture for achieving maximum last mile capacity in satellite communication," *Telecommunication Systems*, vol. 70, no. 1, pp. 27–35, 2019.
- [17] L. Nagpal and K. Samdani, "Project loon: Innovating the connectivity worldwide," in *2017 2nd IEEE International Conference on Recent Trends in Electronics, Information & Communication Technology (RTEICT)*, IEEE, 2017, pp. 1778–1784.
- [18] S. C. Arum, D. Grace, and P. D. Mitchell, "A review of wireless communication using high-altitude platforms for extended coverage and capacity," *Computer Communications*, vol. 157, pp. 232–256, 2020.
- [19] H. Inc. "Hapsmobile's sunlider succeeds in stratospheric test flight." (2020), [Online]. Available: https://www.hapsmobile.com/en/news/press/2020/20201008_01/ (visited on 08/10/2020).
- [20] S. P. Ltd. "Stratospheric platforms ltd proposes complete 5g coverage across scotland, powered by sustainable hydrogen." (2020), [Online]. Available: <https://www.stratosphericplatforms.com/news/telecommunications-for-scotland/> (visited on 08/10/2020).
- [21] Y. Zhou, N. Cheng, N. Lu, and X. S. Shen, "Multi-uav-aided networks: Aerial-ground cooperative vehicular networking architecture," *IEEE vehicular technology magazine*, vol. 10, no. 4, pp. 36–44, 2015.
- [22] S. Khabaz, G. Pujolle, P. Velloso, *et al.*, "A new clustering-based radio resource allocation scheme for c-v2x," in *12th Wireless Days Conference (WD 2021)*, 2021.
- [23] M. Khabbaz, J. Antoun, and C. Assi, "Modeling and performance analysis of uav-assisted vehicular networks," *IEEE Transactions on Vehicular Technology*, vol. 68, no. 9, pp. 8384–8396, 2019.
- [24] H. Gao, C. Liu, Y. Li, and X. Yang, "V2vr: Reliable hybrid-network-oriented v2v data transmission and routing considering rsus and connectivity probability," *IEEE Transactions on Intelligent Transportation Systems*, 2020.

- [25] K. Popoola, D. Grace, and T. Clarke, "Capacity and coverage analysis of high altitude platform (hap) antenna arrays for rural vehicular broadband services," in *2020 IEEE 91st Vehicular Technology Conference (VTC2020-Spring)*, IEEE, 2020, pp. 1–5.
- [26] S. O.-R. A. V. S. Committee *et al.*, "Taxonomy and definitions for terms related to driving automation systems for on-road motor vehicles," *SAE International: Warrendale, PA, USA*, 2018.
- [27] T. S. Rappaport, Y. Xing, G. R. MacCartney, A. F. Molisch, E. Mellios, and J. Zhang, "Overview of millimeter wave communications for fifth-generation (5g) wireless networks—with a focus on propagation models," *IEEE Transactions on antennas and propagation*, vol. 65, no. 12, pp. 6213–6230, 2017.
- [28] G. R. MacCartney and T. S. Rappaport, "Rural macrocell path loss models for millimeter wave wireless communications," *IEEE Journal on selected areas in communications*, vol. 35, no. 7, pp. 1663–1677, 2017.
- [29] 3GPP, "Study on channel model for frequency spectrum above 6 ghz," *TR 38.900 Release 14*, 2016.
- [30] P. S. Bithas, V. Nikolaidis, A. G. Kanatas, and G. K. Karagiannidis, "Uav-to-ground communications: Channel modeling and uav selection," *IEEE Transactions on Communications*, vol. 68, no. 8, pp. 5135–5144, 2020.
- [31] A. A. Khuwaja and Y. Chen, "Channel model for airborne networks," *Autonomous Airborne Wireless Networks*, pp. 7–25, 2021.
- [32] L. Bai, C.-X. Wang, G. Goussetis, *et al.*, "Channel modeling for satellite communication channels at q-band in high latitude," *IEEE Access*, vol. 7, pp. 137 691–137 703, 2019.
- [33] A. Mishurov, S. Panko, A. Gorchakovskiy, T. Zubov, D. Dmitriev, and V. Tyapkin, "Simulation of a multi-frequency satellite communication channel," in *2020 Moscow Workshop on Electronic and Networking Technologies (MWENT)*, IEEE, 2020, pp. 1–6.
- [34] J. Zhao, Q. Wang, Y. Li, J. Zhou, and W. Zhou, "Ka-band based channel modeling and analysis in high altitude platform (hap) system," in *2020 IEEE 91st Vehicular Technology Conference (VTC2020-Spring)*, IEEE, 2020, pp. 1–5.
- [35] M. Guan, Z. Wu, Y. Cui, and M. Yang, "Channel modeling and characteristics for high altitude platform stations communication system," *Journal of Internet Technology*, vol. 21, no. 3, pp. 891–897, 2020.
- [36] K. Heimann, J. Tiemann, D. Yolchyan, and C. Wietfeld, "Experimental 5g mmwave beam tracking testbed for evaluation of vehicular communications," in *2019 IEEE 2nd 5G World Forum (5GWF)*, IEEE, 2019, pp. 382–387.
- [37] V. Semkin and I. Huhtinen, "Millimeter-wave uav-based channel measurement setup," in *2021 IEEE 93rd Vehicular Technology Conference (VTC2021-Spring)*, IEEE, 2021, pp. 1–2.

- [38] J. Huang, C.-X. Wang, H. Chang, J. Sun, and X. Gao, "Multi-frequency multi-scenario millimeter wave mimo channel measurements and modeling for b5g wireless communication systems," *IEEE Journal on Selected Areas in Communications*, vol. 38, no. 9, pp. 2010–2025, 2020.
- [39] 3GPP, "Study on channel model for frequencies from 0.5 to 100 ghz," *3rd Generation Partnership Project (3GPP), Tech. Rep.*, vol. 38, 2018.
- [40] C. R. Storck and F. Duarte-Figueiredo, "A survey of 5g technology evolution, standards, and infrastructure associated with vehicle-to-everything communications by internet of vehicles," *IEEE Access*, vol. 8, pp. 117 593–117 614, 2020.
- [41] L. Zhang, H. Zhao, S. Hou, *et al.*, "A survey on 5g millimeter wave communications for uav-assisted wireless networks," *IEEE Access*, vol. 7, pp. 117 460–117 504, 2019.
- [42] Z. Feng, L. Ji, Q. Zhang, and W. Li, "Spectrum management for mmwave enabled uav swarm networks: Challenges and opportunities," *IEEE Communications Magazine*, vol. 57, no. 1, pp. 146–153, 2018.
- [43] J ITU, "Provisional final acts," in *World Radiocommunication Conference 2019*, ITU Publications, 2019.
- [44] T. S. Rappaport, R. W. Heath Jr, R. C. Daniels, and J. N. Murdock, *Millimeter wave wireless communications*. Pearson Education, 2015.
- [45] P. Series, " P. 530-18, Propagation data and prediction methods required for the design of terrestrial line-of-sight systems", *International Telecommunication Union, Geneva*, 2021.
- [46] S. Shrestha and D.-Y. Choi, "Rain attenuation statistics over millimeter wave bands in south korea," *Journal of Atmospheric and Solar-Terrestrial Physics*, vol. 152, pp. 1–10, 2017.
- [47] A. M. Al-Saman, M. Cheffena, M. Mohamed, M. H. Azmi, and Y. Ai, "Statistical analysis of rain at millimeter waves in tropical area," *IEEE Access*, vol. 8, pp. 51 044–51 061, 2020.
- [48] N. González-Prelcic, R. W. Heath, C. Rusu, and A. Klautau, "High-capacity millimeter wave uav communications," *UAV Communications for 5G and Beyond*, pp. 203–229, 2020.
- [49] H. Jung and I.-H. Lee, "Performance analysis of millimeter-wave uav swarm networks under blockage effects," *Sensors*, vol. 20, no. 16, p. 4593, 2020.
- [50] S. Han, I Chih-Lin, Z. Xu, and C. Rowell, "Large-scale antenna systems with hybrid analog and digital beamforming for millimeter wave 5g," *IEEE Communications Magazine*, vol. 53, no. 1, pp. 186–194, 2015.
- [51] M. Guan, Z. Wu, Y. Cui, *et al.*, "Multi-beam coverage and beamforming technology for high altitude platform station communication system," *EURASIP*

- Journal on Wireless Communications and Networking*, vol. 2019, no. 1, pp. 1–10, 2019.
- [52] L. Dai, B. Wang, M. Wang, *et al.*, “Reconfigurable intelligent surface-based wireless communications: Antenna design, prototyping, and experimental results,” *IEEE Access*, vol. 8, pp. 45 913–45 923, 2020.
- [53] J. Ye, J. Qiao, A. Kammoun, and M.-S. Alouini, “Non-terrestrial communications assisted by reconfigurable intelligent surfaces,” *arXiv preprint arXiv:2109.00876*, 2021.
- [54] S. Alfattani, W. Jaafar, Y. Hmamouche, *et al.*, “Aerial platforms with reconfigurable smart surfaces for 5g and beyond,” *IEEE Communications Magazine*, vol. 59, no. 1, pp. 96–102, 2021.
- [55] D. Grace and M. Mohorcic, *Broadband communications via high altitude platforms*. John Wiley & Sons, 2011.
- [56] M Series, “Guidelines for evaluation of radio interface technologies for imt-2020,” *Report ITU*, pp. 2412–0, 2017.
- [57] V. Semkin, S. Kang, J. Haarla, *et al.*, “Lightweight uav-based measurement system for air-to-ground channels at 28 ghz,” *arXiv preprint arXiv:2103.17149*, 2021.
- [58] Z. Cui, K. Guan, C. Briso-Rodríguez, B. Ai, Z. Zhong, and C. Oestges, “Channel modeling for uav communications: State of the art, case studies, and future directions,” *arXiv preprint arXiv:2012.06707*, 2020.
- [59] Q. Zhu, M. Yao, F. Bai, *et al.*, “A general altitude-dependent path loss model for uav-to-ground millimeter-wave communications,” *Frontiers of Information Technology & Electronic Engineering*, vol. 22, no. 6, pp. 767–776, 2021.
- [60] M. Pang, Q. Zhu, F. Bai, *et al.*, “Height-dependent los probability model for a2g mmwave communications under built-up scenarios,” *arXiv preprint arXiv:2109.02263*, 2021.
- [61] E. M. Vitucci, V. Semkin, M. J. Arpaio, *et al.*, “Experimental characterization of air-to-ground propagation at mm-wave frequencies in dense urban environment,” in *2021 15th European Conference on Antennas and Propagation (EuCAP)*, IEEE, 2021, pp. 1–5.
- [62] V Degli Esposti, F Fuschini, and D Guiducci, “A study on roof-to-street propagation,” *Proc. ICEEA03, September*, pp. 8–12, 2003.
- [63] H. Safi, A. Dargahi, J. Cheng, and M. Safari, “Analytical channel model and link design optimization for ground-to-hap free-space optical communications,” *Journal of Lightwave Technology*, vol. 38, no. 18, pp. 5036–5047, 2020.
- [64] M. T. Dabiri, H. Safi, S. Parsaeefard, and W. Saad, “Analytical channel models for millimeter wave uav networks under hovering fluctuations,” *IEEE Transactions on Wireless Communications*, vol. 19, no. 4, pp. 2868–2883, 2020.

- [65] Z. Lian, L. Jiang, C. He, and Q. Xi, "A novel channel model for 3-d hap-mimo communication systems," in *2016 International Conference on Networking and Network Applications (NaNA)*, IEEE, 2016, pp. 1–6.
- [66] M. Li, M. Yang, G. Lv, and Q. Guo, "Three-state semi-markov channel model for hap-high speed train communication link," in *2011 6th International ICST Conference on Communications and Networking in China (CHINACOM)*, IEEE, 2011, pp. 279–283.
- [67] E. T. V14.0.0, *Study on channel model for frequencies from 0.5 to 100 GHz*, 3GPP TR 38.901 version 14.0.0 Release 14. ETSI, 2017. [Online]. Available: <https://www.etsi.org/standards>.
- [68] G. K. Kurt, M. G. Khoshkholgh, S. Alfattani, *et al.*, "A vision and framework for the high altitude platform station (haps) networks of the future," *IEEE Communications Surveys & Tutorials*, vol. 23, no. 2, pp. 729–779, 2021.
- [69] W. Theunissen, V. Jain, and G. Menon, "Development of a receive phased array antenna for high altitude platform stations using integrated beam-former modules," in *2018 IEEE/MTT-S International Microwave Symposium-IMS*, IEEE, 2018, pp. 779–782.
- [70] W. Tan, S. D. Assimonis, M. Matthaiou, Y. Han, X. Li, and S. Jin, "Analysis of different planar antenna arrays for mmwave massive mimo systems," in *2017 IEEE 85th Vehicular Technology Conference (VTC Spring)*, IEEE, 2017, pp. 1–5.
- [71] M. Stoneback and K. Madsen, "A planar all-silicon 256-element ka-band phased array for high-altitude platforms (haps) application," in *2018 IEEE/MTT-S International Microwave Symposium-IMS*, IEEE, 2018, pp. 783–786.
- [72] F. A. Dicandia and S. Genovesi, "Spectral efficiency improvement of 5g massive mimo systems for high-altitude platform stations by using triangular lattice arrays," *Sensors*, vol. 21, no. 9, p. 3202, 2021.
- [73] G. Federico, D. Caratelli, G. Theis, and A. Smolders, "A review of antenna array technologies for point-to-point and point-to-multipoint wireless communications at millimeter-wave frequencies," *International Journal of Antennas and Propagation*, vol. 2021, 2021.
- [74] H. Asplund, D. Astely, P. von Butovitsch, *et al.*, *Advanced Antenna Systems for 5G Network Deployments: Bridging the Gap Between Theory and Practice*. Academic Press, 2020.
- [75] J. Tong, Y. Lu, D. Zhang, G. Cui, and W. Wang, "Max-min analog beamforming for high altitude platforms communication systems," in *2018 IEEE/CIC International Conference on Communications in China (ICCC)*, IEEE, 2018, pp. 872–876.

- [76] K. Hoshino, S. Sudo, and Y. Ohta, "A study on antenna beamforming method considering movement of solar plane in haps system," in *2019 IEEE 90th Vehicular Technology Conference (VTC2019-Fall)*, IEEE, 2019, pp. 1–5.
- [77] L. Shi, L. Zhao, Y. Liu, and Q. Li, "Spatial-polarization diversity hap-mimo transmission system for emergency high-capacity mobile communications," *AEU-International Journal of Electronics and Communications*, vol. 115, p. 152 816, 2020.
- [78] S. Wang, Y. Li, Q. Wang, M. Su, and W. Zhou, "Dynamic downlink resource allocation based on imperfect estimation in leo-hap cognitive system," in *2019 11th International Conference on Wireless Communications and Signal Processing (WCSP)*, IEEE, 2019, pp. 1–6.
- [79] Z. Lin, M. Lin, Y. Huang, T. De Cola, and W.-P. Zhu, "Robust multi-objective beamforming for integrated satellite and high altitude platform network with imperfect channel state information," *IEEE Transactions on Signal Processing*, vol. 67, no. 24, pp. 6384–6396, 2019.
- [80] J. Li, Y. Sun, L. Xiao, S. Zhou, and C. E. Koksal, "Fast analog beam tracking in phased antenna arrays: Theory and performance," *arXiv preprint arXiv:1710.07873*, 2017.
- [81] "Ieee standard for information technology–telecommunications and information exchange between systems–local and metropolitan area networks–specific requirements–part 11: Wireless lan medium access control (mac) and physical layer (phy) specifications amendment 3: Enhancements for very high throughput in the 60 ghz band," *IEEE Std 802.11ad-2012 (Amendment to IEEE Std 802.11-2012, as amended by IEEE Std 802.11ae-2012 and IEEE Std 802.11aa-2012)*, pp. 1–628, 2012. DOI: 10.1109/IEEESTD.2012.6392842.
- [82] V. Va, H. Vikalo, and R. W. Heath, "Beam tracking for mobile millimeter wave communication systems," in *2016 IEEE Global Conference on Signal and Information Processing (GlobalSIP)*, IEEE, 2016, pp. 743–747.
- [83] S. Shaham, M. Ding, M. Kokshoorn, Z. Lin, S. Dang, and R. Abbas, "Fast channel estimation and beam tracking for millimeter wave vehicular communications," *IEEE Access*, vol. 7, pp. 141 104–141 118, 2019.
- [84] J. Thornton, "A low sidelobe asymmetric beam antenna for high altitude platform communications," *IEEE Microwave and Wireless Components Letters*, vol. 14, no. 2, pp. 59–61, 2004.
- [85] W. Krzysztofik, "Controlled sidelobe level microstrip planar array for haps," in *2008 IEEE Globecom Workshops*, IEEE, pp. 1–5.
- [86] W. Zhong, L. Xu, X. Lu, and L. Wang, "Research on millimeter wave communication interference suppression of uav based on beam optimization," in *International Conference on Machine Learning and Intelligent Communications*, Springer, 2017, pp. 472–481.

- [87] G. Wu, R. Miura, and Y. Hase, "A broadband wireless access system using stratospheric platforms," in *Globecom'00-IEEE. Global Telecommunications Conference. Conference Record (Cat. No. 00CH37137)*, IEEE, vol. 1, 2000, pp. 225–230.
- [88] J. Thornton, D. Grace, C. Spillard, T. Konefal, and T. Tozer, "Broadband communications from a high-altitude platform: The european helinet programme," *Electronics & Communication Engineering Journal*, vol. 13, no. 3, pp. 138–144, 2001.
- [89] D. Grace, M. Mohorcic, M. Oodo, M. Capstick, M. B. Pallavicini, and M. Lalovic, "Capanina-communications from aerial platform networks delivering broadband information for all," *Proceedings of the 14th IST mobile and wireless and communications summit*, 2005.
- [90] A. Inc. "Loon expanding internet connectivity with stratospheric balloons." (2018), [Online]. Available: <https://x.company/projects/loon/> (visited on 08/10/2020).
- [91] C. Engineering. "Case studies - ecosat." (2020), [Online]. Available: https://capgemini-engineering.com/es/en/case_study/ecosat/ (visited on 08/10/2020).
- [92] SCEYE. "Stratospheric platforms to improve life on our planet." (2021), [Online]. Available: <https://www.sceye.com/> (visited on 11/01/2021).
- [93] T. A. Space. "Thales alenia space's stratobus stratospheric airship passes a new development milestone." (2021), [Online]. Available: <https://www.thalesgroup.com/en/worldwide/space/press-release/thales-alenia-spaces-stratobus-stratospheric-airship-passes-new> (visited on 09/23/2021).
- [94] G. P. White and Y. V. Zakharov, "Data communications to trains from high-altitude platforms," *IEEE Transactions on Vehicular Technology*, vol. 56, no. 4, pp. 2253–2266, 2007.
- [95] B. El-Jabu and R. Steele, "Cellular communications using aerial platforms," *IEEE Transactions on Vehicular Technology*, vol. 50, no. 3, pp. 686–700, 2001.
- [96] J. Thornton, D. Grace, M. H. Capstick, and T. C. Tozer, "Optimizing an array of antennas for cellular coverage from a high altitude platform," *IEEE Transactions on Wireless Communications*, vol. 2, no. 3, pp. 484–492, 2003.
- [97] G. Chen, D. Grace, and T. C. Tozer, "Performance of multiple high altitude platforms using directive hap and user antennas," *Wireless Personal Communications*, vol. 32, no. 3-4, pp. 275–299, 2005.
- [98] W. Yang, D. Xie, X. Jing, Q. Jiang, and J. Zeng, "High altitude platform station communication as an enabler for massive internet of things," in *2020 IEEE 20th International Conference on Communication Technology (ICCT)*, IEEE, 2020, pp. 829–833.

- [99] J. Qiu, D. Grace, G. Ding, M. D. Zakaria, and Q. Wu, "Air-ground heterogeneous networks for 5g and beyond via integrating high and low altitude platforms," *IEEE Wireless Communications*, vol. 26, no. 6, pp. 140–148, 2019.
- [100] M. S. Alam, G. K. Kurt, H. Yanikomeroğlu, P. Zhu, and N. D. Đào, "High altitude platform station based super macro base station constellations," *IEEE Communications Magazine*, vol. 59, no. 1, pp. 103–109, 2021.
- [101] M. D. Zakaria, D. Grace, P. D. Mitchell, T. M. Shami, and N. Morozs, "Exploiting user-centric joint transmission-coordinated multipoint with a high altitude platform system architecture," *IEEE Access*, vol. 7, pp. 38 957–38 972, 2019.
- [102] S. C. Arum, D. Grace, P. D. Mitchell, M. D. Zakaria, and N. Morozs, "Energy management of solar-powered aircraft-based high altitude platform for wireless communications," *Electronics*, vol. 9, no. 1, p. 179, 2020.
- [103] O. B. Yahia, E. Erdogan, and G. K. Kurt, "On the performance of haps-assisted hybrid rf-fso multicast communication systems," *arXiv preprint arXiv:2109.10131*, 2021.
- [104] J. Harri, F. Filali, and C. Bonnet, "Mobility models for vehicular ad hoc networks: A survey and taxonomy," *IEEE Communications Surveys & Tutorials*, vol. 11, no. 4, pp. 19–41, 2009.
- [105] A.-L. Beylot and H. Labiod, *Vehicular Networks: Models and Algorithms*. John Wiley & Sons, 2013.
- [106] S. Uppoor, M. Fiore, and J. Härrri, "Synthetic mobility traces for vehicular networking," *Vehicular Networks: Models and Algorithms*, pp. 209–245, 2013.
- [107] C. Celes, A. Boukerche, and A. A. Loureiro, "Revealing and modeling vehicular micro clouds characteristics in a large-scale mobility trace," in *ICC 2021-IEEE International Conference on Communications*, IEEE, 2021, pp. 1–6.
- [108] —, "Mobility trace analysis for intelligent vehicular networks: Methods, models, and applications," *ACM Computing Surveys (CSUR)*, vol. 54, no. 3, pp. 1–38, 2021.
- [109] J. Tian and F. Meng, "Comparison survey of mobility models in vehicular ad-hoc network (vanet)," in *2020 IEEE 3rd International Conference on Automation, Electronics and Electrical Engineering (AUTEEE)*, IEEE, 2020, pp. 337–342.
- [110] K. Koufos and C. P. Dettmann, "Outage in motorway multi-lane vanets with hardcore headway distance using synthetic traces," *IEEE Transactions on Mobile Computing*, 2020.
- [111] D. Krajzewicz, "Traffic simulation with sumo—simulation of urban mobility," in *Fundamentals of traffic simulation*, Springer, 2010, pp. 269–293.
- [112] L. CODECA, J. ERDMANN, V. CAHILL, and J. HARRI, "Saga: An activity-based multi-modal mobility scenario generator for sumo,"

- [113] S. Uppoor, D. Naboulsi, and M. Fiore, "Vehicular mobility trace of the city of cologne, germany," URL: <http://kolntrace.project.citi-lab.fr> (visited on 08/25/2015), 2011.
- [114] L. Bedogni, M. Gramaglia, A. Vesco, M. Fiore, J. Härrri, and F. Ferrero, "The bologna ringway dataset: Improving road network conversion in sumo and validating urban mobility via navigation services," *IEEE Transactions on Vehicular Technology*, vol. 64, no. 12, pp. 5464–5476, 2015.
- [115] P. A. Lopez, M. Behrisch, L. Bieker-Walz, *et al.*, "Microscopic traffic simulation using sumo," in *2018 21st International Conference on Intelligent Transportation Systems (ITSC)*, IEEE, 2018, pp. 2575–2582.
- [116] M. Fellendorf and P. Vortisch, "Microscopic traffic flow simulator vissim," in *Fundamentals of traffic simulation*, Springer, 2010, pp. 63–93.
- [117] K.-C. Lan, "Move: A practical simulator for mobility model in vanet," in *Telematics Communication Technologies and Vehicular Networks: Wireless Architectures and Applications*, IGI Global, 2010, pp. 355–368.
- [118] *Java osm*, <https://josm.openstreetmap.de/>, Accessed: 2019-11-15.
- [119] S. Uppoor, O. Trullols-Cruces, M. Fiore, and J. M. Barcelo-Ordinas, "Generation and analysis of a large-scale urban vehicular mobility dataset," *IEEE Transactions on Mobile Computing*, vol. 13, no. 5, pp. 1061–1075, 2013.
- [120] H. Yu, R. Liu, Z. Li, Y. Ren, and H. Jiang, "An rsu deployment strategy based on traffic demand in vehicular ad hoc networks (vanets)," *IEEE Internet of Things Journal*, vol. 9, no. 9, pp. 6496–6505, 2021.
- [121] C. Liu, H. Huang, H. Du, and X. Jia, "Optimal rsus deployment in vehicular networks," in *International conference on web-age information management*, Springer, 2014, pp. 236–246.
- [122] P. S. Bithas, G. P. Efthymoglou, and A. G. Kanatas, "V2v cooperative relaying communications under interference and outdated csi," *IEEE Transactions on Vehicular Technology*, vol. 67, no. 4, pp. 3466–3480, 2017.
- [123] W. Liu, X. Hou, L. Chen, Y. Hokazono, and J. Zhao, "Interference coordination method for integrated haps-terrestrial networks," Mar. 2022.
- [124] D. for Transport. "National travel survey: 2020." (2020), [Online]. Available: <https://www.gov.uk/government/statistics/national-travel-survey-2020/national-travel-survey-2020> (visited on 03/26/2020).
- [125] M. Mukhtaruzzaman and M. Atiquzzaman, "Clustering in vehicular ad hoc network: Algorithms and challenges," *Computers & Electrical Engineering*, vol. 88, p. 106851, 2020.
- [126] R. Ghebleh, "A comparative classification of information dissemination approaches in vehicular ad hoc networks from distinctive viewpoints: A survey," *Computer Networks*, vol. 131, pp. 15–37, 2018.

- [127] M. S. Talib, A. Hassan, T. Alamery, *et al.*, "A center-based stable evolving clustering algorithm with grid partitioning and extended mobility features for vanets," *IEEE Access*, vol. 8, pp. 169 908–169 921, 2020.
- [128] G. Khayat, C. X. Mavromoustakis, G. Mastorakis, J. M. Batalla, H. Maalouf, and E. Pallis, "Vanet clustering based on weighted trusted cluster head selection," in *2020 International Wireless Communications and Mobile Computing (IWCMC)*, IEEE, 2020, pp. 623–628.
- [129] V. Vèque, F. Kaisser, C. Johnen, and A. Busson, "Convoy: A new cluster-based routing protocol for vehicular networks," *Vehicular Networks: Models and Algorithms*, pp. 91–129, 2013.
- [130] X. Bi, B. Guo, L. Shi, Y. Lu, L. Feng, and Z. Lyu, "A new affinity propagation clustering algorithm for v2v-supported vanets," *IEEE Access*, vol. 8, pp. 71 405–71 421, 2020.
- [131] Z. Wang, L. Liu, M. Zhou, and N. Ansari, "A position-based clustering technique for ad hoc intervehicle communication," *IEEE Transactions on Systems, Man, and Cybernetics, Part C (Applications and Reviews)*, vol. 38, no. 2, pp. 201–208, 2008.
- [132] M. Hadded, P. Muhlethaler, R. Zagrouba, A. Laouiti, and L. A. Saidane, "Using road ids to enhance clustering in vehicular ad hoc networks," in *2015 International Wireless Communications and Mobile Computing Conference (IWCMC)*, IEEE, 2015, pp. 285–290.
- [133] F. Aadil, W. Ahsan, Z. U. Rehman, P. A. Shah, S. Rho, and I. Mehmood, "Clustering algorithm for internet of vehicles (iov) based on dragonfly optimizer (cavdo)," *The Journal of Supercomputing*, vol. 74, no. 9, pp. 4542–4567, 2018.
- [134] G. Husnain and S. Anwar, "An intelligent cluster optimization algorithm based on whale optimization algorithm for vanets (woacnet)," *Plos one*, vol. 16, no. 4, e0250271, 2021.
- [135] N. Kumar, N. Chilamkurti, and J. H. Park, "Alca: Agent learning-based clustering algorithm in vehicular ad hoc networks," *Personal and ubiquitous computing*, vol. 17, no. 8, pp. 1683–1692, 2013.
- [136] L. Codeca, R. Frank, and T. Engel, "Luxembourg sumo traffic (lust) scenario: 24 hours of mobility for vehicular networking research," in *2015 IEEE Vehicular Networking Conference (VNC)*, IEEE, 2015, pp. 1–8.
- [137] M. Behrisch, L. Bieker, J. Erdmann, and D. Krajzewicz, "Sumo—simulation of urban mobility: An overview," in *Proceedings of SIMUL 2011, The Third International Conference on Advances in System Simulation*, ThinkMind, 2011.
- [138] I. MathWorks, *MATLAB: The Language of Technical Computing. Using MATLAB*. MathWorks, 2019, vol. 3.

- [139] J. Song, Y. Wu, Z. Xu, and X. Lin, "Research on car-following model based on sumo," in *The 7th IEEE/International Conference on Advanced Infocomm Technology*, IEEE, 2014, pp. 47–55.
- [140] T. Issariyakul and E. Hossain, *Introduction to network simulator ns2. introduction to network simulator ns2 (vol. 9781461414)*, 2012.
- [141] A. Varga, "Omnet++," in *Modeling and tools for network simulation*, Springer, 2010, pp. 35–59.
- [142] S. Kudva, S. Badsha, S. Sengupta, I. Khalil, and A. Zomaya, "Towards secure and practical consensus for blockchain based vanet," *Information Sciences*, vol. 545, pp. 170–187, 2021.
- [143] L. Codeca and J. Härrri, "Towards multimodal mobility simulation of c-its: The monaco sumo traffic scenario," in *2017 IEEE Vehicular Networking Conference (VNC)*, IEEE, 2017, pp. 97–100.
- [144] I. Saini, S. Saad, and A. Jaekel, "A context aware and traffic adaptive privacy scheme in vanets," in *2020 IEEE 3rd Connected and Automated Vehicles Symposium (CAVS)*, IEEE, 2020, pp. 1–5.
- [145] O. for National Statistics. "Overview of the uk population: January 2021." (2021), [Online]. Available: <https://www.ons.gov.uk/peoplepopulationandcommunity/populationandmigration/populationestimates/articles/overviewoftheukpopulation/january2021> (visited on 01/14/2021).
- [146] T. Y. Post. "Independent commission hears evidence on how north yorkshire's rural economy can achieve its potential." (2020), [Online]. Available: <https://www.yorkshirepost.co.uk/country-and-farming/independent-commission-hears-evidence-how-north-yorkshires-rural-economy-can-achieve-its-potential-1743630> (visited on 01/26/2020).
- [147] N. Y. C. Council. "Historic population estimates." (2016), [Online]. Available: <https://hub.datanorthyorkshire.org/dataset/population-estimates> (visited on 11/12/2021).
- [148] S. Yeung, H. A. Aziz, and S. Madria, "Activity-based shared mobility model for smart transportation," in *2019 20th IEEE International Conference on Mobile Data Management (MDM)*, IEEE, 2019, pp. 599–604.
- [149] J. Schweizer, C. Poliziani, F. Rupi, D. Morgano, and M. Magi, "Building a large-scale micro-simulation transport scenario using big data," *ISPRS International Journal of Geo-Information*, vol. 10, no. 3, p. 165, 2021.
- [150] O. S. Map. "Openstreetmap data extracts." (2021), [Online]. Available: <http://download.geofabrik.de/> (visited on 11/12/2021).
- [151] LearnOSM. "Manipulating data with osmosis." (2021), [Online]. Available: <https://learnosm.org/en/osm-data/osmosis/> (visited on 10/21/2021).

- [152] A. based Demand Generation. "Sumo documentation." (2021), [Online]. Available: https://sumo.dlr.de/docs/Demand/Activity-based_Demand_Generation.htmlurldate={2021-10-21}.
- [153] J. G. Wardrop, "Road paper. some theoretical aspects of road traffic research.," *Proceedings of the institution of civil engineers*, vol. 1, no. 3, pp. 325–362, 1952.
- [154] M. Khabbaz, C. Assi, and S. Sharafeddine, "Multi-hop v2u path availability analysis in uav-assisted vehicular networks," *IEEE Internet of Things Journal*, 2021.
- [155] M. Rapelli, C. Casetti, and G. Gagliardi, "Tust: From raw data to vehicular traffic simulation in turin," in *2019 IEEE/ACM 23rd International Symposium on Distributed Simulation and Real Time Applications (DS-RT)*, IEEE, 2019, pp. 1–8.
- [156] F. B. Carlsen, J. J. Rasmussen, M. M. Sørensen, N. Ø. Jensen, and M. Albano, "Generation of realistic activity scenarios for sumo," in *MobiQuitous 2020-17th EAI International Conference on Mobile and Ubiquitous Systems: Computing, Networking and Services*, 2020, pp. 357–365.
- [157] N. M. Al-Kharasani, Z. A. Zukarnain, S. K. Subramaniam, and Z. M. Hanapi, "An adaptive relay selection scheme for enhancing network stability in vanets," *IEEE Access*, vol. 8, pp. 128 757–128 765, 2020.
- [158] A. Alioua, S.-M. Senouci, S. Moussaoui, E. Alemneh, M.-A.-A. Deradji, and F. Benaziza, "A distributed multi-hop clustering algorithm for infrastructure-less vehicular ad-hoc networks," in *International Conference on Information and Communication Technology for Development for Africa*, Springer, 2017, pp. 68–81.
- [159] G. Rémy, S.-M. Senouci, F. Jan, and Y. Gourhant, "Lte4v2x—collection, dissemination and multi-hop forwarding," in *2012 IEEE international conference on communications (ICC)*, IEEE, 2012, pp. 120–125.
- [160] M. Ahmad, A. A. Ikram, I. Wahid, F. Ullah, A. Ahmad, and F. A. Khan, "Optimized clustering in vehicular ad hoc networks based on honey bee and genetic algorithm for internet of things," *Peer-to-Peer Networking and Applications*, vol. 13, no. 2, pp. 532–547, 2020.
- [161] M. Fahad, F. Aadil, S. Khan, *et al.*, "Grey wolf optimization based clustering algorithm for vehicular ad-hoc networks," *Computers & Electrical Engineering*, vol. 70, pp. 853–870, 2018.
- [162] C. Cooper, D. Franklin, M. Ros, F. Safaei, and M. Abolhasan, "A comparative survey of vanet clustering techniques," *IEEE Communications Surveys & Tutorials*, vol. 19, no. 1, pp. 657–681, 2016.
- [163] M. Ren, J. Zhang, L. Khoukhi, H. Labiod, and V. Vèque, "A review of clustering algorithms in vanets," *Annals of Telecommunications*, pp. 1–23, 2021.

- [164] Y. Xu, F. Fang, D. Cai, and Y. Yuan, "Intelligent user clustering and robust beamforming design for uav-noma downlink," *arXiv preprint arXiv:2006.05852*, 2020.
- [165] R. Kaur, R. K. Ramachandran, R. Doss, and L. Pan, "The importance of selecting clustering parameters in vanets: A survey," *Computer Science Review*, vol. 40, p. 100 392, 2021.
- [166] A. Guidotti, A. Vanelli-Coralli, G. Taricco, and G. Montorsi, "User clustering for multicast precoding in multi-beam satellite systems," *arXiv preprint arXiv:1706.09482*, 2017.
- [167] L. Ju, Q. Du, and M. Gunzburger, "Probabilistic methods for centroidal voronoi tessellations and their parallel implementations," *Parallel Computing*, vol. 28, no. 10, pp. 1477–1500, 2002.
- [168] A. Chowdhury and D. De, "Energy-efficient coverage optimization in wireless sensor networks based on voronoi-glowworm swarm optimization-k-means algorithm," *Ad Hoc Networks*, vol. 122, p. 102 660, 2021.
- [169] W. Wang, F. Xia, H. Nie, *et al.*, "Vehicle trajectory clustering based on dynamic representation learning of internet of vehicles," *IEEE Transactions on Intelligent Transportation Systems*, vol. 22, no. 6, pp. 3567–3576, 2020.
- [170] M. Peixoto, A. Maia, E Mota, *et al.*, "A traffic data clustering framework based on fog computing for vanets," *Vehicular Communications*, vol. 31, p. 100 370, 2021.
- [171] P. J. Rousseeuw, "Silhouettes: A graphical aid to the interpretation and validation of cluster analysis," *Journal of computational and applied mathematics*, vol. 20, pp. 53–65, 1987.
- [172] M. Dorigo, M. Birattari, and T. Stutzle, "Ant colony optimization," *IEEE computational intelligence magazine*, vol. 1, no. 4, pp. 28–39, 2006.
- [173] A. M. Jabbar, K. R. Ku-Mahamud, and R. Sagban, "Ant-based sorting and aco-based clustering approaches: A review," in *2018 IEEE Symposium on Computer Applications & Industrial Electronics (ISCAIE)*, IEEE, 2018, pp. 217–223.
- [174] C Mageshkumar, S Karthik, and V. Arunachalam, "Hybrid metaheuristic algorithm for improving the efficiency of data clustering," *Cluster Computing*, vol. 22, no. 1, pp. 435–442, 2019.
- [175] X. Liu, "Routing protocols based on ant colony optimization in wireless sensor networks: A survey," *IEEE Access*, vol. 5, pp. 26 303–26 317, 2017.
- [176] Z. Khan, S. Fang, A. Koubaa, P. Fan, F. Abbas, and H. Farman, "Street-centric routing scheme using ant colony optimization-based clustering for bus-based vehicular ad-hoc network," *Computers & Electrical Engineering*, vol. 86, p. 106 736, 2020.

- [177] S. Ebadinezhad, Z. Dereboylu, and E. Ever, "Clustering-based modified ant colony optimizer for internet of vehicles (cacoiov)," *Sustainability*, vol. 11, no. 9, p. 2624, 2019.
- [178] F. Aadil, K. B. Bajwa, S. Khan, N. M. Chaudary, and A. Akram, "Caconet: Ant colony optimization (aco) based clustering algorithm for vanet," *PloS one*, vol. 11, no. 5, e0154080, 2016.
- [179] Y. Hua, Q. Liu, K. Hao, and Y. Jin, "A survey of evolutionary algorithms for multi-objective optimization problems with irregular pareto fronts," *IEEE/CAA Journal of Automatica Sinica*, vol. 8, no. 2, pp. 303–318, 2021.
- [180] Y. A. Shah, H. A. Habib, F. Aadil, M. F. Khan, M. Maqsood, and T. Nawaz, "Camonet: Moth-flame optimization (mfo) based clustering algorithm for vanets," *IEEE Access*, vol. 6, pp. 48 611–48 624, 2018.
- [181] M. Ko, H. Lee, and J. Choi, "Planar lte/sub-6 ghz 5g mimo antenna integrated with mmwave 5g beamforming phased array antennas for v2x applications," *IET Microwaves, Antennas & Propagation*, vol. 14, no. 11, pp. 1283–1295, 2020.
- [182] F. Alraddady, "Performance of high-altitude platforms cellular communications using hamming-tapered concentric circular arrays," 2014.
- [183] C. A. Balanis, *Antenna theory: analysis and design*. John wiley & sons, 2016.
- [184] Y. Shibata, N. Kanazawa, M. Konishi, K. Hoshino, Y. Ohta, and A. Nagate, "System design of gigabit haps mobile communications," *IEEE Access*, vol. 8, pp. 157 995–158 007, 2020.
- [185] S. Barrie and D. B. O. Konditi, "Evaluation of adjacent channel interference from land-earth station in motion to 5g radio access network in the ka-frequency band," *Heliyon*, vol. 7, no. 6, e07412, 2021.
- [186] P. Series," P. 838-3, Specific attenuation model for rain for use in prediction methods," *International Telecommunication Union, Geneva*, 1997.
- [187] P. Series, " P. 618-13, Propagation data and prediction methods required for the design of earth-space telecommunication systems," *International Telecommunication Union, Geneva*, 2017.
- [188] P. Series, " P. 676-12, Attenuation by atmospheric gases and related effects," *International Telecommunication Union, Geneva*, 2013.
- [189] Z. Pi and F. Khan, "An introduction to millimeter-wave mobile broadband systems," *IEEE communications magazine*, vol. 49, no. 6, pp. 101–107, 2011.
- [190] V. Va and R. W. Heath, "Basic relationship between channel coherence time and beamwidth in vehicular channels," in *2015 IEEE 82nd Vehicular Technology Conference (VTC2015-Fall)*, IEEE, 2015, pp. 1–5.
- [191] A. Tassi, M. Egan, R. J. Piechocki, and A. Nix, "Modeling and design of millimeter-wave networks for highway vehicular communication," *IEEE Transactions on Vehicular Technology*, vol. 66, no. 12, pp. 10 676–10 691, 2017.

- [192] M. Ozpolat, K. Bhargava, E. Kampert, and M. D. Higgins, "Multi-lane urban mmwave v2v networks: A path loss behaviour dependent coverage analysis," *Vehicular Communications*, vol. 30, p. 100 348, 2021.
- [193] A. Papadogiannis and A. G. Burr, "Multi-beam assisted mimo—a novel approach to fixed beamforming," in *2011 Future Network & Mobile Summit*, IEEE, 2011, pp. 1–8.
- [194] A. Burr, A. Papadogiannis, and T. Jiang, "Mimo truncated shannon bound for system level capacity evaluation of wireless networks," in *2012 IEEE Wireless Communications and Networking Conference Workshops (WCNCW)*, IEEE, 2012, pp. 268–272.
- [195] M. H. C. Garcia, A. Molina-Galan, M. Boban, *et al.*, "A tutorial on 5g nr v2x communications," *arXiv preprint arXiv:2102.04538*, 2021.
- [196] E. 3GPP, *5g nr: Physical layer procedures for data (3gpp ts 38.214 version 16.2.0 release 16)*, 2020.
- [197] A. Bazzi, G. Cecchini, M. Menarini, B. M. Masini, and A. Zanella, "Survey and perspectives of vehicular wi-fi versus sidelink cellular-v2x in the 5g era," *Future Internet*, vol. 11, no. 6, p. 122, 2019.
- [198] U. A. Mughal, J. Xiao, I. Ahmad, and K. Chang, "Cooperative resource management for c-v2i communications in a dense urban environment," *Vehicular Communications*, vol. 26, p. 100 282, 2020.
- [199] E. Ahmed and H. Gharavi, "Cooperative vehicular networking: A survey," *IEEE Transactions on Intelligent Transportation Systems*, vol. 19, no. 3, pp. 996–1014, 2018.
- [200] O. Rehman, M. Ould-Khaoua, and H. Bourdouden, "An adaptive relay nodes selection scheme for multi-hop broadcast in vanets," *Computer Communications*, vol. 87, pp. 76–90, 2016.
- [201] S. Atapattu, Y. Jing, H. Jiang, and C. Tellambura, "Relay selection and performance analysis in multiple-user networks," *IEEE Journal on Selected Areas in Communications*, vol. 31, no. 8, pp. 1517–1529, 2012.
- [202] K. Belbase, Z. Zhang, H. Jiang, and C. Tellambura, "Coverage analysis of millimeter wave decode-and-forward networks with best relay selection," *IEEE Access*, vol. 6, pp. 22 670–22 683, 2018.
- [203] H. Zhang, X. Zhang, and D. K. Sung, "An efficient cooperative transmission based opportunistic broadcast scheme in vanets," *IEEE Transactions on Mobile Computing*, 2021.
- [204] D. Yang, X. Fang, and G. Xue, "Opra: Optimal relay assignment for capacity maximization in cooperative networks," in *2011 IEEE International Conference on Communications (ICC)*, IEEE, 2011, pp. 1–6.

- [205] G. Sun, M. Yu, D. Liao, and V. Chang, "Analytical exploration of energy savings for parked vehicles to enhance vanet connectivity," *IEEE Transactions on Intelligent Transportation Systems*, vol. 20, no. 5, pp. 1749–1761, 2018.
- [206] D. Abada, A. Massaq, A. Boulouz, and M. B. Salah, "An adaptive vehicular relay and gateway selection scheme for connecting vanets to internet via 4g lte cellular network," in *Emerging technologies for connected internet of vehicles and intelligent transportation system networks*, Springer, 2020, pp. 149–163.
- [207] B. Kim, S. Kim, H. Yoon, *et al.*, "Nearest-first: Efficient relaying scheme in heterogeneous v2v communication environments," *IEEE Access*, vol. 7, pp. 23 615–23 627, 2019.
- [208] X. Fan, D. Liu, B. Fu, and S. Wen, "Optimal relay selection for uav-assisted v2v communications," *Wireless Networks*, pp. 1–17, 2021.
- [209] Y. He, D. Zhai, D. Wang, X. Tang, and R. Zhang, "A relay selection protocol for uav-assisted vanets," *Applied Sciences*, vol. 10, no. 23, p. 8762, 2020.
- [210] H. W. Kuhn, "The hungarian method for the assignment problem," *Naval research logistics quarterly*, vol. 2, no. 1-2, pp. 83–97, 1955.
- [211] K Erciyes, "Graph applications," in *Discrete Mathematics and Graph Theory*, Springer, 2021, pp. 307–328.
- [212] B. C. Nguyen, N. N. Thang, T. M. Hoang, *et al.*, "Analysis of outage probability and throughput for energy harvesting full-duplex decode-and-forward vehicle-to-vehicle relay system," *Wireless Communications and Mobile Computing*, vol. 2020, 2020.
- [213] H. Fernández, L. Rubio, V. M. Rodrigo-Peñarrocha, and J. Reig, "Path loss characterization for vehicular communications at 700 mhz and 5.9 ghz under los and nlos conditions," *IEEE Antennas and Wireless Propagation Letters*, vol. 13, pp. 931–934, 2014.
- [214] F. Li, W. Chen, Y. Shui, *et al.*, "Connectivity probability analysis of vanets at different traffic densities using measured data at 5.9 ghz," *Physical Communication*, vol. 35, p. 100 709, 2019.
- [215] A. Cardote, S. Sargento, and P. Steenkiste, "On the connection availability between relay nodes in a vanet," in *2010 IEEE Globecom Workshops*, IEEE, 2010, pp. 181–185.
- [216] A. Benslimane, S. Barghi, and C. Assi, "An efficient routing protocol for connecting vehicular networks to the internet," *Pervasive and Mobile Computing*, vol. 7, no. 1, pp. 98–113, 2011.